

CONTACT MECHANICS OF GRADED ORTHOTROPIC COATINGS

A THESIS SUBMITTED TO
THE GRADUATE SCHOOL OF NATURAL AND APPLIED SCIENCES
OF
MIDDLE EAST TECHNICAL UNIVERSITY

BY

ONUR ARSLAN

IN PARTIAL FULFILLMENT OF THE REQUIREMENTS
FOR
THE DEGREE OF DOCTOR OF PHILOSOPHY
IN
MECHANICAL ENGINEERING

FEBRUARY 2016

Approval of the thesis:

CONTACT MECHANICS OF GRADED ORTHOTROPIC COATINGS

submitted by **ONUR ARSLAN** in partial fulfillment of the requirements for the degree of **Doctor of Philosophy in Mechanical Engineering Department, Middle East Technical University** by,

Prof. Dr. Gülbin Dural Ünver

Dean, Graduate School of **Natural and Applied Sciences**

Prof. Dr. Tuna Balkan

Head of Department, **Mechanical Engineering**

Prof. Dr. Serkan Dağ

Supervisor, **Mechanical Engineering Dept., METU**

Examining Committee Members:

Assit. Prof. Dr. Gökhan Özgen

Mechanical Engineering Dept., METU

Prof. Dr. Serkan Dağ

Mechanical Engineering Dept., METU

Prof. Dr. Altan Kayran

Aerospace Engineering Dept., METU

Prof. Dr. Mehmet Ali Güler

Mechanical Engineering Dept., TOBB ETU

Assoc. Prof. Dr. Recep Güneş

Mechanical Engineering Dept., Erciyes University

Date: 02/02/2016

I hereby declare that all information in this document has been obtained and presented in accordance with academic rules and ethical conduct. I also declare that, as required by these rules and conduct, I have fully cited and referenced all material and results that are not original to this work.

Name, Last name : Onur ARSLAN

Signature:

ABSTRACT

CONTACT MECHANICS OF GRADED ORTHOTROPIC COATINGS

Arslan, Onur

Ph.D., Department of Mechanical Engineering

Supervisor: Prof. Dr. Serkan Dağ

February 2016, 147 pages

Analytic and computational studies are performed for contact problems of orthotropic functionally graded material (FGM) coatings which are bonded to isotropic homogeneous substrates without any interfacial defects. The orthotropic FGM coatings possess orthotropic stiffness gradations through the coating thickness direction. The variations of each orthotropic stiffness constants are assumed to behave as exponential functions. In the analytical procedure, the problems of orthotropic graded coatings which are subjected to contact loads by an arbitrarily shaped inelastic stamp are examined under plane strain assumption. After getting the Navier equations of the elasticity problem, Fourier transformation techniques are used to determine the field expressions that satisfy the boundary conditions of the related problem. A deformation gradient on the contact region is used to obtain a singular integral equation (SIE) which is collocated through a discretization procedure on the roots of Chebyshev polynomials. Computational approach for the same contact problem is based on the finite element method in which the coating-substrate systems are divided into finite elements having the material parameters defined at their centroids. The results produced by using the analytical technique and the finite element method are compared to assess the accuracy achieved by both methods. Finally, the complete contact problems on the orthotropic homogeneous coatings are also investigated.

Keywords: Frictional sliding contact problems, Singular Integral Equation of the second kind, Orthotropic FGM coatings, Finite element procedure.

ÖZ

DERECELENDİRİLMİŞ ORTOTROPİK KAPLAMALARIN TEMAS MEKANİĞİ

Arslan, Onur

Doktora, Makina Mühendisliği Bölümü

Tez Yöneticisi: Prof. Dr. Serkan Dağ

Şubat 2016, 147 sayfa

Bu tez izotropik yarı-sonsuz homojen gövde ile mükemmel şekilde yapıştırılmış olan ortotropik fonksiyonel derecelendirilmiş malzeme (FDM) kaplamaların temas mekaniği üzerinedir. Kaplama içerisindeki elastik derecelendirme kaplama kalınlığı boyuncadır. Ortotropik katılık sabitlerinin eksene bağlı olarak değişen değerleri üstel fonksiyonlar ile gösterilmiştir. Geliştirilen Analitik metotta; çeşitli yüzey profillerine sahip rijit zımbalar ile derecelendirilmiş ortotropik kaplama yüzeyi arasındaki sürtünmeli temas düzlem-gerinimi varsayımı ile ele alınmıştır. Problemin temelini oluşturan kısmi diferansiyel denklemler ve problemdeki sınır koşulları Fourier dönüşüm teknikleri ile formüle edilmiştir. Daha sonra problem bir tekil integral denklemine dönüştürülmüş ve bu integralin numerik çözümü “expansion-collocation” tekniği ile sağlanmıştır. Hesaplamalı yöntemde ise; çeşitli yüzey profillerine sahip rijit zımbalar ile derecelendirilmiş ortotropik kaplama yüzeyi arasındaki sürtünmeli temas, sonlu elemanlar metodu ile modellenmiştir. Sözü geçen sonlu elemanlar analizinde; derecelendirilmiş kaplama-homojen gövde sistemi sonlu elemanlara bölünerek, her bir sonlu elemanın malzeme özelliği kendi ağırlık merkezinde tanımlanmıştır. Geliştirilen iki yöntemin farklı zımba profilleri için üretilen sonuçları birbirleri ile karşılaştırılarak her iki metodun da doğruluğu ispat edilmiştir. Son olarak ise homojen ortotropik kaplamaların temas mekaniği düz zımba profili için incelenmiştir.

Anahtar Kelimeler: Sürtünmeli kayma temas problemleri, Tekil İntegral Denklemleri, Ortotropik FDM kaplamaları, Sonlu elemanlar metodu.

To My Dear Mother Hatice ARSLAN

ACKNOWLEDGMENTS

The author would like to express his gratitude to his advisor Prof. Dr. Serkan Dağ for his support and insightful guidance throughout the Ph.D. study.

The useful discussions of the Ph.D. committee members, Prof. Dr. Altan Kayran, Assist. Prof. Dr. Gökhan Özgen, Prof. Dr. Mehmet Ali Güler and Assoc. Prof. Dr. Recep Güneş are also very much appreciated.

TABLE OF CONTENTS

| | |
|---|------|
| ABSTRACT | v |
| ÖZ..... | vi |
| ACKNOWLEDGMENTS..... | viii |
| TABLE OF CONTENTS | ix |
| LIST OF TABLES | xi |
| LIST OF FIGURES..... | xiv |
| CHAPTERS | |
| 1. INTRODUCTION..... | 1 |
| 1.1 Literature Survey | 1 |
| 1.2 Scope of the research..... | 6 |
| 2. PROBLEM STATEMENT AND THE ANALYTICAL METHOD | 9 |
| 2.1 Definition of the problem | 9 |
| 2.2 Formulation | 14 |
| 2.2.1 The orthotropic FGM coating..... | 14 |
| 2.2.2 The homogeneous substrate..... | 17 |
| 2.2.3 Determination of unknown constants | 19 |
| 2.2.4 Derivation of the Singular Integral Equation..... | 24 |
| 2.2.5 The in plane lateral surface stress | 33 |

| | |
|--|-----|
| 2.2.6 On the solutions of the Singular Integral Equation..... | 34 |
| 2.2.6.1 Flat stamp..... | 36 |
| 2.2.6.2 Triangular stamp | 39 |
| 2.2.6.3 Circular stamp | 42 |
| 3. THE FINITE ELEMENT METHOD | 47 |
| 4. NUMERICAL RESULTS | 53 |
| 4.1 Flat stamp | 55 |
| 4.2 Triangular stamp..... | 59 |
| 4.3 Circular stamp | 62 |
| 4.4 Homogeneous coating | 66 |
| 4.5 Tables | 69 |
| 4.6 Figures | 86 |
| 5. CONCLUDING REMARKS | 127 |
| 5.1 Conclusions | 127 |
| 5.2 Future work | 129 |
| REFERENCES..... | 131 |
| APPENDICES | |
| A. ASYMPTOTIC EXPANSION COEFFICIENTS | 139 |
| B. CLOSED FORM AND RECURRENCE TYPE SOLUTIONS OF CAUCHY PRINCIPAL VALUE INTEGRALS..... | 141 |
| C. FUNCTION THEORECTIC ANALYSES | 143 |
| VITA | 147 |

LIST OF TABLES

TABLES

| | |
|--|----|
| Table 2.1: Engineering parameters utilized in the parametric analyses | 26 |
| Table 4.1: Convergence of the normalized contact stresses evaluated for various values of γh , N and r regarding the flat stamp, $\eta = 0.3$, $(b - a)/h = 0.4$, $r = (2y - (b + a))/(b - a)$ | 69 |
| Table 4.2: Convergence of the normalized contact stresses evaluated for various values of γh , N and r regarding the flat stamp, $\eta = 0.3$, $(b - a)/h = 1.0$, $r = (2y - (b + a))/(b - a)$ | 70 |
| Table 4.3: Normalized forces $P/(\mu_{xy} \tan(\theta)(b - a))$ evaluated for various magnitudes of the friction coefficient η , the normalized non-homogeneity constant γh and the normalized contact length $(b - a)/h$ regarding the triangular stamp for which the coating surface is Alumina. | 71 |
| Table 4.4: Normalized forces $P/(\mu_{xy} \tan(\theta)(b - a))$ evaluated for various magnitudes of the friction coefficient η , the normalized non-homogeneity parameter γh and the normalized contact length $(b - a)/h$ regarding the triangular stamp, $E_x/E_y = 0.6$ | 72 |
| Table 4.5: Normalized forces $P/(\mu_{xy} \tan(\theta)(b - a))$ evaluated for various magnitudes of the friction coefficient η , the normalized non-homogeneity parameter γh and the normalized contact length $(b - a)/h$ regarding the triangular stamp, $E_x/E_y = 1.5$ | 73 |

Table 4.6: Normalized forces $P/(\mu_{xy} \tan(\theta)(b-a))$ evaluated for various magnitudes of the friction coefficient η , the normalized non-homogeneity parameter γh and the normalized contact length $(b-a)/h$ regarding the triangular stamp, $E_x/E_z = 0.6$ 74

Table 4.7: Normalized forces $P/(\mu_{xy} \tan(\theta)(b-a))$ evaluated for various magnitudes of the friction coefficient η , the normalized non-homogeneity parameter γh and the normalized contact length $(b-a)/h$ regarding the triangular stamp, $E_x/E_z = 3.0$ 74

Table 4.8: Normalized forces $P/(\mu_{xy}(b-a))$ evaluated for various magnitudes of the friction coefficient η , the normalized non-homogeneity parameter γh and the normalized contact length $(b-a)/h$ regarding the circular stamp, for which the coating surface is Alumina, $a/R = 0$, $b/R = 0.02$ 76

Table 4.9: Normalized forces $P/(\mu_{xy}(b-a))$ evaluated for various magnitudes of the friction coefficient η , the normalized non-homogeneity parameter γh and the normalized contact length $(b-a)/h$ regarding the circular stamp, $a/R = 0$, $b/R = 0.02$, $E_x/E_y = 0.6$ 77

Table 4.10: Normalized forces $P/(\mu_{xy}(b-a))$ evaluated for various values of the friction coefficient η , the normalized non-homogeneity parameter γh and the normalized contact length $(b-a)/h$ regarding the circular stamp, $a/R = 0$, $b/R = 0.02$, $E_x/E_y = 1.5$ 78

Table 4.11: Normalized forces $P/(\mu_{xy}(b-a))$ evaluated for various magnitudes of the friction coefficient η , the normalized non-homogeneity parameter γh and the normalized contact length $(b-a)/h$ regarding the circular stamp, $a/R = 0$, $b/R = 0.02$, $E_x/E_z = 0.6$ 79

Table 4.12: Normalized forces $P/(\mu_{xy}(b-a))$ evaluated for various magnitudes of the coefficient of friction η , the normalized non-homogeneity parameter γh and the normalized contact length $(b-a)/h$ regarding the circular stamp, $a/R=0$, $b/R=0.02$, $E_x/E_z=3.0$ 80

Table 4.13: Centerline position c/R of the circular stamp problem for various magnitudes of the friction coefficient η , the normalized non-homogeneity parameter γh and normalized contact length $(b-a)/h$, $a/R=0$, $b/R=0.02$, for which the coating surface is Alumina. 81

Table 4.14: Centerline position c/R of the circular stamp problem for various magnitudes of friction coefficient η , the normalized non-homogeneity parameter γh and normalized contact length $(b-a)/h$, $a/R=0$, $b/R=0.02$, $E_x/E_y=0.6$ 82

Table 4.15: Centerline position c/R of the circular stamp problem for various magnitudes of the friction coefficient η , the normalized non-homogeneity parameter γh and normalized contact length $(b-a)/h$, $a/R=0$, $b/R=0.02$, $E_x/E_y=1.5$ 83

Table 4.16: Centerline position c/R of the circular stamp problem for various magnitudes of the friction coefficient η , the normalized non-homogeneity parameter γh and normalized contact length $(b-a)/h$, $a/R=0$, $b/R=0.02$, $E_x/E_z=0.6$ 84

Table 4.17: Centerline position c/R of the circular stamp problem for various magnitudes of the friction coefficient η , the normalized non-homogeneity parameter γh and normalized contact length $(b-a)/h$, $a/R=0$, $b/R=0.02$, $E_x/E_z=3.0$ 85

LIST OF FIGURES

FIGURES

| | |
|---|----|
| Figure 2.1: An orthotropic FGM coating subjected to a contact load by an arbitrarily shaped inelastic stamp. | 9 |
| Figure 2.2: The geometry of the flat stamp problem..... | 36 |
| Figure 2.3: The geometry of the triangular stamp problem. | 39 |
| Figure 2.4: The geometry of the circular stamp problem..... | 42 |
| Figure 3.1: (a) (a) A quadrangular FE located in the Cartesian coordinate frame; (b) A triangular FE located in the Cartesian coordinate frame; (c) Quadrangular and the triangular FE's located in the iso-parametric coordinate frame. | 48 |
| Figure 3.2: Contact Detection Points. | 50 |
| Figure 3.3: FE mesh utilized for the flat stamp problem..... | 51 |
| Figure 4.1: Gradation of orthotropic stiffness constants for $\gamma h > 0.0$ | 86 |
| Figure 4.2: Comparison plots of the normalized stresses evaluated by the analytical and computational procedures for a flat stamp problem, $(b - a)/h = 1.0$, $\eta = 0.3$, $\gamma h = 0.1$. a) Normalized contact stress, b) Normalized lateral contact stress.. ... | 87 |
| Figure 4.3: Comparison plots of the normalized stresses evaluated by the analytical and computational procedures for a flat stamp problem, $(b - a)/h = 1.0$, $\eta = 0.3$, $\gamma h = 0.712$. a) Normalized contact stress, b) Normalized lateral contact stress. | 88 |

| | |
|--|----|
| Figure 4.4: Scaled deformed shape of the contact region, which is produced by using the FE solution of a flat stamp problem, $(b - a)/h = 1.0$, $\eta = 0.3$, $\gamma h = 0.712$. | 89 |
| Figure 4.5: Effect of normalized non-homogeneity parameter γh variations on the normalized contact stress for a flat stamp problem, $(b - a)/h = 1.0$, $\eta = 0.3$ | 90 |
| Figure 4.6: Effect of friction coefficient η variations on the normalized contact stress for a flat stamp problem, $(b - a)/h = 1.0$, $\gamma h = 0.712$. | 90 |
| Figure 4.7: Effect of normalized contact length $(b - a)/h$ variations on the normalized contact stress for a flat stamp problem, $\eta = 0.3$, $\gamma h = 0.712$ | 91 |
| Figure 4.8: Effect of elastic modulus ratio E_x/E_y variations on the normalized contact stress for a flat stamp problem, $(b - a)/h = 1.0$, $\eta = 0.3$, $\gamma h = 0.712$ | 91 |
| Figure 4.9: Effect of elastic modulus ratio E_x/E_z variations on the normalized contact stress for a flat stamp problem, $(b - a)/h = 1.0$, $\eta = 0.3$, $\gamma h = 0.712$ | 92 |
| Figure 4.10: Effect of normalized non-homogeneity parameter γh variations on the normalized lateral contact stress for a flat stamp problem, $(b - a)/h = 1.0$, $\eta = 0.3$. | 93 |
| Figure 4.11: Effect of friction coefficient η variations on the normalized lateral contact stress for a flat stamp problem, $(b - a)/h = 1.0$, $\gamma h = 0.712$ | 93 |
| Figure 4.12: Effect of normalized contact length $(b - a)/h$ variations on the normalized lateral contact stress for a flat stamp problem, $\eta = 0.3$, $\gamma h = 0.712$.. | 94 |
| Figure 4.13: Effect of elastic modulus ratio E_x/E_y variations on the normalized lateral contact stress for a flat stamp problem, $(b - a)/h = 1.0$, $\eta = 0.3$, $\gamma h = 0.712$ | 94 |

| | |
|---|-----|
| Figure 4.14: Effect of elastic modulus ratio E_x/E_z variations on the normalized lateral contact stress for a flat stamp problem, $(b-a)/h=1.0$, $\eta=0.3$, $\gamma h=0.712$ | 95 |
| Figure 4.15: Comparison plots of the normalized stresses evaluated by the analytical and computational procedures for a triangular stamp problem, $(b-a)/h=1.0$, $\eta=0.3$, $\gamma h=0.1$. a) Normalized contact stress, b) Normalized lateral contact stress..... | 96 |
| Figure 4.16: Comparison plots of the normalized stresses evaluated by the analytical and computational procedures for a triangular stamp problem, $(b-a)/h=1.0$, $\eta=0.3$, $\gamma h=0.712$. a) Normalized contact stress, b) Normalized lateral contact stress..... | 97 |
| Figure 4.17: Scaled deformed shape of the contact region, which is produced by using the FE solution of a triangular stamp problem, $\eta=0.3$, $\gamma h=0.712$, $(b-a)/h=1.0$ | 98 |
| Figure 4.18: Effect of normalized non-homogeneity parameter γh variations on the normalized contact stress for a triangular stamp problem, $(b-a)/h=1.0$, $\eta=0.3$ | 99 |
| Figure 4.19: Effect of friction coefficient η variations on the normalized contact stress for a triangular stamp problem, $(b-a)/h=1.0$, $\gamma h=0.712$ | 99 |
| Figure 4.20: Effect of normalized contact length $(b-a)/h$ variations on the normalized contact stress for a triangular stamp problem, $\eta=0.3$, $\gamma h=0.712$ | 100 |
| Figure 4.21: Effect of elastic modulus ratio E_x/E_y variations on the normalized contact stress for a triangular stamp problem, $(b-a)/h=1.0$, $\eta=0.3$, $\gamma h=0.712$ | 100 |

| | |
|---|-----|
| Figure 4.22: Effect of elastic modulus ratio E_x/E_z variations on the normalized contact stress for a triangular stamp problem, $(b-a)/h=1.0, \eta=0.3, \gamma h=0.712$ | 101 |
| Figure 4.23: Effect of normalized non-homogeneity parameter γh variations on the normalized lateral contact stress for a triangular stamp problem, $(b-a)/h=1.0, \eta=0.3$ | 102 |
| Figure 4.24: Effect of friction coefficient η variations on the normalized lateral contact stress for a triangular stamp problem, $(b-a)/h=1.0, \gamma h=0.712$ | 102 |
| Figure 4.25: Effect of normalized contact length $(b-a)/h$ variations on the normalized lateral contact stress for a triangular stamp problem, $\eta=0.3, \gamma h=0.712$ | 103 |
| Figure 4.26: Effect of elastic modulus ratio E_x/E_y variations on the normalized lateral contact stress for a triangular stamp problem, $(b-a)/h=1.0, \eta=0.3, \gamma h=0.712$ | 103 |
| Figure 4.27: Effect of elastic modulus ratio E_x/E_z variations on the normalized lateral contact stress for a triangular stamp problem, $(b-a)/h=1.0, \eta=0.3, \gamma h=0.712$ | 104 |
| Figure 4.28: Scaled deformed shape of the contact region, which is produced by using the FE solution of a circular stamp problem, $\eta=0.3, \gamma h=0.712, (b-a)/h=1.0$ | 105 |
| Figure 4.29: Comparison plots of the normalized stresses evaluated by the analytical and computational procedures for a circular stamp problem, $(b-a)/h=1.0, \eta=0.3, \gamma h=0.1$. a) Normalized contact stress, b) Normalized lateral contact stress..... | 106 |

| | |
|---|-----|
| Figure 4.30: Comparison plots of the normalized stresses evaluated by the analytical and computational procedures for a circular stamp problem, $(b-a)/h=1.0$, $\eta=0.3$, $\gamma h=0.712$. a) Normalized contact stress, b) Normalized lateral contact stress..... | 107 |
| Figure 4.31: Effect of normalized non-homogeneity parameter γh variations on the normalized contact stress for a circular stamp problem, $(b-a)/h=1.0$, $\eta=0.3$ | 108 |
| Figure 4.32: Effect of friction coefficient η variations on the normalized contact stress for a circular stamp problem, $(b-a)/h=1.0$, $\gamma h=0.712$ | 108 |
| Figure 4.33: Effect of normalized contact length $(b-a)/h$ variations on the normalized contact stress for a circular stamp problem, $\eta=0.3$, $\gamma h=0.712$. .. | 109 |
| Figure 4.34: Effect of elastic modulus ratio E_x/E_y variations on the normalized contact stress for a circular stamp problem, $(b-a)/h=1.0$, $\eta=0.3$, $\gamma h=0.712$ | 109 |
| Figure 4.35: Effect of elastic modulus ratio E_x/E_z variations on the normalized lateral contact stress for a circular stamp problem, $(b-a)/h=1.0$, $\eta=0.3$, $\gamma h=0.712$ | 110 |
| Figure 4.36: Effect of normalized non-homogeneity parameter γh variations on the normalized lateral contact stress for a triangular stamp problem, $(b-a)/h=1.0$, $\eta=0.3$ | 111 |
| Figure 4.37: Effect of friction coefficient η variations on the normalized lateral contact stress for a circular stamp problem, $(b-a)/h=1.0$, $\gamma h=0.712$ | 111 |
| Figure 4.38: Effect of normalized contact length $(b-a)/h$ variations on the normalized lateral contact stress for a circular stamp problem, $\eta=0.3$, $\gamma h=0.712$ | 112 |

| | |
|--|-----|
| Figure 4.39: Effect of elastic modulus ratio E_x/E_y variations on the normalized lateral contact stress for a circular stamp problem, $(b-a)/h=1.0$, $\eta=0.3$, $\gamma h=0.712$. | 112 |
| Figure 4.40: Effect of elastic modulus ratio E_x/E_z variations on the normalized lateral contact stress for a circular stamp problem, $(b-a)/h=1.0$, $\eta=0.3$, $\gamma h=0.712$. | 113 |
| Figure 4.41: The complete contact problem of an orthotropic homogeneous coating | 114 |
| Figure 4.42: Comparison plots of the normalized surface stresses evaluated by the analytical and computational procedures for a flat stamp problem of the homogeneous orthotropic Alumina coating, $(b-a)/h=1.0$, $\eta=0.3$, a) Normalized contact stress, b) Normalized lateral contact stress. | 115 |
| Figure 4.43: Comparison plots of the normalized surface stresses evaluated by the analytical and computational procedures for a flat stamp problem of the homogeneous orthotropic Alumina coating, $(b-a)/h=0.4$, $\eta=0.3$, a) Normalized contact stress, b) Normalized lateral contact stress. | 116 |
| Figure 4.44: Comparison plots of the normalized surface stresses evaluated by the analytical and computational procedures for a flat stamp problem of an homogeneous orthotropic coating, $(b-a)/h=1.0$, $\eta=0.3$, $E_1/E_2=1.5$, a) Normalized contact stress, b) Normalized lateral contact stress. | 117 |
| Figure 4.45: Effect of friction coefficient η variations on the normalized surface stresses for a flat stamp problem of the orthotropic homogeneous Alumina coating, $(b-a)/h=1.0$, a) Normalized contact stress, b) Normalized lateral contact stress. | 118 |
| Figure 4.46: Effect of normalized contact length $(b-a)/h$ variations on the normalized surface stresses for a flat stamp problem of the orthotropic homogeneous Alumina coating, $\eta=0.3$, a) Normalized contact stress, b) Normalized lateral contact stress. | 119 |

Figure 4.47: Effect of elastic modulus ratio E_x/E_y variations on the normalized surface stresses for a flat stamp problem of orthotropic homogeneous coatings, $(b-a)/h=1.0$, $\eta=0.3$, a) Normalized contact stress, b) Normalized lateral contact stress..... 120

Figure 4.48: Effect of elastic modulus ratio E_x/E_z variations on the normalized surface stresses for a flat stamp problem of orthotropic homogeneous coatings, $(b-a)/h=1.0$, $\eta=0.3$, a) Normalized contact stress, b) Normalized lateral contact stress..... 121

Figure 4.49: Effect of friction coefficient η variations on the normalized interfacial stresses for a flat stamp problem of the orthotropic homogeneous Alumina coating, $(b-a)/h=1.0$, a) Normalized normal stress, b) Normalized shear stress. 122

Figure 4.50: Effect of normalized contact length $(b-a)/h$ variations on the normalized interfacial stresses for a flat stamp problem of the orthotropic homogeneous Alumina coating, $\eta=0.3$, a) Normalized normal stress, b) Normalized shear stress..... 123

Figure 4.51: Effect of elastic modulus ratio E_x/E_y variations on the normalized interfacial stresses for a flat stamp problem of orthotropic homogeneous coatings, $(b-a)/h=1.0$, $\eta=0.3$, a) Normalized normal stress, b) Normalized shear stress. 124

Figure 4.52: Effect of elastic modulus ratio E_x/E_z variations on the normalized interfacial stresses for a flat stamp problem of orthotropic homogeneous coatings, $(b-a)/h=1.0$, $\eta=0.3$, a) Normalized normal stress, b) Normalized shear stress. 125

CHAPTER 1

INTRODUCTION

This study is performed to investigate frictional contact problems of orthotropic functionally graded material (FGM) coatings which are bonded to isotropic homogeneous substrates without any interfacial defects. The problems of orthotropic graded coatings which are subjected to contact loads by an arbitrarily shaped rigid stamp are examined under plane strain assumption. In this chapter, literature review for the related contact mechanics problems is presented. After all, the purpose of this study is explained.

1.1 Literature Survey

Machine components are generally made of common engineering materials such as Nickel, Aluminum and Steel alloys. Although such materials are low-cost, ductile and easy to reform, they do not possess effective bearing performance when they are exposed to contact tractions. This deficiency results from their weak hardness and low wear resistance. In such problems, the parts which are made of the common engineering materials are coated with ceramic based layers to improve the load bearing capability of the structure. For that reason, the coating materials are desired to have superior hardness and stiffness compared to the base materials. The second main necessity for the layered structures is to have a good bonding strength between two media. Even though the ceramic homogeneous coating surfaces satisfy the surface hardness and wear resistance requirements, they generally have weak bonding strength when used with the common engineering materials. Because a material property mismatch occurs at the interface between two different homogeneous materials, which may lead to the delamination of the structure under contact loads. It is possible to remedy the debonding problems if

the coating is produced of FGMs (Functionally Graded Materials) which also have good surface resistance to mechanical loadings. Because some of the material properties of an FGM coating at the interface can be matched with the material properties of the substrate material, which improves the bonding strength between two media. From a broad perspective, FGMs can be defined as the combination of two different materials by using special processing techniques (i.e. Plasma spray and Electron beam techniques) to be able to optimize the material properties at any spatial location. FGMs have continuously changing material properties due to the change in the volume fractions of constituent phases. The material gradations are defined by continuous functions for the analytical and computational purposes and can be in different characteristics to improve the thermal [1], mechanical [2], electrical [3] or optical [4] performance of FGMs.

Some practical examples can be mentioned for the graded coatings involving contact problems. They can be mainly categorized as the load transfer members and abradable seals. Abradable seals are utilized in gas turbines to provide leak proofing between the shroud and the turbine blades. The seal is defined as a ceramic-based graded layer which is bonded to the metallic shroud. The stiffness of the blade is very large relative to the stiffness of the ceramic coating. Due to this fact, the blade can be modelled as a rigid stamp forced against the surface of the elastic seal with a relative frictional motion. In this application, the purpose of introducing material gradation to the seal is to alleviate the interfacial stresses improving the bonding strength between two media. Similar concept can be considered for internal combustion engines. There exists a relative motion between the piston ring and the coated cylinder potentially yielding a sliding frictional contact in-between. Due to the graded coating on the aluminum cylinder surface, wear control is accomplished. The force transferring members such as gears, bearings, cams and cutting tools can be modelled as contact problems involving two elastic solids. The contacting surfaces of these members can be coated with graded ceramic layers to increase the surface wear resistance, which also improves the bonding strength. The grading in these coatings also plays a vital role to avoid the loss of toughness, as the surface wear resistance is increased.

Although the utilization of FGM coatings reduces the delamination risks, their brittle ceramic surfaces could be prone to cracking problems as long as the surfaces

are subjected to contact tractions. For that reason, some research in the technical literature focused on the surface performance of the FGM coatings. They mainly investigate the optimization of the system parameters to alleviate the surface deficiencies. Experimental investigations reveal the necessity of FGMs in the engineering applications which are under the risk of contact driven failures. Yue and Li [5] and Zhang et al. [6] showed that usage of FGM surfaces enables wear control that results from frictional contact. It can be inferred from the experimental results generated by Kim et al. [7] that the graded specimens possess significant resistance to contact driven failures. Additionally, a graded elastic modulus in thickness direction is proved to avoid cone-shaped cracks that results from surface penetration [8-10] and prevents the initiation of herringbone crackings due to the contact loads with friction [11]. Improving the response of the FGMs to frictional contact, their utilization can be extended to the fields such as high performance cutting tools [12] and prostheses [13].

Theoretical studies on contact mechanics of elastic solids were originated by Hertz [14] in which the contact area is accepted very small with respect to the elastic body. Therefore, a contacting body can be modeled semi-infinitely, which facilitates mathematical modeling. Some guiding solutions for contact problems in a semi-infinite graded medium are given in [15–19]. The contact problems are commonly divided into two types as frictional and frictionless contact problems. There are some studies associated with frictionless contact mechanics problems [20-24]. Upon the application of normal contact tractions to a surface, the tangential forces arise between two bodies. In such problems, Coulomb law of friction is used. Some studies examining sliding frictional contact problems based on finite element method are given in [25–27].

In the recent literature, various procedures, loading conditions and geometries are regarded to investigate the behavior of functionally graded materials involving contact mechanics problems. Contact mechanics analyses of homogeneous substrates which are coated with isotropic FGM layers having positive or negative gradations in the thickness direction are carried out by Guler [28]. Detailed analytical results considering stress distribution via sliding frictional contact under plane strain condition are given in this study. Giannakopoulos and Pallot [29] generated some fully analytical solutions to examine in-plane contact between rigid

rollers and graded half planes. When a contact problem can not be solved in closed form, a singular integral equation (SIE) is enabled to evaluate desired field variables of the system. Guler and Erdogan [30-32] examined the response of FGM coatings which are subjected to contact tractions by rigid indenters of various profiles by using the SIE approach in plane assumptions. Ke and Wang [33-34] presented a solution based on the SIE method in order to observe the behavior of FGM's possessing various material gradations, and loaded by contact tractions with friction. Partial slip condition can be taken into account in contact problems when the contacting bodies are in oscillatory motion. Ke and Wang [35-36] investigated some partial slip contact problems of FGMs. Yang and Ke [37] examined a 2D problem of FGM - substrate system which is exposed to contact tractions by a rigid roller. Choi and Paulino [38] investigated the SIE solution by considering the influences of heat generation resulting from the frictional sliding motion on the surfaces of interlayered FGM-substrate structures. Guler [39] presented a SIE solution technique to examine the behavior of some strips and plates that are fully bonded to FGM media. Dag et al. [40-41] analytically and computationally solved the contact problem of a semi-infinite medium having lateral gradations, which is loaded by inelastic indenters of various surface profiles. Dag [42] outlined an SIE procedure for the complete contact problem of a semi-infinite medium possessing lateral gradations in such a way that, the coefficient of friction varies along the horizontal coordinate axis.

As far as the studies dealing with the response of cracks under contact stresses are concerned, we can mention some articles. Hasebe et al. [43] derived an analytical formulation for a surface crack on an elastic half-plane under complete contact loadings by using rational mapping function and complex stress functions. Choi [44] considered a non-homogeneous medium which includes a homogeneous coating and a base material, which are combined to each other utilizing a bonding strip having material gradations. In the related study, the stress intensity factors of a full-crack lying on the base material are evaluated analytically for which the coating surface is exposed to contact tractions. Dag and Erdogan [45] analytically computed the mixed mode stress intensity factors of an edge crack located on the surface of a semi-infinite medium having gradations in the thickness direction, such that the medium is under the effect of contact tractions with friction.

developed an analytical procedure which is based on the singular integral equation (SIE) approach to compute mixed mode SIFs for a surface crack existing in a graded half-plane loaded by a sliding flat stamp. Choi and Paulino [46] handled an interface crack problem between an FGM layer and a semi-infinite medium for which the system is subjected to contact loadings involving friction. Dag [47] analytically calculated the crack tip parameters of an edge cracking located in a semi-infinite half plane possessing material gradations. The graded medium is exposed to contact stresses by frictional sliding stamps of various surface profiles in this study. The work reported by Dag et al. [48] and Apatay [49] consider an edge crack lying on the free surface of an FGM strip bonded to a semi-infinite medium, that are under complete contact loadings. In the related study, the cracking and contacting phenomena are treated separately. Lajnef and El Borgi [50, 51] examined an edge crack problem located on a graded coating by using a SIE-based analytical procedure. In their studies, an FGM layer which is bonded to a semi-infinite medium is subjected to simple tensional and shear loadings.

In all of the research mentioned above, the materials having spatial gradations are accepted as isotropic. It is also required to mention some of the studies concerning contact mechanics problems of anisotropic materials. Borodich [52] analyzed some dynamic-elastic contact mechanics problems by considering the integral characteristics procedure in the boundary-initial value problems for anisotropic structures. Ciavarella et al. [53] generated a numerical procedure to investigate the response of three dimensional anisotropic materials which are in contact with second-order surface geometries. Lin and Ovaert [54] focused on examining the behavior of a generally anisotropic material under plane assumptions, for which the asperous surface of the medium is subjected to iso-thermal contact loads involving Coulomb friction. Rand and Rovenskii [55] studied some theoretical techniques and methodologies needed to build the fundamentals of the elasticity of anisotropic materials. Ning et al. [56] solved the penetration problem between a rigid globe and a transversely isotropic strip which locates on an inelastic semi-infinite medium. Li and Wang [57] investigated the contact phenomenon on piezoelectric generally anisotropic parts utilizing Fourier-transformation techniques. He and Ovaert [58] examined the response of an anisotropic half plane having asperous free surface to a contacting with an asperous inelastic ball by

handling the Barnett-Lothe tensors based line integral on 3D inclined surfaces. Larijani et al. [59] examined effects of degree of anisotropy on surface crack propagations in rail head coatings subjected to rolling contacts.

Due to the processing techniques used in their production, FGM structures could gain anisotropic behavior. Sampath et al. [60] revealed that coatings having gradations which are manufactured by Plasma-Spray Method mostly possess a microscopic anatomy with cleavage planes which is collimated to the boundary. Additionally, Kaysser and Ilschner [61] found that the coatings having gradations which are manufactured by the Electron-Beam method possess a shaft-like anatomy which causes greater stiffness through the thickness direction and non-stiff surfaces normal to the medium edges. As a conclusion, FGM models should be considered as elastic orthotropic nonhomogeneous medium, if more realistic representations of the layered structures are demanded. There are a few studies performed on the mechanical behavior of orthotropic materials that are under contact loads. Bakirtas [62] focused on the contact phenomenon of an inelastic stamp with no friction in an orthotropic nonhomogeneous semi-infinite medium. Hwu and Fan [63] presented the complete contact phenomenon involving the penetration of a stamp with no friction through an orthotropic half plane by applying a similar solution method of interfacial crackings. Shi et al. [64] analyzed a contacting phenomenon with no friction on orthotropic semi-infinite medium loaded with an inelastic ellipsoid stamp. Swanson [65] evaluated the stresses that result from the contact loadings on orthotropic materials by synthesizing two previously studied solution methods [66-67]. The behavior of a multi-layered piezoelectric orthotropic half-space forced by a frictionless inelastic parabolic indenter was examined by Ramirez [68]. Guler [69] demonstrated the closed-form solutions of plane strain frictional contacting phenomenon of an inelastic stamp sliding on an orthotropic semi-infinite medium by using the SIE based analytical technique.

1.2 Scope of the Research

In the technical literature, there are no computational or analytical studies on contact mechanics of orthotropic FGM coatings. Hence, the purpose of this study

is to perform analytic and computational studies for contact problems of orthotropic functionally graded material (FGM) coatings which are bonded to isotropic homogeneous substrates without any interfacial defects. The orthotropic FGM coatings possess orthotropic stiffness gradations through the coating thickness direction. The variations of each orthotropic stiffness constants are assumed to behave as exponential functions. In the analytical procedure, the problems of orthotropic graded coatings that are subjected to contact loads by an arbitrarily shaped inelastic stamp are examined. In engineering applications, coating thickness is generally very small relative to the other dimensions of a coated member. Hence, in this study, the orthotropic coating thickness should be considered very small relative to the depth of the model. Under this consideration, the aforementioned contact problem is modelled using the plane strain assumption. After deriving the Navier equations of the problem, the Fourier transformation techniques are used to determine the field expressions that satisfy the boundary conditions. A deformation gradient on the contact region is used to obtain a singular integral equation (SIE) which is collocated through a discretization procedure on the roots of Chebyshev polynomials. Computational approach for the same contact problem is based on the finite element method in which the coating-substrate systems are divided into finite elements having the material parameters defined at their centroids. The solution of the present problem by using two different solution techniques enables us to assess the accuracy of both methods by directly comparing their results. Numerical results are obtained regarding flat, triangular and circular stamp surfaces, which reveal the effects of nonhomogeneity, degree of orthotropy, friction coefficient and coating thickness on the contact stresses.

Note that the risks of contact driven damages for orthotropic homogeneous coatings such as interfacial delamination or surface crackings can be alleviated with the properly selected orthotropic material and the other problem parameters. Therefore, in this study, the surface and interfacial stresses of an orthotropic homogeneous coating under the action of complete contact loading is also investigated, which is not examined in the technical literature so far.

CHAPTER 2

PROBLEM STATEMENT AND THE ANALYTICAL METHOD

2.1. Definition of the Problem

The analytical method presented in this study is based on the derivation of a SIE to examine the stress distribution in orthotropic FGM coatings subjected to contact stresses by a sliding inelastic stamp having an arbitrarily shaped surface (Fig 2.1).

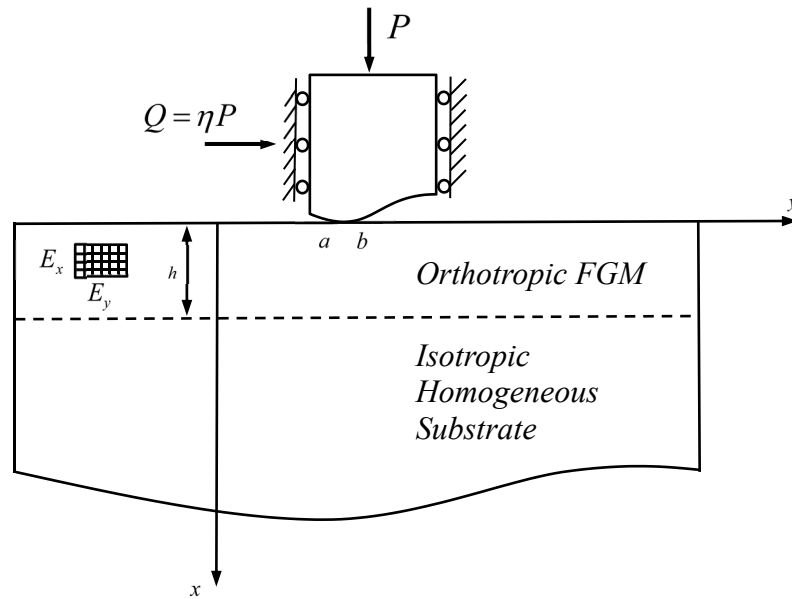


Figure 2.1: An orthotropic FGM coating subjected to a contact load by an arbitrarily shaped inelastic stamp.

It is assumed that the orthotropic FGM coating is bonded to an isotropic homogeneous semi-infinite substrate without any interfacial defects. Coulomb friction is assumed to exist between the stamp and the coating, which yields lateral force on the FGM surface. The composite structure is modeled under plane strain

assumption. The stiffness constants of the orthotropic coating are assumed to behave as exponential functions through the thickness direction. The endpoints of the inelastic stamp which is in contact with the FGM surface are located at the coordinates $y=a$ and $y=b$.

The presented contact problem is handled by using the plane elasticity and formulated with the utilization of Fourier transformation techniques. In the analytical formulation of the problem, contact stresses in the orthotropic FGM coating and the homogeneous semi-infinite substrate are formulated separately. After that the required field quantities of the problem are derived by considering the following continuity and boundary conditions:

$$\sigma_{xx}(0, y) = \sigma(y) \quad a < y < b \quad (2.1a)$$

$$\sigma_{xy}(0, y) = \eta \sigma(y) \quad a < y < b \quad (2.1b)$$

$$u(h^+, y) = u(h^-, y) \quad (2.1c)$$

$$v(h^+, y) = v(h^-, y) \quad (2.1d)$$

$$\sigma_{xx}(h^+, y) = \sigma_{xx}(h^-, y) \quad (2.1e)$$

$$\sigma_{xy}(h^+, y) = \sigma_{xy}(h^-, y) \quad (2.1f)$$

$$\frac{\partial}{\partial y} u(0, y) = f(y) \quad a < y < b \quad (2.1g)$$

$$\int_a^b \sigma_{xx}(0, y) dy = -P \quad (2.1h)$$

where $\sigma(y)$ is the contact traction existing due to the contact of inelastic stamp, and which is the primary unknown of the problem. η is the coulomb friction coefficient. $f(y)$ is a known function indicating the surface profile of the inelastic stamp. The contact stresses and the field quantities are expressed in terms of the surface normal stress $\sigma(y)$. The displacement gradient in (2.1g) is then used

to derive a SIE of the second kind. With the numerical solution of the SIE by utilizing an expansion-collocation procedure, the unknown function of the problem $\sigma(y)$ is obtained.

The inverse Fourier transformations utilized throughout the derivations of field quantities are given as

$$u(x, y) = \frac{1}{2\pi} \int_{-\infty}^{\infty} U(x, \rho) e^{i\rho y} d\rho \quad (2.2a)$$

$$v(x, y) = \frac{1}{2\pi} \int_{-\infty}^{\infty} V(x, \rho) e^{i\rho y} d\rho \quad (2.2b)$$

where $u(x, y)$ and $v(x, y)$ stand for the displacement components in x and y axes, respectively. The Navier equations for the orthotropic FGM coating and the homogeneous semi-infinite medium are formulated using plane elasticity as follows:

For orthotropic FGM ($0 < x < h$):

The constitutive relation for plane orthotropy of FGMs is stated in the following form [42]

$$\begin{Bmatrix} \sigma_{xx}^c \\ \sigma_{yy}^c \\ \sigma_{xy}^c \end{Bmatrix} = \begin{bmatrix} c_{11}(x) & c_{12}(x) & 0 \\ c_{12}(x) & c_{22}(x) & 0 \\ 0 & 0 & c_{66}(x) \end{bmatrix} \begin{Bmatrix} \varepsilon_{xx}^c \\ \varepsilon_{yy}^c \\ 2\varepsilon_{xy}^c \end{Bmatrix} \quad (2.3)$$

where σ_{ij}^c ($i, j = x, y$) and ε_{ij}^c ($i, j = x, y$) are the stress and strain tensors, respectively. The superscripts c donates the FGM coating. $c_{11}(x)$, $c_{22}(x)$, $c_{12}(x)$, and $c_{66}(x)$ are the stiffness coefficients which vary with respect to x axis as [70]

$$c_{11}(x) = c_{110} e^{\gamma x}, \quad c_{22}(x) = c_{220} e^{\gamma x}, \quad c_{12}(x) = c_{120} e^{\gamma x}, \quad c_{66}(x) = c_{660} e^{\gamma x}. \quad (2.4)$$

where γ is the non-homogeneity parameter. c_{110} , c_{220} , c_{120} and c_{660} are the stiffness constants at the coating surface (at $x = 0$) and defined in terms of the engineering parameters as

$$c_{110} = \begin{cases} \frac{E_x^2}{E_x - \nu_{xy}^2 E_y} & \text{for plane stress} \\ \frac{E_x^2 (\nu_{yz}^2 \nu_{zx} E_x - \nu_{xz} E_y)}{\Delta} & \text{for plane strain} \end{cases} \quad (2.5a)$$

$$c_{220} = \begin{cases} \frac{E_x E_y}{E_x - \nu_{xy}^2 E_y} & \text{for plane stress} \\ \frac{\nu_{xz} E_x E_y (\nu_{xz} \nu_{zx} - 1)}{\Delta} & \text{for plane strain} \end{cases} \quad (2.5b)$$

$$c_{120} = \begin{cases} \frac{\nu_{xy} E_x E_y}{E_x - \nu_{xy}^2 E_y} & \text{for plane stress} \\ -\frac{\nu_{xz} E_x E_y (\nu_{yz} \nu_{zx} E_x + \nu_{xy} E_y)}{\Delta} & \text{for plane strain} \end{cases} \quad (2.5c)$$

$$c_{660} = \mu_{xy} \quad (2.5d)$$

where

$$\Delta = \nu_{yz}^2 \nu_{zx} E_x^2 + \nu_{xy}^2 \nu_{xz} E_y^2 + \nu_{xz} E_x E_y (\nu_{xz} \nu_{zx} + 2\nu_{xy} \nu_{yz} \nu_{zx} - 1) \quad (2.5e)$$

The engineering parameters have to satisfy the restrictions given below

$$\frac{\nu_{ij}}{E_i} = \frac{\nu_{ji}}{E_j}, \quad \nu_{ij} < \sqrt{\frac{E_j}{E_i}}. \quad (2.6)$$

The strain-displacement relations in plane are

$$\varepsilon_{xx}^c(x, y) = \frac{\partial u^c}{\partial x}, \quad \varepsilon_{yy}^c(x, y) = \frac{\partial v^c}{\partial y}, \quad \varepsilon_{xy}^c(x, y) = \frac{1}{2} \left(\frac{\partial u^c}{\partial y} + \frac{\partial v^c}{\partial x} \right). \quad (2.7)$$

Considering (2.3), (2.4) and (2.7) together, the stress field for orthotropic FGM coating is obtained as

$$\sigma_{xx}^c(x, y) = e^{\gamma x} \left(c_{110} \frac{\partial u^c}{\partial x} + c_{120} \frac{\partial v^c}{\partial y} \right) \quad (2.8a)$$

$$\sigma_{yy}^c(x, y) = e^{\gamma x} \left(c_{120} \frac{\partial u^c}{\partial x} + c_{220} \frac{\partial v^c}{\partial y} \right) \quad (2.8b)$$

$$\sigma_{xy}^c(x, y) = e^{\gamma x} c_{660} \left(\frac{\partial u^c}{\partial y} + \frac{\partial v^c}{\partial x} \right) \quad (2.8c)$$

The equilibrium equations $\sigma_{ij,j}^c = 0$ ($i, j = x, y$) yield the governing equations for the orthotropic FGM coating as

$$c_{110} \gamma \frac{\partial u^c}{\partial x} + c_{110} \frac{\partial^2 u^c}{\partial x^2} + c_{120} \gamma \frac{\partial v^c}{\partial y} + (c_{120} + c_{660}) \frac{\partial^2 v^c}{\partial x \partial y} + c_{660} \frac{\partial^2 u^c}{\partial y^2} = 0 \quad (2.9a)$$

$$c_{660} \gamma \left(\frac{\partial u^c}{\partial y} + \frac{\partial v^c}{\partial x} \right) + (c_{120} + c_{660}) \frac{\partial^2 u^c}{\partial x \partial y} + c_{660} \frac{\partial^2 v^c}{\partial x^2} + c_{220} \frac{\partial^2 v^c}{\partial y^2} = 0 \quad (2.9b)$$

For homogeneous substrate ($h < x < \infty$):

The stress components for the homogeneous half plane are written by using plane elasticity as

$$\sigma_{xx}^m(x, y) = \frac{\mu}{\kappa - 1} \left\{ (\kappa + 1) \frac{\partial u^m}{\partial x} + (3 - \kappa) \frac{\partial v^m}{\partial y} \right\} \quad (2.10a)$$

$$\sigma_{yy}^m(x, y) = \frac{\mu}{\kappa - 1} \left\{ (3 - \kappa) \frac{\partial u^m}{\partial x} + (\kappa + 1) \frac{\partial v^m}{\partial y} \right\} \quad (2.10b)$$

$$\sigma_{xy}^m(x, y) = \mu \left(\frac{\partial u^m}{\partial y} + \frac{\partial v^m}{\partial x} \right) \quad (2.10c)$$

where κ , μ and ν are the Kolosov constant, shear modulus and Poisson's ratio of the homogeneous substrate, respectively. The superscript m denotes the homogeneous substrate. The Kolosov constant is given for plane stress and plane strain assumptions as

$$\kappa = \begin{cases} \frac{3-\nu}{1+\nu} & \text{for plane stress} \\ 3-4\nu & \text{for plane strain} \end{cases} \quad (2.11)$$

The equilibrium equations $\sigma_{ij,j}^m = 0$ ($i, j = x, y$) yield the governing equations for the homogeneous substrate

$$(\kappa+1)\frac{\partial^2 u^m}{\partial x^2} + 2\frac{\partial^2 v^m}{\partial x \partial y} + (\kappa-1)\frac{\partial^2 u^m}{\partial y^2} = 0 \quad (2.12a)$$

$$(\kappa-1)\frac{\partial^2 v^m}{\partial x^2} + 2\frac{\partial^2 u^m}{\partial x \partial y} + (\kappa+1)\frac{\partial^2 v^m}{\partial y^2} = 0 \quad (2.12b)$$

2.2 Formulation

2.2.1 The orthotropic FGM coating

The inverse Fourier transformations given in (2.2) are used to convert (2.9) into the system of ordinary differential equations (ODE's) as follows,

$$c_{110}\gamma\frac{dU^c}{dx} + c_{110}\frac{d^2U^c}{dx^2} - c_{660}\rho^2U^c + c_{120}\gamma\rho iV^c + (c_{120} + c_{660})i\rho\frac{dV^c}{dx} = 0 \quad (2.13a)$$

$$c_{660}\frac{d^2V^c}{dx^2} + c_{660}\gamma\frac{dV^c}{dx} - c_{220}\rho^2V^c + c_{660}\gamma i\rho U^c + (c_{120} + c_{660})i\rho\frac{dU^c}{dx} = 0 \quad (2.13b)$$

Letting

$$V^c(x) = x_1, \quad U^c(x) = x_2, \quad \frac{dV^c}{dx} = x_3 \quad \text{and} \quad \frac{dU^c}{dx} = x_4. \quad (2.14)$$

The system of ODE's can be written in the form of $\dot{x}_i = Ax_i$ as

$$\begin{Bmatrix} \dot{x}_1 \\ \dot{x}_2 \\ \dot{x}_3 \\ \dot{x}_4 \end{Bmatrix} = \begin{bmatrix} 0 & 0 & 1 & 0 \\ 0 & 0 & 0 & 1 \\ \frac{c_{220}}{c_{660}}\rho^2 & -\gamma\rho i & -\gamma & -\frac{(c_{120}+c_{660})\rho i}{c_{660}} \\ -\frac{c_{120}}{c_{110}}\gamma\rho i & \frac{c_{660}}{c_{110}}\rho^2 & -\frac{(c_{120}+c_{660})}{c_{110}}\rho i & -\gamma \end{bmatrix} \begin{Bmatrix} x_1 \\ x_2 \\ x_3 \\ x_4 \end{Bmatrix} \quad (2.15)$$

The characteristic equation of the differential equation system is defined as

$|A - rI| = 0$ and its open form becomes

$$r^4 + 2\gamma r^3 + (\gamma^2 + C_1\rho^2)r^2 + \rho^2\gamma C_1 r + \frac{\rho^2}{c_{110}}(\gamma^2 c_{120} + \rho^2 c_{220}) = 0 \quad (2.16)$$

Rearranging (2.16)

$$\left(r^2 + \gamma r + \frac{\rho^2 C_1}{2}\right)^2 + \rho^2 \gamma^2 \frac{c_{120}}{c_{110}} + \rho^4 \left(\frac{c_{220}}{c_{110}} - \frac{C_1^2}{4}\right) = 0 \quad (2.17a)$$

where

$$C_1 = \frac{c_{120}^2 + 2c_{120}c_{660} - c_{110}c_{220}}{c_{110}c_{660}} \quad (2.17b)$$

Consider the solutions of differential equations are in the following exponential forms

$$U^c(x, \rho) = M_1 e^{r_1 x} + M_2 e^{r_2 x} + M_3 e^{r_3 x} + M_4 e^{r_4 x} \quad (2.18a)$$

$$V^c(x, \rho) = N_1 M_1 e^{r_1 x} + N_2 M_2 e^{r_2 x} + N_3 M_3 e^{r_3 x} + N_4 M_4 e^{r_4 x} \quad (2.18b)$$

Substituting (2.18) into (2.13a), N_j yields

$$N_j = i \frac{c_{110} r_j (r_j + \gamma) - c_{660} \rho^2}{\rho \{c_{120} (r_j + \gamma) + c_{660} r_j\}}, \quad j = 1, \dots, 4 \quad (2.19)$$

Solving (2.17a), the roots r_j ($j = 1, \dots, 4$) are obtained as

$$r_1 = -\frac{\gamma}{2} + \frac{1}{2}\sqrt{\gamma^2 - 2\rho^2 C_1 + 4\sqrt{\delta_1}} \quad \Re(r_1) > 0 \quad (2.20a)$$

$$r_2 = -\frac{\gamma}{2} + \frac{1}{2}\sqrt{\gamma^2 - 2\rho^2 C_1 - 4\sqrt{\delta_1}} \quad \Re(r_2) > 0 \quad (2.20b)$$

$$r_3 = -\frac{\gamma}{2} - \frac{1}{2}\sqrt{\gamma^2 - 2\rho^2 C_1 + 4\sqrt{\delta_1}} \quad \Re(r_3) < 0 \quad (2.20c)$$

$$r_4 = -\frac{\gamma}{2} - \frac{1}{2}\sqrt{\gamma^2 - 2\rho^2 C_1 - 4\sqrt{\delta_1}} \quad \Re(r_4) < 0 \quad (2.20d)$$

where

$$\delta_1 = \rho^4 \left(\frac{C_1^2}{4} - \frac{c_{220}}{c_{110}} \right) - \rho^2 \gamma^2 \frac{c_{120}}{c_{110}} \quad (2.20e)$$

Substituting (2.18) into (2.2), the planar displacement constituents are obtained as

$$u^c(x, y) = \frac{1}{2\pi} \int \sum_{j=1}^4 M_j e^{r_j x + i\rho y} d\rho \quad (2.21a)$$

$$v^c(x, y) = \frac{1}{2\pi} \int \sum_{j=1}^4 M_j N_j e^{r_j x + i\rho y} d\rho \quad (2.21b)$$

Therefore, the field quantities of the orthotropic FGM coating are restated in the following form

$$\sigma_{xx}^c(x, y) = \frac{1}{2\pi} \int \sum_{j=1}^4 M_j (c_{110} r_j + c_{120} N_j i\rho) e^{(r_j + \gamma)x + i\rho y} d\rho \quad (2.22a)$$

$$\sigma_{yy}^c(x, y) = \frac{1}{2\pi} \int \sum_{j=1}^4 M_j (c_{120} r_j + c_{220} N_j i\rho) e^{(r_j + \gamma)x + i\rho y} d\rho \quad (2.22b)$$

$$\sigma_{xy}^c(x, y) = \frac{c_{660}}{2\pi} \int \sum_{j=1}^4 M_j (N_j r_j + i\rho) e^{(r_j + \gamma)x + i\rho y} d\rho \quad (2.22c)$$

$$\frac{\partial}{\partial y} u^c(x, y) = \frac{1}{2\pi} \int \sum_{j=1}^4 i\rho M_j e^{r_j x + i\rho y} d\rho \quad (2.22d)$$

2.2.2 The homogeneous substrate

The inverse Fourier transformations given in (2.2) are used to convert (2.12) into ODE's as follows

$$(\kappa+1)\frac{d^2U^m}{dx^2} + 2\rho i \frac{dV^m}{dx} - (\kappa-1)\rho^2 U^m = 0 \quad (2.23a)$$

$$(\kappa-1)\frac{d^2V^m}{dx^2} + 2\rho i \frac{dU^m}{dx} - (\kappa+1)\rho^2 V^m = 0 \quad (2.23b)$$

The differentials of $U^m(x, \rho)$ and $V^m(x, \rho)$ with respect to x axis in (2.23) are separated by using basic calculus as

$$\frac{d^4U^m}{dx^4} - 2\rho^2 \frac{d^2U^m}{dx^2} + \rho^4 U^m = 0 \quad (2.24a)$$

$$\frac{d^4V^m}{dx^4} - 2\rho^2 \frac{d^2V^m}{dx^2} + \rho^4 V^m = 0 \quad (2.24b)$$

The two differential equations above have similar structure, so do their solutions. The characteristic equation of (2.24) are then defined as

$$r^4 - 2\rho^2 r^2 + \rho^4 = 0 \quad (2.25)$$

(2.25) have two double roots as $r_{1,2} = |\rho|$ and $r_{3,4} = -|\rho|$. Hence the solutions of (2.24) are expressed as

$$U^m(x, \rho) = [A_1(\rho) + xA_2(\rho)]e^{|\rho|x} + [A_3(\rho) + xA_4(\rho)]e^{-|\rho|x} \quad (2.26a)$$

$$V^m(x, \rho) = [B_1(\rho) + xB_2(\rho)]e^{|\rho|x} + [B_3(\rho) + xB_4(\rho)]e^{-|\rho|x} \quad (2.26b)$$

The relations between $A_j(\rho)$ and $B_j(\rho)$ are defined substituting (2.26) into (2.23) as

$$B_1(\rho) = i \frac{|\rho| A_1(\rho) + \kappa A_2(\rho)}{\rho} \quad (2.27a)$$

$$B_2(\rho) = i \frac{|\rho|}{\rho} A_2(\rho) \quad (2.27b)$$

$$B_3(\rho) = -i \frac{|\rho| A_3(\rho) - \kappa A_4(\rho)}{\rho} \quad (2.27c)$$

$$B_4(\rho) = -i \frac{|\rho|}{\rho} A_4(\rho) \quad (2.27d)$$

The stresses $\sigma_{yy}^m(x, y)$ and $\sigma_{xy}^m(x, y)$ should be bounded as $(x^2 + y^2)$ tends to infinity. Thus, $A_1(\rho) = A_2(\rho) = B_1(\rho) = B_2(\rho) = 0$ should be satisfied and then (2.26a-b) reduce to

$$U^m(x, \rho) = [A_3(\rho) + x A_4(\rho)] e^{-|\rho|x} \quad (2.28a)$$

$$V^m(x, \rho) = [B_3(\rho) + x B_4(\rho)] e^{-|\rho|x} \quad (2.28b)$$

Substituting (2.28) into (2.2), the planar displacement components are obtained as

$$u^m(x, y) = \frac{1}{2\pi} \int_{-\infty}^{\infty} [A_3(\rho) + x A_4(\rho)] e^{i\rho y - |\rho|x} d\rho \quad (2.29a)$$

$$v^m(x, y) = \frac{1}{2\pi} \int_{-\infty}^{\infty} [B_3(\rho) + x B_4(\rho)] e^{i\rho y - |\rho|x} d\rho \quad (2.29b)$$

Therefore, the stress components of the homogeneous substrate in (2.10) are restated as:

$$\sigma_{xx}^m(x, y) = \frac{\mu}{2\pi(\kappa-1)} \int_{-\infty}^{\infty} \left\{ \begin{aligned} &(\kappa+1)[(1-|\rho|x)A_4 - |\rho|A_3] \\ &+ (3-\kappa)i\rho[B_3 + xB_4] \end{aligned} \right\} e^{i\rho y - |\rho|x} d\rho \quad (2.30a)$$

$$\sigma_{yy}^m(x, y) = \frac{\mu}{2\pi(\kappa-1)} \int_{-\infty}^{\infty} \left\{ \begin{aligned} &(3-\kappa)[(1-|\rho|x)A_4 - |\rho|A_3] \\ &+ (\kappa+1)i\rho[B_3 + xB_4] \end{aligned} \right\} e^{i\rho y - |\rho|x} d\rho \quad (2.30b)$$

$$\sigma_{xy}^m(x, y) = \frac{\mu}{2\pi} \int_{-\infty}^{\infty} \left\{ (1 - |\rho| x) B_4 - |\rho| B_3 + i\rho (A_3 + x A_4) \right\} e^{i\rho y - |\rho| x} d\rho \quad (2.30c)$$

2.2.3 Determination of unknown constants

The unknown constants in (2.22) and (2.30) are obtained handling the continuity conditions between the graded coating and the homogeneous half plane, as shown below. Hence the constants are defined in terms of the unknown of the problem $\sigma(y)$.

$$u^c(h, y) = u^m(h, y) \quad (2.31a)$$

$$v^c(h, y) = v^m(h, y) \quad (2.31b)$$

$$\sigma_{xx}^c(h, y) = \sigma_{xx}^m(h, y) \quad (2.31c)$$

$$\sigma_{xy}^c(h, y) = \sigma_{xy}^m(h, y) \quad (2.31d)$$

(2.31a) and (2.31b) are recast considering (2.2) as

$$\frac{1}{2\pi} \lim_{x \rightarrow h} \int_{-\infty}^{\infty} U^c(x, \rho) e^{i\rho y} d\rho = \frac{1}{2\pi} \lim_{x \rightarrow h} \int_{-\infty}^{\infty} U^m(x, \rho) e^{i\rho y} d\rho \quad (2.32a)$$

$$\frac{1}{2\pi} \lim_{x \rightarrow h} \int_{-\infty}^{\infty} V^c(x, \rho) e^{i\rho y} d\rho = \frac{1}{2\pi} \lim_{x \rightarrow h} \int_{-\infty}^{\infty} V^m(x, \rho) e^{i\rho y} d\rho \quad (2.32b)$$

Substituting (2.18) and (2.28) into (2.2):

$$M_1 e^{r_1 h} + M_2 e^{r_2 h} + M_3 e^{r_3 h} + M_4 e^{r_4 h} = (A_3 + h A_4) e^{-|\rho| h} \quad (2.33a)$$

$$N_1 M_1 e^{r_1 h} + N_2 M_2 e^{r_2 h} + N_3 M_3 e^{r_3 h} + N_4 M_4 e^{r_4 h} = (B_3 + h B_4) e^{-|\rho| h} \quad (2.33b)$$

Considering (2.27c-d), (2.33) is rewritten as

$$M_1 e^{r_1 h} + M_2 e^{r_2 h} + M_3 e^{r_3 h} + M_4 e^{r_4 h} = (A_3 + h A_4) e^{-|\rho| h} \quad (2.34a)$$

$$N_1 M_1 e^{r_1 h} + N_2 M_2 e^{r_2 h} + N_3 M_3 e^{r_3 h} + N_4 M_4 e^{r_4 h} = \frac{i e^{-|\rho| h}}{\rho} [(\kappa - h|\rho|) A_4 - |\rho| A_3] \quad (2.34b)$$

$A_3(\rho)$ and $A_4(\rho)$ can be defined in terms of M_j using (2.34) as

$$A_3(\rho) = \sum_{j=1}^4 e^{h(r_j + |\rho|)} M_j \left[1 - \frac{h(|\rho| - i\rho N_j)}{\kappa} \right] \quad (2.35a)$$

$$A_4(\rho) = \sum_{j=1}^4 \frac{M_j}{\kappa} e^{h(r_j + |\rho|)} (|\rho| - i\rho N_j) \quad (2.35b)$$

The continuity relations in (2.31c-d) are used to define the relations between M_j ($j=1, \dots, 4$) components. Considering (2.2) the stress components in (2.8) and (2.10) are expressed as

For orthotropic FGM ($0 < x < h$):

$$\sigma_{xx}^c(x, y) = \frac{e^{\gamma x}}{2\pi} \int_{-\infty}^{\infty} \left(c_{110} \frac{dU^c}{dx} + c_{120} i\rho V^c \right) e^{i\rho y} d\rho \quad (2.36a)$$

$$\sigma_{yy}^c(x, y) = \frac{e^{\gamma x}}{2\pi} \int_{-\infty}^{\infty} \left(c_{120} \frac{dU^c}{dx} + c_{220} i\rho V^c \right) e^{i\rho y} d\rho \quad (2.36b)$$

$$\sigma_{xy}^c(x, y) = \frac{e^{\gamma x}}{2\pi} \int_{-\infty}^{\infty} c_{660} \left(\frac{dV^c}{dx} + i\rho U^c \right) e^{i\rho y} d\rho \quad (2.36c)$$

For homogeneous substrate ($h < x < \infty$):

$$\sigma_{xx}^m(x, y) = \frac{\mu}{2\pi(\kappa - 1)} \int_{-\infty}^{\infty} \left((\kappa + 1) \frac{dU^m}{dx} + (3 - \kappa) i\rho V^m \right) e^{i\rho y} d\rho \quad (2.37a)$$

$$\sigma_{yy}^m(x, y) = \frac{\mu}{2\pi(\kappa - 1)} \int_{-\infty}^{\infty} \left((3 - \kappa) \frac{dU^m}{dx} + (\kappa + 1) i\rho V^m \right) e^{i\rho y} d\rho \quad (2.37b)$$

$$\sigma_{xy}^m(x, y) = \frac{\mu}{2\pi} \int_{-\infty}^{\infty} \left(\frac{dV^m}{dx} + i\rho U^m \right) e^{i\rho y} d\rho \quad (2.37c)$$

Hence the normal and shear stress components at the interface ($x = h$) rewritten as

$$\sigma_{xx}^c(h, y) = \frac{e^{\gamma h}}{2\pi} \lim_{x \rightarrow h} \left[\int_{-\infty}^{\infty} \left(c_{110} \frac{dU^c}{dx} + c_{120} i\rho V^c \right) e^{i\rho y} d\rho \right] \quad (2.38a)$$

$$\sigma_{xy}^c(h, y) = \frac{e^{\gamma h}}{2\pi} \lim_{x \rightarrow h} \left[\int_{-\infty}^{\infty} c_{660} \left(\frac{dV^c}{dx} + i\rho U^c \right) e^{i\rho y} d\rho \right] \quad (2.38b)$$

$$\sigma_{xx}^m(h, y) = \frac{\mu}{2\pi(\kappa-1)} \lim_{x \rightarrow h} \left[\int_{-\infty}^{\infty} \left((\kappa+1) \frac{dU^m}{dx} + (3-\kappa) i\rho V^m \right) e^{i\rho y} d\rho \right] \quad (2.38c)$$

$$\sigma_{xy}^m(h, y) = \frac{\mu}{2\pi} \lim_{x \rightarrow h} \left[\int_{-\infty}^{\infty} \left(\frac{dV^m}{dx} + i\rho U^m \right) e^{i\rho y} d\rho \right] \quad (2.38d)$$

Taking (2.18) and (2.28) into account, (2.38) are substituted into the continuity equations in (2.31c-d). This operation yields the following expressions

$$M_1 = p_1 M_2 + p_2 M_4 \quad (2.39a)$$

$$M_3 = p_3 M_2 + p_4 M_4 \quad (2.39b)$$

where

$$p_1 = \frac{k_2 l_3 - k_3 l_2}{k_3 l_1 - k_1 l_3}, \quad p_2 = \frac{k_4 l_3 - k_3 l_4}{k_3 l_1 - k_1 l_3}, \quad p_3 = \frac{k_1 l_2 - k_2 l_1}{k_3 l_1 - k_1 l_3}, \quad p_4 = \frac{k_1 l_4 - k_4 l_1}{k_3 l_1 - k_1 l_3}. \quad (2.40)$$

$$k_j = e^{hr_j} \left\{ i\rho N_j \left[e^{h\gamma} c_{120} + \mu \left(\frac{\kappa-1}{\kappa} \right) \right] + e^{h\gamma} c_{110} r_j + \mu |\rho| \left(\frac{\kappa+1}{\kappa} \right) \right\} \quad (2.41a)$$

$$l_j = e^{hr_j} \left\{ N_j \left[c_{660} r_j e^{h\gamma} + \mu |\rho| \left(\frac{\kappa+1}{\kappa} \right) \right] + i\rho \left[c_{660} e^{h\gamma} + \mu \left(\frac{\kappa+1}{\kappa} \right) - 2\mu \right] \right\} \quad (2.41b)$$

The traction boundary conditions on the contact surface are used to obtain M_2 and M_4 as follows: Applying Fourier transformation on (2.36a) and (2.36c), following expressions are obtained

$$c_{110} \frac{dU^c}{dx} + c_{120} i\rho V^c = e^{-\gamma x} \int_{-\infty}^{\infty} \sigma_{xx}^c(x, s) e^{-i\rho s} ds \quad (2.42a)$$

$$\frac{dV^c}{dx} + i\rho U^c = \frac{e^{-\gamma x}}{c_{660}} \int_{-\infty}^{\infty} \sigma_{xy}^c(x, s) e^{-i\rho s} ds \quad (2.42b)$$

The surface stresses are expressed in terms of the unknown of the problem $\sigma(y)$ as

$$\sigma_{xx}(0, y) = \sigma(y) \quad a < y < b \quad (2.43a)$$

$$\sigma_{xy}(0, y) = \eta \sigma(y) \quad a < y < b \quad (2.43b)$$

After taking the Fourier transforms, (2.43) is written rearranging the integral boundaries as

$$\int_{-\infty}^{\infty} \sigma_{xx}(0, s) e^{-i\rho s} ds = \int_a^b \sigma(s) e^{-i\rho s} ds = P(\rho) \quad (2.44a)$$

$$\int_{-\infty}^{\infty} \sigma_{xy}(0, s) e^{-i\rho s} ds = \eta \int_a^b \sigma(s) e^{-i\rho s} ds = \eta P(\rho) \quad (2.44b)$$

(2.44) are substituted into (2.42), then following equations are obtained

$$c_{110} \frac{dU^c}{dx}(x, \rho) + c_{120} i\rho V^c(x, \rho) = e^{-\gamma x} P(\rho) \quad (2.45a)$$

$$\frac{dV^c}{dx}(x, \rho) + i\rho U^c(x, \rho) = \frac{e^{-\gamma x}}{c_{660}} \eta P(\rho) \quad (2.45b)$$

where

$$U^c(0, \rho) = M_1 + M_2 + M_3 + M_4 \quad (2.46a)$$

$$\frac{dU^c}{dx}(0, \rho) = M_1 r_1 + M_2 r_2 + M_3 r_3 + M_4 r_4 \quad (2.46b)$$

$$V^c(0, \rho) = M_1 N_1 + M_2 N_2 + M_3 N_3 + M_4 N_4 \quad (2.46c)$$

$$\frac{dV^c}{dx}(0, \rho) = M_1 N_1 r_1 + M_2 N_2 r_2 + M_3 N_3 r_3 + M_4 N_4 r_4 \quad (2.46d)$$

Substituting (2.46) into (2.45), following expressions are obtained

$$\varphi_1 M_1 + \varphi_2 M_2 + \varphi_3 M_3 + \varphi_4 M_4 = e^{-\gamma x} P(\rho) \quad (2.47a)$$

$$\theta_1 M_1 + \theta_2 M_2 + \theta_3 M_3 + \theta_4 M_4 = \eta e^{-\gamma x} P(\rho) \quad (2.47b)$$

where

$$\varphi_j = c_{110} r_j + c_{120} i \rho N_j \quad (2.48a)$$

$$\theta_j = c_{660} (N_j r_j + i \rho) \quad (2.48b)$$

Substituting (2.39) into (2.47), the equations of M_2 and M_4 are written as

$$t_1 M_2 + t_2 M_4 = e^{-\gamma x} P(\rho) \quad (2.49a)$$

$$t_3 M_2 + t_4 M_4 = \eta e^{-\gamma x} P(\rho) \quad (2.49b)$$

where

$$t_1 = \varphi_1 p_1 + \varphi_2 + \varphi_3 p_3 \quad (2.50a)$$

$$t_2 = \varphi_1 p_2 + \varphi_4 + \varphi_3 p_4 \quad (2.50b)$$

$$t_3 = \theta_1 p_1 + \theta_2 + \theta_3 p_3 \quad (2.50c)$$

$$t_4 = \theta_1 p_2 + \theta_4 + \theta_3 p_4 \quad (2.50d)$$

Then M_2 and M_4 are obtained from (2.49) as

$$M_2 = P(\rho) e^{-\gamma x} \frac{\eta t_2 - t_4}{t_2 t_3 - t_1 t_4} \quad (2.51a)$$

$$M_4 = P(\rho) e^{-\gamma x} \frac{t_3 - \eta t_1}{t_2 t_3 - t_1 t_4} \quad (2.51b)$$

Therefore, all the terms are defined in terms of the unknown function $\sigma(s)$.

2.2.4 Derivation of the Singular Integral Equation

In this section, a singular integral equation is constructed using the stress and displacement expressions obtained in the previous sections. Then the kernels of the stress distributions on the coating surface are determined. The boundary conditions (2.1g) and (2.1h) are used in the construction and solution of singular integral equations. Hence the term (2.22d) is rewritten considering (2.51) and (2.44a) as

$$\frac{\partial}{\partial y} u^c(x, y) = \frac{1}{2\pi} \int_{-\infty}^{\infty} \int_{-\infty}^{\infty} \sigma(s) e^{-i\rho s} ds \Gamma_{33}(\rho, x) e^{i\rho y} d\rho \quad (2.52a)$$

where

$$\Gamma_{33}(\rho, x) = i\rho e^{-\gamma x} \left[\frac{(\eta t_2 - t_4)(p_1 e^{r_1 x} + e^{r_2 x} + p_3 e^{r_3 x}) + (t_3 - \eta t_1)(p_2 e^{r_1 x} + p_4 e^{r_3 x} + e^{r_4 x})}{t_2 t_3 - t_1 t_4} \right] \quad (2.52b)$$

Changing the sequences of the integrals and rearranging the integral boundaries, (2.52a) is restated as

$$\frac{\partial}{\partial y} u^c(x, y) = \int_a^b k_{33}(x, y, s) \sigma(s) ds \quad (2.53a)$$

where

$$k_{33}(x, y, s) = \frac{1}{2\pi} \int_{-\infty}^{\infty} \Gamma_{33}(\rho, x) e^{-i\rho(s-y)} d\rho \quad (2.53b)$$

Rewriting (2.53b) in trigonometric form

$$k_{33}(x, y, s) = \frac{1}{2\pi} \int_{-\infty}^{\infty} \Gamma_{33}(\rho, x) [\cos((y-s)\rho) + i \sin((y-s)\rho)] d\rho \quad (2.54)$$

Changing the integral boundaries from 0 to ∞ , (2.54) is written as

$$k_{33}(x, y, s) = \frac{1}{2\pi} \int_0^{\infty} [K_{331} \cos((y-s)\rho) + K_{332} \sin((y-s)\rho)] d\rho \quad (2.55)$$

where

$$K_{331}(\rho, x) = \Gamma_{33}(\rho, x) + \Gamma_{33}(-\rho, x) \quad (2.56a)$$

$$K_{332}(\rho, x) = i [\Gamma_{33}(\rho, x) - \Gamma_{33}(-\rho, x)] \quad (2.56b)$$

The asymptotic expansions of the roots in (2.20) are obtained using Maple as

$$r_1^{\infty} = 0.5 C_{r1} \rho - 0.5 \gamma \quad (2.57a)$$

$$r_2^{\infty} = 0.5 C_{r2} \rho - 0.5 \gamma \quad (2.57b)$$

$$r_3^{\infty} = -0.5 C_{r1} \rho - 0.5 \gamma \quad (2.57c)$$

$$r_4^{\infty} = -0.5 C_{r2} \rho - 0.5 \gamma \quad (2.57d)$$

where

$$C_{r1} = \sqrt{2 \sqrt{C_1^2 - 4 \frac{C_{220}}{C_{110}}} - 2C_1} \quad (2.57e)$$

$$C_{r2} = \sqrt{-2 \sqrt{C_1^2 - 4 \frac{C_{220}}{C_{110}}} - 2C_1} \quad (2.57f)$$

Note that the error between r_i and r_i^{∞} ($i=1, \dots, 4$) are less than 0.06 % for $\rho > 10$.

The square rooted terms C_{r1} and C_{r2} are realized to be real and greater than

zero for most of the orthotropic materials either in plane stress or in plane strain assumptions. This information is used during the extraction of dominant terms as $\rho \rightarrow \infty$. The engineering constants of materials used in this study are given in Table 2.1. Alumina is used as the coating surface material and Nickel is used as a substrate material in most of the parametric analyses.

Table 2.1: Engineering parameters utilized in the parametric analyses.

| <i>Property</i> | <i>Alumina (Al_2O_3)</i> | <i>Nickel</i> |
|-----------------|---------------------------------------|---------------|
| E_x | 116.36 GPa | 204 GPa |
| E_y | 90.43 GPa | 204 GPa |
| E_z | 90.43 GPa | 204 GPa |
| μ_{xy} | 38.21 GPa | 77.86 GPa |
| ν_{xy} | 0.28 | 0.31 |
| ν_{xz} | 0.27 | 0.31 |
| ν_{zx} | 0.21 | 0.31 |
| ν_{zy} | 0.14 | 0.31 |
| ν_{yz} | 0.14 | 0.31 |

Therefore, the asymptotic expansions of (2.56) are calculated as $\rho \rightarrow \infty$ using Maple and some algebra as in the following form

$$K_{331}^{\infty}(\rho, x) = \left[f_{10} + \frac{f_{11}}{\rho} + \frac{f_{12}}{\rho^2} + \frac{f_{13}}{\rho^3} + \frac{f_{14}}{\rho^4} + O\left(\frac{1}{\rho^5}\right) + \dots \right] e^{-0.5x(C_{r2}\rho + 3\gamma)} \\ + \left[s_{10} + \frac{s_{11}}{\rho} + \frac{s_{12}}{\rho^2} + \frac{s_{13}}{\rho^3} + \frac{s_{14}}{\rho^4} + O\left(\frac{1}{\rho^5}\right) + \dots \right] e^{-0.5x(C_{r1}\rho + 3\gamma)} \quad (2.58a)$$

$$K_{332}^{\infty}(\rho, x) = \left[f_{20} + \frac{f_{21}}{\rho} + \frac{f_{22}}{\rho^2} + \frac{f_{23}}{\rho^3} + \frac{f_{24}}{\rho^4} + O\left(\frac{1}{\rho^5}\right) + \dots \right] e^{-0.5x(C_{r2}\rho + 3\gamma)} \\ + \left[s_{20} + \frac{s_{21}}{\rho} + \frac{s_{22}}{\rho^2} + \frac{s_{23}}{\rho^3} + \frac{s_{24}}{\rho^4} + O\left(\frac{1}{\rho^5}\right) + \dots \right] e^{-0.5x(C_{r1}\rho + 3\gamma)} \quad (2.58b)$$

where the first terms f_{ij} and s_{ij} are given in Appendix A.

f_{10} , s_{10} , f_{20} , s_{20} terms are added and subtracted from K_{331} and K_{332} in order to omit the singular behavior of the integrals. Then taking limit as $x \rightarrow 0$, $k_{33}(x, y, s)$ in (2.55) has the following form:

$$\begin{aligned}
k_{33}(0, y, s) = & \lim_{x \rightarrow 0} \frac{1}{2\pi} \int_0^\infty \left[\left(K_{331}(\rho, x) - f_{10} e^{-0.5x(C_{r2}\rho + 3\gamma)} \right. \right. \\
& \left. \left. - s_{10} e^{-0.5x(C_{r1}\rho + 3\gamma)} \right) \cos((y-s)\rho) \right] d\rho \\
& + \lim_{x \rightarrow 0} \frac{1}{2\pi} \int_0^\infty \left[\left(K_{332}(\rho, x) - f_{20} e^{-0.5x(C_{r2}\rho + 3\gamma)} \right. \right. \\
& \left. \left. - s_{20} e^{-0.5x(C_{r1}\rho + 3\gamma)} \right) \sin((y-s)\rho) \right] d\rho \\
& + \lim_{x \rightarrow 0} \frac{e^{-1.5\gamma x}}{2\pi} \int_0^\infty f_{10} e^{-0.5C_{r2}\rho x} \cos((y-s)\rho) d\rho \\
& + \lim_{x \rightarrow 0} \frac{e^{-1.5\gamma x}}{2\pi} \int_0^\infty f_{20} e^{-0.5C_{r2}\rho x} \sin((y-s)\rho) d\rho \\
& + \lim_{x \rightarrow 0} \frac{e^{-1.5\gamma x}}{2\pi} \int_0^\infty s_{10} e^{-0.5C_{r1}\rho x} \cos((y-s)\rho) d\rho \\
& + \lim_{x \rightarrow 0} \frac{e^{-1.5\gamma x}}{2\pi} \int_0^\infty s_{20} e^{-0.5C_{r1}\rho x} \sin((y-s)\rho) d\rho
\end{aligned} \tag{2.59}$$

The 3rd to 6th integrals in (2.59) are calculated considering dirac delta distribution as

$$\lim_{x \rightarrow 0} \frac{e^{-1.5\gamma x}}{2\pi} \int_0^\infty f_{10} e^{-0.5C_{r2}\rho x} \cos((y-s)\rho) d\rho = \frac{f_{10}}{2} \delta(s-y) \tag{2.60a}$$

$$\lim_{x \rightarrow 0} \frac{e^{-1.5\gamma x}}{2\pi} \int_0^\infty s_{10} e^{-0.5C_{r1}\rho x} \cos((y-s)\rho) d\rho = \frac{s_{10}}{2} \delta(s-y) \tag{2.60b}$$

$$\lim_{x \rightarrow 0} \frac{e^{-1.5\gamma x}}{2\pi} \int_0^\infty f_{20} e^{-0.5C_{r2}\rho x} \sin((y-s)\rho) d\rho = -\frac{f_{20}}{2\pi} \frac{1}{s-y} \tag{2.60c}$$

$$\lim_{x \rightarrow 0} \frac{e^{-1.5\gamma x}}{2\pi} \int_0^\infty s_{20} e^{-0.5C_{r1}\rho x} \sin((y-s)\rho) d\rho = -\frac{s_{20}}{2\pi} \frac{1}{s-y} \tag{2.60d}$$

Then (2.59) is rewritten as

$$\begin{aligned}
k_{33}(0, y, s) = & \lim_{x \rightarrow 0} \frac{1}{2\pi} \int_0^\infty \left[\left(\begin{array}{c} K_{331}(\rho, x) - f_{10} e^{-0.5x(C_{r2}\rho + 3\gamma)} \\ - s_{10} e^{-0.5x(C_{r1}\rho + 3\gamma)} \end{array} \right) \cos((y-s)\rho) \right] d\rho \\
& + \lim_{x \rightarrow 0} \frac{1}{2\pi} \int_0^\infty \left[\left(\begin{array}{c} K_{332}(\rho, x) - f_{20} e^{-0.5x(C_{r2}\rho + 3\gamma)} \\ - s_{20} e^{-0.5x(C_{r1}\rho + 3\gamma)} \end{array} \right) \sin((y-s)\rho) \right] d\rho \quad (2.61) \\
& + \left(\frac{f_{10} + s_{10}}{2} \right) \delta(s-y) - \left(\frac{f_{20} + s_{20}}{2\pi} \right) \frac{1}{s-y}
\end{aligned}$$

In (2.61), dividing the integral boundaries of the first integral into two as $0 - A_1$ and $A_1 - \infty$ and also the second integral into two as $0 - A_2$ and $A_2 - \infty$, then (2.61) can be rearranged as

$$\begin{aligned}
k_{33}(0, y, s) = & \frac{1}{2\pi} \int_0^{A_1} [(K_{331}(\rho, x) - f_{10} - s_{10}) \cos((y-s)\rho)] d\rho \\
& + \frac{1}{2\pi} \int_{A_1}^\infty [(K_{331}(\rho, x) - f_{10} - s_{10}) \cos((y-s)\rho)] d\rho \\
& + \frac{1}{2\pi} \int_0^{A_2} [(K_{332}(\rho, x) - f_{20} - s_{20}) \sin((y-s)\rho)] d\rho \quad (2.62) \\
& + \frac{1}{2\pi} \int_{A_2}^\infty [(K_{332}(\rho, x) - f_{20} - s_{20}) \sin((y-s)\rho)] d\rho \\
& + \left(\frac{f_{10} + s_{10}}{2} \right) \delta(s-y) - \left(\frac{f_{20} + s_{20}}{2\pi} \right) \frac{1}{s-y}
\end{aligned}$$

where A_1 and A_2 are the integration cut-off points. $(f_{11} + s_{11})/\rho$ and $(f_{21} + s_{21})/\rho$ terms cause logarithmic singularities in the integrals. Hence $(f_{11} + s_{11})/\rho$ term is added and subtracted from the integral which have the boundary $A_1 - \infty$, and the term $(f_{21} + s_{21})/\rho$ can be added and subtracted from the integral having integral boundaries $0 - \infty$. Because the integral having sine term is definite at $\rho = 0$. Therefore (2.62) is rearranged as

$$\begin{aligned}
k_{33}(0, y, s) = & \frac{1}{2\pi} \left\{ \int_0^{A_1} (K_{331}(\rho, 0) - (f_{10} + s_{10})) \cos((y-s)\rho) d\rho \right. \\
& + \int_{A_1}^{\infty} (K_{331}(\rho, 0) - K_{331}^{\infty}(\rho, 0)) \cos((y-s)\rho) d\rho \\
& + \int_{A_1}^{\infty} \left(K_{331}^{\infty}(\rho, 0) - (f_{10} + s_{10}) - \frac{f_{11} + s_{11}}{\rho} \right) \cos((y-s)\rho) d\rho \\
& + \int_{A_1}^{\infty} \frac{f_{11} + s_{11}}{\rho} \cos((y-s)\rho) d\rho + \int_0^{\infty} \frac{f_{21} + s_{21}}{\rho} \sin((y-s)\rho) d\rho \\
& + \int_0^{A_2} \left(K_{332}(\rho, 0) - (f_{20} + s_{20}) - \frac{f_{21} + s_{21}}{\rho} \right) \sin((y-s)\rho) d\rho \\
& + \int_{A_2}^{\infty} (K_{332}(\rho, 0) - K_{332}^{\infty}(\rho, 0)) \sin((y-s)\rho) d\rho \\
& + \int_{A_2}^{\infty} \left(K_{332}^{\infty}(\rho, 0) - (f_{20} + s_{20}) - \frac{f_{21} + s_{21}}{\rho} \right) \sin((y-s)\rho) d\rho \Big\} \\
& + \left(\frac{f_{10} + s_{10}}{2} \right) \delta(s-y) - \left(\frac{f_{20} + s_{20}}{2\pi} \right) \frac{1}{s-y}
\end{aligned} \tag{2.63}$$

4th integral in (2.63) is rearranged in the following form

$$\int_{A_1}^{\infty} \frac{f_{11} + s_{11}}{\rho} \cos((y-s)\rho) d\rho = -(f_{11} + s_{11}) Ci(|A_1(s-y)|) \tag{2.64}$$

where Ci is the cosine integral and formulated as

$$Ci(|A_1(s-y)|) = \gamma_e + \ln|A_1(s-y)| + \int_0^{|A_1(s-y)|} \frac{\cos(\alpha) - 1}{\alpha} d\alpha \tag{2.65}$$

and γ_e is the Euler-Mascheroni constant ($\gamma_e = 0.57721566$).

The 5th integral in (2.63) is calculated as

$$\begin{aligned}
\int_0^{\infty} \frac{f_{21} + s_{21}}{\rho} \sin((y-s)\rho) d\rho &= -(f_{21} + s_{21}) \int_0^{\infty} \frac{\sin((s-y)\rho)}{\rho(s-y)} d(\rho(s-y)) \\
&= -(f_{21} + s_{21}) Si((s-y)\infty) = -(f_{21} + s_{21}) \frac{\pi}{2} \text{sign}(s-y)
\end{aligned} \tag{2.66}$$

where Si is the sine integral.

If the magnitudes of A_1 and A_2 are selected large enough, the 2nd and 7th integrals in (2.63) can be neglected. Then (2.63) is rewritten as

$$\begin{aligned}
k_{33}(0, y, s) = & \frac{1}{2\pi} \left\{ \int_0^{A_1} (K_{331}(\rho, 0) - (f_{10} + s_{10})) \cos((y-s)\rho) d\rho \right. \\
& + \int_{A_1}^{\infty} \left(K_{331}^{\infty}(\rho, 0) - (f_{10} + s_{10}) - \frac{f_{11} + s_{11}}{\rho} \right) \cos((y-s)\rho) d\rho \\
& - (f_{11} + s_{11}) Ci(|A_1(s-y)|) - \frac{\pi}{2} (f_{21} + s_{21}) \text{sign}(s-y) \\
& + \int_0^{A_2} \left(K_{332}(\rho, 0) - (f_{20} + s_{20}) - \frac{f_{21} + s_{21}}{\rho} \right) \sin((y-s)\rho) d\rho \\
& + \int_{A_2}^{\infty} \left(K_{332}^{\infty}(\rho, 0) - (f_{20} + s_{20}) - \frac{f_{21} + s_{21}}{\rho} \right) \sin((y-s)\rho) d\rho \Big\} \\
& + \left(\frac{f_{10} + s_{10}}{2} \right) \delta(s-y) - \left(\frac{f_{20} + s_{20}}{2\pi} \right) \frac{1}{s-y}
\end{aligned} \tag{2.67}$$

Using (2.53a) and (2.67), we conclude a second kind singular integral equation as

$$\frac{\partial u}{\partial y}(y) = \left(\frac{f_{10} + s_{10}}{2} \right) \sigma(y) - \frac{f_{20} + s_{20}}{2\pi} \int_a^b \frac{\sigma(s)}{s-y} ds + \frac{1}{2\pi} \int_a^b K(s, y) \sigma(s) ds \tag{2.68}$$

and the kernel $K(s, y)$ is given as

$$\begin{aligned}
K(y, s) = & \int_0^{A_1} (K_{331}(\rho, 0) - (f_{10} + s_{10})) \cos((y-s)\rho) d\rho \\
& + \int_{A_1}^{\infty} \left(K_{331}^{\infty}(\rho, 0) - (f_{10} + s_{10}) - \frac{f_{11} + s_{11}}{\rho} \right) \cos((y-s)\rho) d\rho \\
& - (f_{11} + s_{11}) Ci(|A_1(s-y)|) - \frac{\pi}{2} (f_{21} + s_{21}) \text{sign}(s-y) \\
& + \int_0^{A_2} \left(K_{332}(\rho, 0) - (f_{20} + s_{20}) - \frac{f_{21} + s_{21}}{\rho} \right) \sin((y-s)\rho) d\rho \\
& + \int_{A_2}^{\infty} \left(K_{332}^{\infty}(\rho, 0) - (f_{20} + s_{20}) - \frac{f_{21} + s_{21}}{\rho} \right) \sin((y-s)\rho) d\rho
\end{aligned} \tag{2.69}$$

The gradient of the displacement component $v(x, y)$ with respect to y axis in (2.21b) is written as

$$\frac{\partial v}{\partial y}(x, y) = \frac{1}{2\pi} \int_{-\infty}^{\infty} i\rho \sum_{j=1}^4 M_j N_j e^{r_j x + i\rho y} d\rho = \frac{1}{2\pi} \int_{-\infty}^{\infty} \int_{-\infty}^{\infty} \sigma(s) e^{-i\rho s} ds \Gamma_{13}(\rho, x) e^{i\rho y} d\rho \quad (2.70a)$$

where

$$\Gamma_{13}(\rho, x) = e^{-\gamma x} i \rho \frac{\left[(\eta_2 - t_4)(p_1 N_1 e^{r_1 x} + N_2 e^{r_2 x} + p_3 N_3 e^{r_3 x}) + (t_3 - \eta_1)(p_2 N_1 e^{r_1 x} + p_4 N_3 e^{r_3 x} + N_4 e^{r_4 x}) \right]}{t_2 t_3 - t_1 t_4} \quad (2.70b)$$

Changing the sequences of the integrals and rearranging the integral boundaries, (2.70a) is restated as

$$\frac{\partial v}{\partial y}(x, y) = \int_a^b k_{13}(x, y, s) \sigma(s) ds \quad (2.71a)$$

where

$$k_{13}(x, y, s) = \frac{1}{2\pi} \int_{-\infty}^{\infty} \Gamma_{13}(\rho, x) e^{-i\rho(s-y)} d\rho \quad (2.71b)$$

Rewriting (2.71b) in trigonometric form

$$k_{13}(x, y, s) = \frac{1}{2\pi} \int_{-\infty}^{\infty} \Gamma_{13}(\rho, x) [\cos((y-s)\rho) + i \sin((y-s)\rho)] d\rho \quad (2.72)$$

Changing the integral boundaries from 0 to ∞ , (2.72) is written as

$$k_{13}(x, y, s) = \frac{1}{2\pi} \int_0^{\infty} [K_{131} \cos((y-s)\rho) + K_{132} \sin((y-s)\rho)] d\rho \quad (2.73)$$

where

$$K_{131}(\rho, x) = \Gamma_{13}(\rho, x) + \Gamma_{13}(-\rho, x) \quad (2.74a)$$

$$K_{132}(\rho, x) = i [\Gamma_{13}(\rho, x) - \Gamma_{13}(-\rho, x)] \quad (2.74b)$$

The asymptotic expansions of (2.74a) and (2.74b) are calculated as $\rho \rightarrow \infty$ as

$$K_{131}^{\infty}(\rho, x) = \left[d_{10} + \frac{d_{11}}{\rho} + \frac{d_{12}}{\rho^2} + \frac{d_{13}}{\rho^3} + \frac{d_{14}}{\rho^4} + O\left(\frac{1}{\rho^5}\right) + \dots \right] e^{-0.5x(C_{r2}\rho + 3\gamma)} \\ + \left[h_{10} + \frac{h_{11}}{\rho} + \frac{h_{12}}{\rho^2} + \frac{h_{13}}{\rho^3} + \frac{h_{14}}{\rho^4} + O\left(\frac{1}{\rho^5}\right) + \dots \right] e^{-0.5x(C_{r1}\rho + 3\gamma)} \quad (2.75a)$$

$$K_{132}^{\infty}(\rho, x) = \left[d_{20} + \frac{d_{21}}{\rho} + \frac{d_{22}}{\rho^2} + \frac{d_{23}}{\rho^3} + \frac{d_{24}}{\rho^4} + O\left(\frac{1}{\rho^5}\right) + \dots \right] e^{-0.5x(C_{r2}\rho + 3\gamma)} \\ + \left[h_{20} + \frac{h_{21}}{\rho} + \frac{h_{22}}{\rho^2} + \frac{h_{23}}{\rho^3} + \frac{h_{24}}{\rho^4} + O\left(\frac{1}{\rho^5}\right) + \dots \right] e^{-0.5x(C_{r1}\rho + 3\gamma)} \quad (2.75b)$$

where the terms d_{ij} and h_{ij} are given in the Appendix A.

The kernel $k_{13}(0, y, s)$ is obtained using similar operations in the previous section.

Hence the displacement derivative is derived as

$$\frac{\partial v}{\partial y}(y) = \left(\frac{d_{10} + h_{10}}{2} \right) \sigma(y) - \frac{d_{20} + h_{20}}{2\pi} \int_a^b \frac{\sigma(s)}{s - y} ds + \frac{1}{2\pi} \int_a^b K_2(s, y) \sigma(s) ds \quad (2.76)$$

And $K_2(s, y)$ is given as

$$K_2(y, s) = \int_0^{A_1} (K_{131}(\rho, 0) - (d_{10} + h_{10})) \cos((y - s)\rho) d\rho \\ + \int_{A_1}^{\infty} \left(K_{131}^{\infty}(\rho, 0) - (d_{10} + h_{10}) - \frac{d_{11} + h_{11}}{\rho} \right) \cos((y - s)\rho) d\rho \\ - (d_{11} + h_{11}) Ci(|A_1(s - y)|) - \frac{\pi}{2} (d_{21} + h_{21}) \text{sign}(s - y) \quad (2.77) \\ + \int_0^{A_2} \left(K_{132}(\rho, 0) - (d_{20} + h_{20}) - \frac{d_{21} + h_{21}}{\rho} \right) \sin((y - s)\rho) d\rho \\ + \int_{A_2}^{\infty} \left(K_{132}^{\infty}(\rho, 0) - (d_{20} + h_{20}) - \frac{d_{21} + h_{21}}{\rho} \right) \sin((y - s)\rho) d\rho$$

2.2.5 The in plane lateral surface stress $\sigma_{yy}(0, y)$

Once the contact normal stress $\sigma(y)$ is obtained, the in plane stress $\sigma_{yy}(0, y)$ can be derived. The strains for an orthotropic medium in y and z directions are written as

$$\varepsilon_{xx} = \frac{\sigma_{xx}}{E_x} - \frac{\nu_{yx}}{E_y} \sigma_{yy} - \frac{\nu_{zx}}{E_z} \sigma_{zz} \quad (2.78)$$

$$\varepsilon_{zz} = -\frac{\nu_{xz}}{E_x} \sigma_{xx} - \frac{\nu_{yz}}{E_y} \sigma_{yy} + \frac{\sigma_{zz}}{E_z} \quad (2.79)$$

For plane strain assumption ($\varepsilon_{zz}=0$), σ_{zz} reduces to

$$\sigma_{zz} = E_z \left(\frac{\nu_{xz}}{E_x} \sigma_{xx} + \frac{\nu_{yz}}{E_y} \sigma_{yy} \right) \quad (2.80)$$

Substituting σ_{zz} in (2.78) and taking the limit as $x \rightarrow 0$, we obtain

$$\varepsilon_{xx}(0, y) = \frac{\partial u}{\partial x}(0, y) = c_{330} \sigma_{xx}(0, y) - c_{440} \sigma_{yy}(0, y) \quad (2.81)$$

where

$$c_{330} = \frac{1 - \nu_{xz} \nu_{zx}}{E_x} \quad (2.82a)$$

$$c_{440} = \frac{\nu_{yx} + \nu_{zx} \nu_{yz}}{E_y} \quad (2.82b)$$

Note that the in plane stress $\sigma_{yy}(0, y)$ is formulated by using (2.76), (2.81) and (2.82b) as

$$\sigma_{yy}(0, y) = \frac{1}{1 + c_{220} c_{440}} \left[\left(\frac{c_{220}(d_{10} + h_{10})}{2} + c_{120} c_{330} \right) \sigma(y) - \frac{c_{220}(d_{20} + h_{20})}{2\pi} \int_a^b \frac{\sigma(s)}{s - y} ds + \frac{c_{220}}{2\pi} \int_a^b K_2(s, y) \sigma(s) ds \right] \quad (2.83)$$

2.2.6 On the solutions of the Singular Integral Equation

In this section, the unknown function $\sigma(y)$ is obtained with the numerical solution of the SIE for various stamp profiles. In order to handle numerical solution of the SIE in (2.68) for various stamp profiles, we first introduce the relations below

$$y = \frac{b-a}{2}r + \frac{b+a}{2} \quad -1 < r < 1 \quad (2.84a)$$

$$s = \frac{b-a}{2}t + \frac{b+a}{2} \quad -1 < t < 1 \quad (2.84b)$$

$$\bar{\rho} = \frac{b-a}{2}\rho, \quad \bar{\gamma} = \frac{b-a}{2}\gamma, \quad \bar{h} = \frac{2}{b-a}h. \quad (2.84c-e)$$

$$\bar{A}_1 = \frac{b-a}{2}A_1, \quad \bar{A}_2 = \frac{b-a}{2}A_2. \quad (2.84f,g)$$

$$\sigma(y) = \sigma\left(\frac{b-a}{2}r + \frac{b+a}{2}\right) = \tilde{\sigma}(r) \quad (2.84h)$$

Considering the normalizations in (2.84), the kernel $K(y,s)$ in (2.69) is expressed as:

$$K(y,s) = \frac{2}{b-a} \bar{K}(r,t) \quad (2.85)$$

$$\begin{aligned}
\bar{K}(r,t) = & \int_0^{\bar{A}_1} \left(\bar{K}_{331}(\bar{\rho}) - (f_{10} + s_{10}) \right) \cos((r-t) \bar{\rho}) d\bar{\rho} \\
& + \int_{\bar{A}_1}^{\infty} \left(\frac{\bar{f}_{12} + \bar{s}_{12}}{\bar{\rho}^2} + \frac{\bar{f}_{13} + \bar{s}_{13}}{\bar{\rho}^3} + \frac{\bar{f}_{14} + \bar{s}_{14}}{\bar{\rho}^4} + \dots \right) \cos((r-t) \bar{\rho}) d\bar{\rho} \\
& + \int_0^{\bar{A}_2} \left(\bar{K}_{332}(\bar{\rho}) - (f_{20} + s_{20}) - \frac{\bar{f}_{21} + \bar{s}_{21}}{\bar{\rho}} \right) \sin((r-t) \bar{\rho}) d\bar{\rho} \\
& + \int_{\bar{A}_2}^{\infty} \left(\frac{\bar{f}_{22} + \bar{s}_{22}}{\bar{\rho}^2} + \frac{\bar{f}_{23} + \bar{s}_{23}}{\bar{\rho}^3} + \frac{\bar{f}_{24} + \bar{s}_{24}}{\bar{\rho}^4} + \dots \right) \sin((r-t) \bar{\rho}) d\bar{\rho} \\
& - (\bar{f}_{11} + \bar{s}_{11}) Ci\left(\left| \bar{A}_1(r-t) \right|\right) - (\bar{f}_{21} + \bar{s}_{21}) \frac{\pi}{2} \text{sign}(t-r)
\end{aligned} \tag{2.86a}$$

$$K_{331}(\rho) = K_{331}\left(\frac{2}{b-a} \bar{\rho}\right) = \bar{K}_{331}(\bar{\rho}) \tag{2.86b}$$

$$K_{332}(\rho) = K_{332}\left(\frac{2}{b-a} \bar{\rho}\right) = \bar{K}_{332}(\bar{\rho}) \tag{2.86c}$$

$$\bar{f}_{ij} = \frac{b-a}{2} f_{ij}, \quad \bar{s}_{ij} = \frac{b-a}{2} s_{ij}. \quad (i=1,2), \quad (j=1,\dots,4) \tag{2.86d,e}$$

Hence the solution of singular integral equation in (2.68) is obtained for flat, triangular and circular stamp profiles in the following sections.

2.2.6.1 Flat stamp

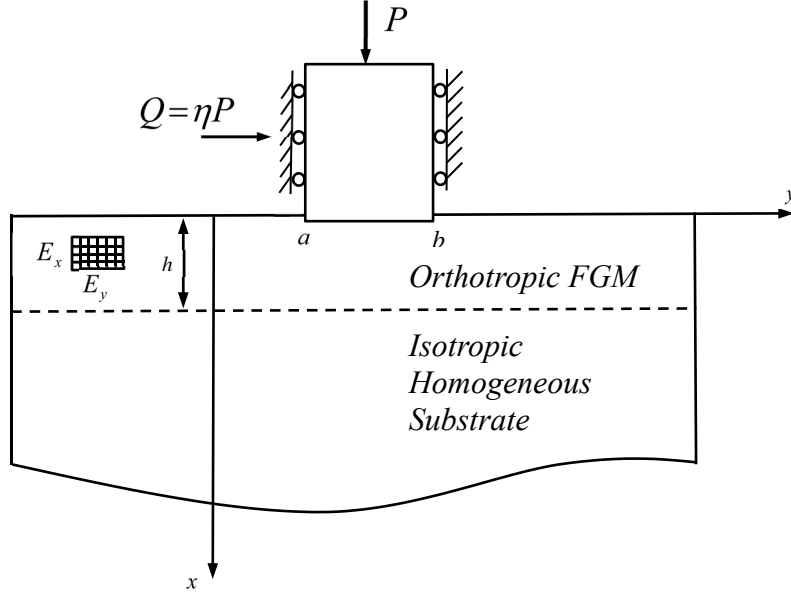


Figure 2.2: The geometry of the flat stamp problem.

The flat stamp contact problem of an orthotropic FGM coating which is bonded to a homogeneous semi-infinite medium is shown in Fig.2.2. The FGM surface is subjected to contact force P by a flat stamp. In this case, consider that the contact length $(b-a)$ is independent of the normal contact force P (i.e. complete contact) and the stamp profile is expressed by

$$\frac{\partial}{\partial y} u^c(0, y) = 0 \quad a < y < b \quad (2.87)$$

The Kernel in (2.85) is substituted into the (2.68) considering the normalizations in (2.84). Hence the integral equation (2.68) and the equilibrium equation (2.1h) become

$$\frac{f_{10} + s_{10}}{f_{20} + s_{20}} \bar{\sigma}(r) - \frac{1}{\pi} \int_{-1}^1 \frac{\bar{\sigma}(t)}{t-r} dt + \frac{1}{(f_{20} + s_{20})\pi} \int_{-1}^1 \bar{K}(t, r) \bar{\sigma}(t) dt = 0 \quad -1 < r < 1 \quad (2.88)$$

$$\int_{-1}^1 \bar{\sigma}(r) dr = -2 \quad (2.89)$$

where

$$\bar{\sigma}(r) = \frac{\tilde{\sigma}(r)}{P/(b-a)} \quad (2.90)$$

According to the theoretic analysis [71, 72], the unknown function $\bar{\sigma}(r)$ can be expanded into the series of Jacobi polynomials as in the following form

$$\bar{\sigma}(r) = \omega(r) \sum_{n=0}^{\infty} A_n P_n^{\alpha, \beta}(r), \quad \omega(r) = (1-r)^{\alpha} (1+r)^{\beta}. \quad (2.91a,b)$$

where $P_n^{\alpha, \beta}(r)$ are the Jacobi polynomials of order n and A_n 's are the unknown coefficients. α and β are the strengths of singularities at $y=b$ and $y=a$ respectively (see Appendix C). These exponents are selected such that $-1 < \alpha < 0$, $-1 < \beta < 0$ and $\alpha + \beta = 1$ [28] depending on the value of A/B as

$$\alpha = \frac{\phi}{\pi} - 1, \quad \beta = -\frac{\phi}{\pi}, \quad \text{for } \frac{A}{B} \geq 0 \quad (2.92a,b)$$

$$\alpha = -\frac{\phi}{\pi}, \quad \beta = \frac{\phi}{\pi} - 1, \quad \text{for } \frac{A}{B} < 0 \quad (2.92c,d)$$

where

$$A = f_{10} + s_{10}, \quad B = f_{20} + s_{20}. \quad (2.93a,b)$$

$$\phi = \arctan \left| \frac{B}{A} \right|, \quad 0 < \phi \leq \frac{\pi}{2} \quad (2.93c)$$

Substituting (2.91) into (2.89) and using orthogonality relations [73], A_0 is obtained as

$$A_0 = -\frac{2}{\theta_0}, \quad \theta_0 = \frac{2^{\alpha+\beta+1} \Gamma(\alpha+1) \Gamma(\beta+1)}{\Gamma(\alpha+\beta+2)}. \quad (2.94a,b)$$

where Γ is the Gamma function. The relation needed to regularize singular parts of Cauchy principal value integrals are formulated by Tricomi [74] in closed form and by Guler [28] in recurrence formulation form. These formulations are given in

Appendix B. Hence the singular integral equation in (2.88) is rewritten truncating the infinite series at N as

$$\sum_{n=0}^N A_n F_n(r) = 0 \quad -1 < r < 1 \quad (2.95a)$$

where

$$F_n(r) = \frac{A}{B} (1-r)^\alpha (1+r)^\beta P_n^{\alpha,\beta}(r) - \frac{L_n(r)}{\pi} + \frac{1}{\pi B} \int_{-1}^1 \bar{K}(t, r) (1-t)^\alpha (1+t)^\beta P_n^{\alpha,\beta}(t) dt \quad (2.95b)$$

The unknown constants A_n ($n=1,2,3,\dots,N$) are determined with the numerical solution of the singular integral equation (2.95) by using a collocation technique outlined by Erdogan [71]. In the flat stamp case, $(N+1)$ linear equations are constructed by applying a collocation method on (2.95) at N points and by using (2.94). The obtained $(N+1)$ equations are handled together to calculate A_n ($n=0,\dots,N$). The roots of Chebyshev polynomials of first kind are used as the collocation points and given as

$$r_i = \cos\left(\frac{\pi(2i-1)}{2N}\right) \quad i=1,2,\dots,N \quad (2.96)$$

Hence the contact stress is calculated using the truncated form of (2.91) at N points as

$$\frac{\sigma\left(\frac{b-a}{2}r + \frac{b+a}{2}\right)}{P/(b-a)} = (1-r)^\alpha (1+r)^\beta \sum_{n=0}^N A_n P_n^{\alpha,\beta}(r) \quad -1 < r < 1 \quad (2.97)$$

2.2.6.2 Triangular stamp

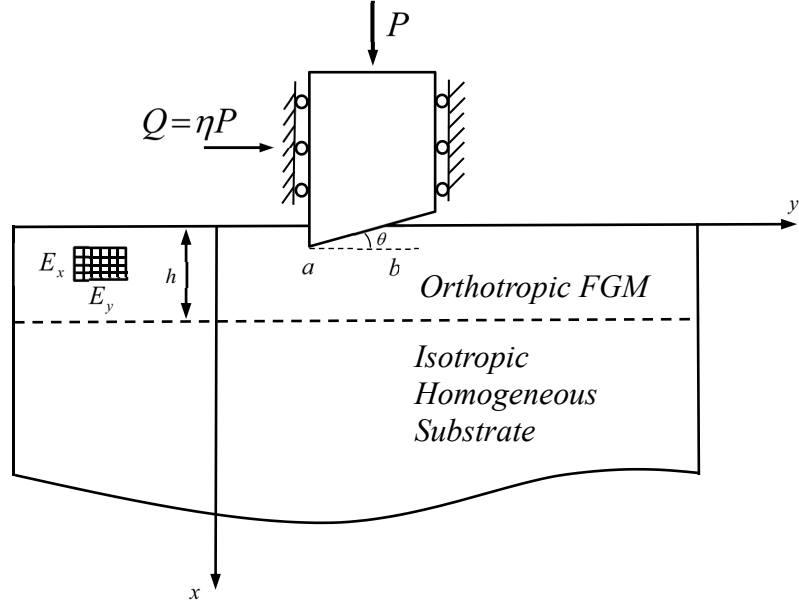


Figure 2.3: The geometry of the triangular stamp problem.

The triangular stamp contact problem of an orthotropic FGM coating which is bonded to a homogeneous semi-infinite medium is shown in Fig.2.3. The FGM surface is subjected to contact force P by a triangular stamp. In this case, consider that contact length $(b-a)$ is strongly dependent on the normal contact force P and the stamp profile is given by

$$\frac{\partial}{\partial y} u^c(0, y) = -\tan(\theta) \quad a < y < b \quad (2.98)$$

where θ is the stamp inclination angle. Considering (2.98) and the normalizations in (2.84), the integral equation (2.68) and the equilibrium equation (2.1h) become

$$\begin{aligned} \frac{f_{10} + s_{10}}{f_{20} + s_{20}} \bar{\sigma}(r) - \frac{1}{\pi} \int_{-1}^1 \frac{\bar{\sigma}(t)}{t-r} dt + \frac{1}{(f_{20} + s_{20})\pi} \int_{-1}^1 \bar{K}(t, r) \bar{\sigma}(t) dt \\ = -\frac{2}{(f_{20} + s_{20})\mu_{xy}} \quad -1 < r < 1 \end{aligned} \quad (2.99)$$

$$\int_{-1}^1 \bar{\sigma}(r) dr = -\frac{2P}{\mu_{xy} \tan(\theta)(b-a)} \quad (2.100)$$

where

$$\bar{\sigma}(r) = \frac{\tilde{\sigma}(r)}{\mu_{xy} \tan(\theta)} \quad (2.101)$$

According to the theoretic analysis [71, 72], the unknown function $\bar{\sigma}(r)$ can be expanded into the series of Jacobi polynomials as in the following form

$$\bar{\sigma}(r) = \omega(r) \sum_{n=0}^{\infty} A_n P_n^{\alpha, \beta}(r), \quad \omega(r) = (1-r)^{\alpha} (1+r)^{\beta}. \quad (2.102a,b)$$

where $P_n^{\alpha, \beta}(r)$ are the Jacobi polynomials of order n and A_n 's are the unknown coefficients. α and β are the strengths of singularities at $y=b$ and $y=a$ respectively (see Appendix C). These exponents are selected such that $0 < \alpha < 1$, $-1 < \beta < 0$ and $\alpha + \beta = 0$ [28, 73] depending on the value of A/B as

$$\alpha = \frac{\phi}{\pi}, \quad \beta = -\frac{\phi}{\pi}, \quad \text{for} \quad \frac{A}{B} \geq 0 \quad (2.103a,b)$$

$$\alpha = 1 - \frac{\phi}{\pi}, \quad \beta = \frac{\phi}{\pi} - 1, \quad \text{for} \quad \frac{A}{B} < 0 \quad (2.103c,d)$$

where A , B and ϕ are given in (2.93a-c).

Substituting (2.102) into (2.100) and using orthogonality relations [48], the normalized contact force $P/(b-a)$ is obtained as

$$\frac{P}{b-a} = -\frac{A_0 \theta_0 \mu_{xy} \tan(\theta)}{2} \quad (2.104)$$

where θ_0 is given in (2.94b).

Considering the relations in Appendix B, the singular integral equation in (2.99) is rewritten truncating the infinite series at N as

$$\sum_{n=0}^N A_n F_{2n}(r) = -\frac{2}{B\mu_{xy}} \quad -1 < r < 1 \quad (2.105a)$$

where

$$F_{2n}(r) = \left[\begin{aligned} &\frac{A}{B}(1-r)^\alpha(1+r)^\beta P_n^{\alpha,\beta}(r) - \frac{L_n(r)}{\pi} \\ &+ \frac{1}{\pi B} \int_{-1}^1 \bar{K}(t,r)(1-t)^\alpha(1+t)^\beta P_n^{\alpha,\beta}(t) dt \end{aligned} \right] \quad (2.105b)$$

The unknown constants A_n ($n=1,2,3,\dots,N$) are determined with the numerical solution of the SIE (2.105) by using a collocation technique outlined by Erdogan [71]. In the case of the triangular stamp, $(N+1)$ linear equations are constructed by applying a collocation method on (2.105) at $(N+1)$ points. These $(N+1)$ equations are handled together to calculate A_n ($n=0,\dots,N$). The roots of Chebyshev polynomials of first kind are utilized as the points of collocation and given as

$$r_i = \cos\left(\frac{\pi(2i-1)}{2(N+1)}\right) \quad i=1,2,\dots,N+1 \quad (2.106)$$

Hence the contact stress is calculated using the truncated form of (2.91) at N points as

$$\frac{\sigma\left(\frac{b-a}{2}r + \frac{b+a}{2}\right)}{P/(b-a)} = -\frac{2}{A_0\theta_0}(1-r)^\alpha(1+r)^\beta \sum_{n=0}^N A_n P_n^{\alpha,\beta}(r) \quad -1 < r < 1 \quad (2.107)$$

2.2.6.3 Circular stamp

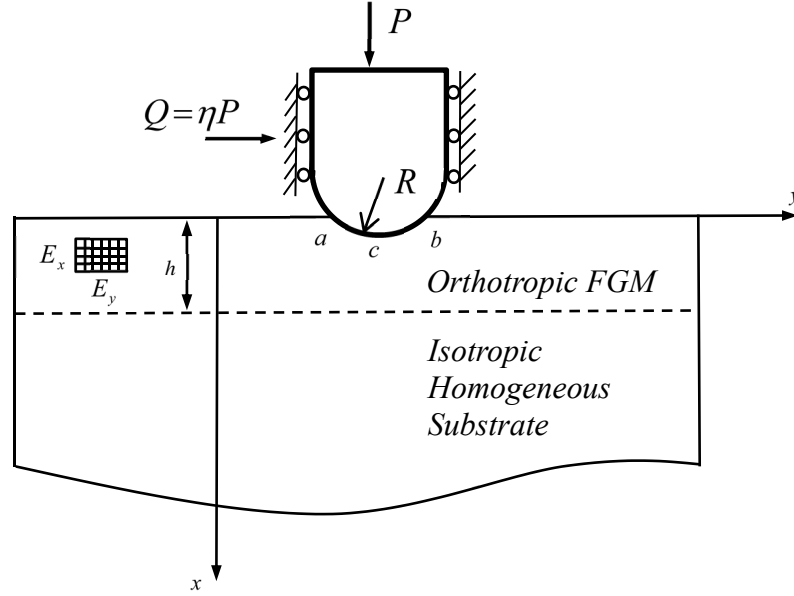


Figure 2.4: The geometry of the circular stamp problem.

The circular stamp contact problem of an orthotropic FGM coating which is bonded to a homogeneous semi-infinite medium is shown in Fig.2.4. The FGM surface is subjected to contact force P by a circular stamp. In this case, note that the contact length $(b - a)$ is strongly dependent on the normal contact force P similar to the triangular stamp case. The stamp profile is approximated as in the following form for $R \gg b - a$

$$\frac{\partial}{\partial y} u^c(0, y) = \frac{c - y}{R} \quad (2.108)$$

where c and R are the centerline position and the radius of the circular stamp, respectively. Considering (2.108) and the normalizations in (2.84), the integral equation (2.68) and the equilibrium equation (2.1h) become

$$\frac{f_{10} + s_{10}}{f_{10} + s_{10}} \bar{\sigma}(r) - \frac{1}{\pi} \int_{-1}^1 \frac{\bar{\sigma}(t)}{t-r} dt + \frac{1}{(f_{20} + s_{20})\pi} \int_{-1}^1 \bar{K}(t, r) \bar{\sigma}(t) dt = \frac{(2c - (b-a)r - (b+a))}{\mu_{xy}(f_{20} + s_{20})R} \quad -1 < r < 1 \quad (2.109)$$

$$\int_{-1}^1 \bar{\sigma}(r) dr = -\frac{2P}{\mu_{xy}(b-a)} \quad (2.110)$$

where

$$\bar{\sigma}(r) = \frac{\tilde{\sigma}(r)}{\mu_{xy}} \quad (2.111)$$

According to the theoretic analysis [71, 72], the unknown function $\bar{\sigma}(r)$ can be expanded into the series of Jacobi polynomials as in the following form

$$\bar{\sigma}(r) = \omega(r) \sum_{n=0}^{\infty} A_n P_n^{\alpha, \beta}(r), \quad \omega(r) = (1-r)^{\alpha} (1+r)^{\beta}. \quad (2.112a,b)$$

where $P_n^{\alpha, \beta}(r)$ are the Jacobi polynomials of order n and A_n 's are the unknown coefficients. The α and β are selected such that $0 < \alpha < 1$, $0 < \beta < 1$ and $\alpha + \beta = 1$ [28, 73] depending on the value of A/B as

$$\alpha = \frac{\phi}{\pi}, \quad \beta = 1 - \frac{\phi}{\pi}, \quad \text{for } \frac{A}{B} \geq 0 \quad (2.113a,b)$$

$$\alpha = 1 - \frac{\phi}{\pi}, \quad \beta = \frac{\phi}{\pi}, \quad \text{for } \frac{A}{B} < 0 \quad (2.113c,d)$$

where A , B and ϕ are given in (2.93a-c).

Substituting (2.112) into (2.110) and using orthogonality relations [48], the normalized contact force $P/(b-a)$ is obtained as

$$\frac{P}{b-a} = -\frac{A_0 \theta_1 \mu_{xy}}{2} \quad (2.114a)$$

where

$$\theta_1 = \frac{2\pi\alpha(1-\alpha)}{\sin(\pi\alpha)} \quad (2.114b)$$

For the circular stamp case ($\alpha + \beta = 1$), the property of Jacobi polynomial given in Appendix B reduces to:

$$\frac{1}{\pi} \int_{-1}^1 \frac{(1-t)^\alpha (1+t)^\beta P_n^{\alpha,\beta}(t)}{t-r} dt = \left[\begin{array}{c} \cot(\pi\alpha)(1-r)^\alpha (1+r)^\beta P_n^{\alpha,\beta}(r) \\ -\frac{2}{\sin(\pi\alpha)} P_{n+1}^{-\alpha,-\beta}(r) \end{array} \right] \quad (2.115)$$

Considering (2.112) and (2.115), the singular integral equation (2.109) is rewritten truncating the infinite series at N as

$$\left(\frac{A}{B} - \cot(\pi\alpha) \right) (1-r)^\alpha (1+r)^\beta \sum_{n=0}^N A_n P_n^{\alpha,\beta}(r) + \sum_{n=0}^N A_n m_{1n}(r) + \frac{1}{B\pi} \sum_{n=0}^N A_n m_{2n}(r) = \frac{(2c - (b-a)r - (b+a))}{\mu_{xy} B R} \quad -1 < r < 1 \quad (2.116)$$

where

$$m_{1n}(r) = \frac{2}{\sin(\pi\alpha)} P_{n+1}^{-\alpha,-\beta}(r) \quad -1 < r < 1 \quad (2.117a)$$

$$m_{2n}(r) = \int_{-1}^1 \bar{K}(t,r) P_n^{\alpha,\beta}(t) (1-t)^\alpha (1+t)^\beta dt \quad -1 < r < 1 \quad (2.117b)$$

When the material of the contact surface is Alumina ($A/B < 0$), the first term in (2.116) becomes zero. Hence (2.116) yields as

$$\sum_{n=0}^N A_n m_{1n}(r) + \frac{1}{B\pi} \sum_{n=0}^N A_n m_{2n}(r) = \frac{(2c - (b-a)r - (b+a))}{\mu_{xy} B R} \quad -1 < r < 1 \quad (2.118)$$

Expressing the right-hand side of (2.118) in terms of Jacobi polynomial of the first order, the following equation is obtained

$$\sum_{n=0}^N A_n m_{1n}(r) + \frac{1}{B\pi} \sum_{n=0}^N A_n m_{2n}(r) = \frac{(2c - (b-a)(2\alpha-1) - (b+a))}{\mu_{xy} B R} - \frac{2(b-a)}{\mu_{xy} B R} P_1^{-\alpha, -\beta}(r) \quad -1 < r < 1 \quad (2.119)$$

The variables a/R , b/R and c/R are not independent in the circular stamp problem. One of them is dependent on the other two. To be able to define the relationship between a/R , b/R and c/R ; first multiply both sides of (2.119) by $(1-r)^{-\alpha}(1+r)^{-\beta}$ then integrate from -1 to 1 as follows

$$\begin{aligned} \sum_{n=0}^N A_n \int_{-1}^1 m_{1n}(r) (1-r)^{-\alpha} (1+r)^{-\beta} dr + \frac{1}{B\pi} \sum_{n=0}^N A_n \int_{-1}^1 m_{2n}(r) (1-r)^{-\alpha} (1+r)^{-\beta} dr = \\ \frac{(2c - (b-a)(2\alpha-1) - (b+a))}{\mu_{xy} B R} \int_{-1}^1 (1-r)^{-\alpha} (1+r)^{-\beta} dr \\ - \frac{2(b-a)}{\mu_{xy} B R} \int_{-1}^1 (1-r)^{-\alpha} (1+r)^{-\beta} P_1^{-\alpha, -\beta}(r) dr \end{aligned} \quad (2.120)$$

It is proved by Erdogan [46] that the some of the integrals located in (2.120) become zero. Note also that the first integral on the right-hand side of (2.120) are evaluated as

$$\int_{-1}^1 (1-r)^{-\alpha} (1+r)^{-\beta} dr = \frac{\pi}{\sin(\pi\alpha)} \quad \alpha + \beta = 1 \quad (2.121)$$

Hence, rearranging (2.120) the following expression is obtained

$$\frac{1}{\pi} \sum_{n=0}^N A_n M_n = \frac{\pi(2c - (b-a)(2\alpha-1) - (b+a))}{\sin(\pi\alpha) \mu_{xy} R} \quad (2.122a)$$

where

$$M_n = \int_{-1}^1 m_{2n}(r) (1-r)^{-\alpha} (1+r)^{-\beta} dr \quad (2.122b)$$

Considering (2.122) and (2.119) together, the following expression is obtained

$$\sum_{n=0}^N A_n F_{3n}(r) = -\frac{2(b-a)}{B\mu_{xy}R} P_1^{-\alpha,-\beta}(r) \quad -1 < r < 1 \quad (2.123a)$$

$$F_{3n}(r) = m_{1n}(r) + \frac{1}{B\pi} \left(m_{2n}(r) - \frac{\sin(\pi\alpha)}{\pi} M_n \right) \quad -1 < r < 1 \quad (2.123b)$$

Note that M_n in (2.122b) is a double integral whose computation requires much more time compared to the integrals in flat and triangular stamp cases. By using (2.122) the centerline position is obtained as

$$\frac{c}{R} = \frac{1}{2} \left[\frac{\sin(\pi\alpha)\mu_{xy}}{\pi^2} \sum_{n=0}^N A_n M_n + \frac{(b+a)}{R} + \frac{(b-a)(2\alpha-1)}{R} \right] \quad (2.124)$$

In the numerical solution, first a/R and b/R are specified, then (2.123) is collocated at $(N+1)$ points to calculate the unknown constants A_n ($n=0, \dots, N$). The roots of Chebyshev polynomials of first kind are used as the collocation points and given as

$$r_i = \cos\left(\frac{\pi(2i-1)}{2(N+1)}\right) \quad i=1, 2, \dots, N+1 \quad (2.125)$$

Considering (2.114) and the truncated form of (2.91) at N points, the normalized contact stress is calculated as

$$\frac{\sigma\left(\frac{b-a}{2}r + \frac{b+a}{2}\right)}{P/(b-a)} = -\frac{2}{A_0\theta_1} (1-r)^\alpha (1+r)^\beta \sum_{n=0}^N A_n P_n^{\alpha,\beta}(r) \quad -1 < r < 1 \quad (2.126)$$

After all the normalized force and the centerline position are calculated using (2.114) and (2.124), respectively.

CHAPTER 3

THE FINITE ELEMENT METHOD

Beside the analytical method defined in the preceding section, a finite element (FE) approach is also conducted to examine the response of orthotropic FGM coatings under contact loads. The solution of the contact problem by using two different solution techniques enables assessing the accuracy of both methods directly comparing their results. By this way, a dependable computational approach can be generated.

This computational solution procedure is carried out utilizing the finite element analysis software ANSYS [75]. FE simulations are performed to investigate flat, triangular and circular stamp contact problems that are shown in Figures 2.2-2.4. The 2D models of the FGM coating and homogeneous medium are divided into quadrangular and triangular solid elements. These quadrangular and the triangular finite elements can be seen in Figure 3.1. In the FE discretization of graded structures, two foremost procedures are utilized to consider the continuous spatial gradations in the stiffness constants. In this study, they are named as graded FE and homogeneous FE methods. The gauss points are used to attribute engineering parameters for each finite element in the graded FE method (Santare and Lambros [76]). However, the engineering parameters are computed at the centroids of the finite elements in the homogeneous FE technique (Yıldırım et. al [77] and Dag et al. [78]).

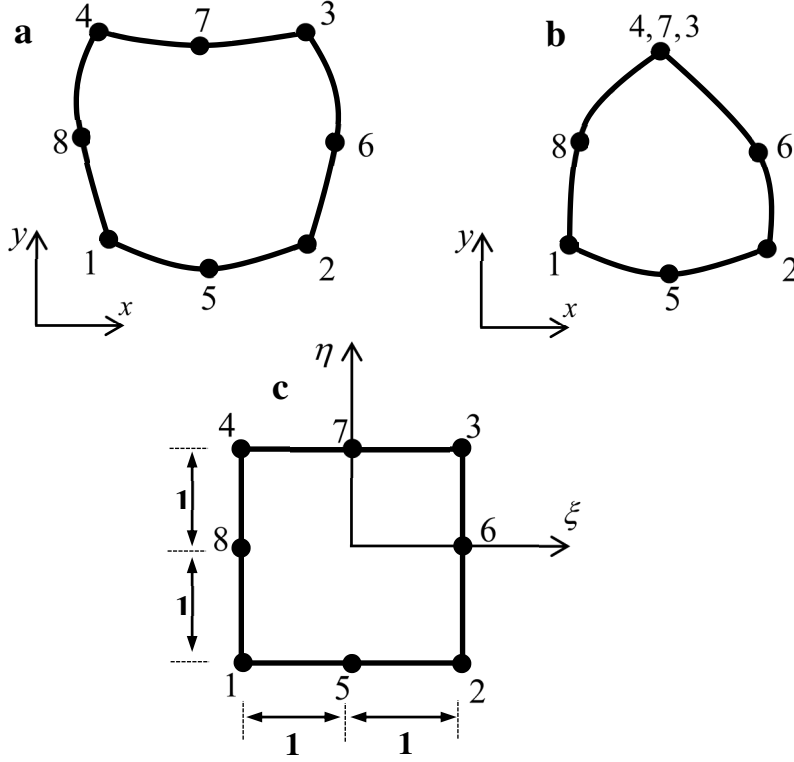


Figure 3.1: (a) A quadrangular FE located in the Cartesian coordinate frame; (b) A triangular FE located in the Cartesian coordinate frame; (c) Quadrangular and the triangular FE's located in the iso-parametric coordinate frame.

Hence, in the homogeneous FE method, the material properties attributed to the elements are constant all through the surface of an element. Previous studies demonstrate that when an FGM structure is discretized finely enough, one can capture very correct results utilizing both of these approaches [77, 78]. The homogeneous FE method is used in this study. The following parametric analyses illustrates that the results of analytical and computational techniques fit to each other with a high level accuracy. In the computational analyses, the flat, triangular and circular stamp boundaries are taken as rigid target elements. The surface of the FGM coating that might contact with the target surfaces are described as the contact elements lying on the solid elements. The rigid stamp surfaces are divided into a group of target segment elements and are coupled with its contacting surfaces.

These rigid and contact surfaces share the same real constant set [75]. The target segment elements can be exposed to any translational or rotational displacement, voltage, magnetic potential and temperature. Moments and forces can also be applied on target elements. Although these elements can easily model arbitrary target shapes, the target surfaces are smooth in this study. Each target surface can be coupled with only one contact surface. However, more than one contact elements may compose the contact surface and contact with the same target surface. Similarly, more than one target elements may form the target surface and gets the contact with the same contact surface. It is valid for both the target and contact surfaces that any number of elements can be defined in a one target or contact surface. Alternatively, the contact and target surfaces can be discretized by dividing the large surfaces into smaller ones which include fewer number of elements [75].

The augmented Lagrangian method is utilized as an iterative procedure of the contact problem. The theory details of the Augmented Lagrangian method is given in a review paper by Mijar and Arora [79]. In this method, the contact pressure and frictional stresses are increased step by step during equilibrium iterations. the Augmented Lagrangian method generally yields better conditioning and is less dependent on the magnitude of the contact stiffness compared to the penalty method. However, the augmented Lagrangian method might require extra iterations in some analyses for which the deformed mesh is too distorted [75].

Contact detection points are defined at the Gauss integration points of the contact elements which are located on the element surface (see Fig. 3.2). The indentation of the contact element into the target surface is constrained at its integration points. However, the target surface can penetrate into the contact surface. Surface-to-surface contact elements are used in this study treating the Gauss integration points as detection points. This treatment yields more stable stresses than the nodal detection scheme for which the nodes are used for the contact detection [75].

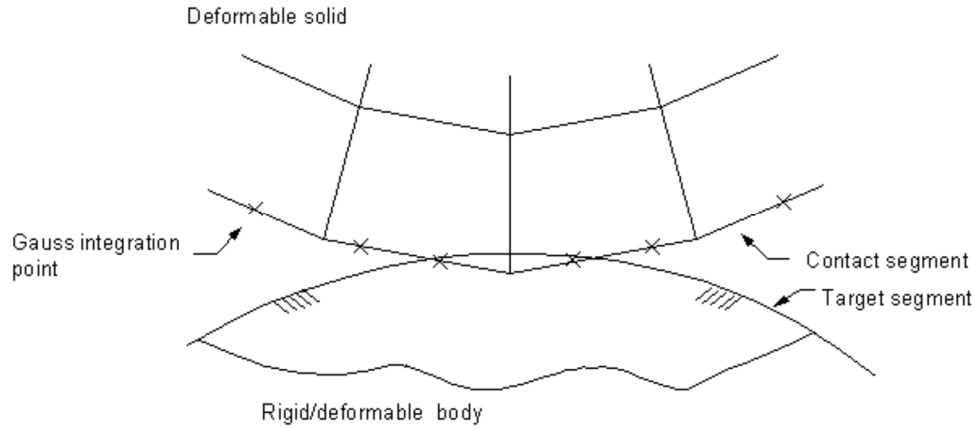


Figure 3.2: Contact Detection Points [75].

FE mesh utilized for the flat stamp problem is presented in Figure 3.3. This finite element mesh includes 500 contact line elements and 60,759 quadrangular and triangular 2D solid elements. The inelastic flat stamp possesses three rigid target surfaces, the inelastic triangular stamp possesses two rigid target surfaces and the inelastic circular stamp has a unique rigid target surface in the FE simulations. In Figure 3.3; B , H , W and h stand for the width of the inelastic stamp, the vertical size of the coating-substrate system, the horizontal size of the coating-substrate system and the thickness of the coating, respectively. H and W are taken large enough not to cause any influences on the results of the simulation. Hence, $B=W$ is assigned as $1=10$. $H=W$ and $B=h$ are set as $1=1.625$ and $1=1$, respectively. The FE mesh denseness is refined apparently on the contact zone to be able to take the abrupt changes of the field quantities into account particularly near the edges of the stamps. In the meantime, the FE mesh denseness is also raised through the coating thickness in order to maintain smooth exponential material gradations.

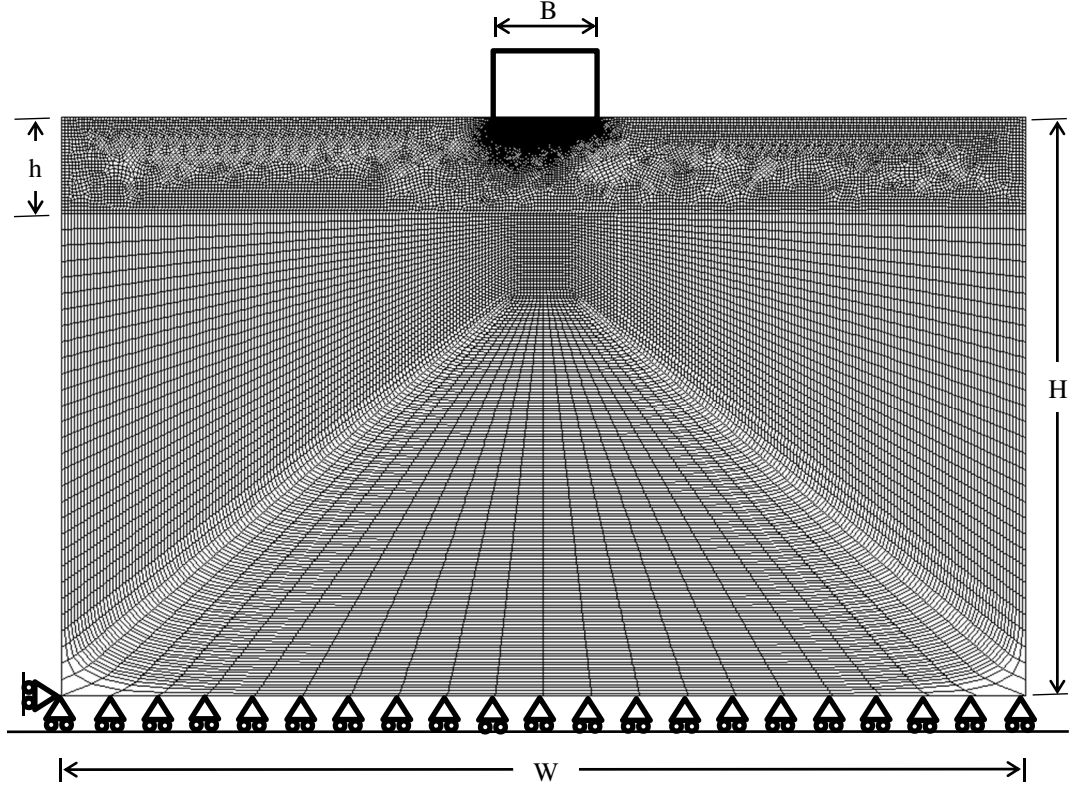


Figure 3.3: FE mesh utilized for the flat stamp problem.

The most critical issue managed in the computational contact analysis of this study is the attribution of different material properties for each finite element depending on their position in the vertical x axis. This feature is not available in ANSYS and it is enabled by adding a proper subroutine into the related ANSYS code.

Note that the computational analyses are optimized such that $R \gg (b-a)$ for the circular stamp problem ($(b-a)/R = 8 \times 10^{-5}$) and $(b-a)\tan(\theta) \ll (b-a)$ for the triangular stamp problem ($\tan(\theta) = 8.73 \times 10^{-5}$). Upon these conditions, the convergence of iterative method (Augmented Lagrange) is remedied remarkably.

CHAPTER 4

NUMERICAL RESULTS

This chapter presents the results produced with the analytical and computational techniques. In this section, it is needed to mention about the normalizations enabled in the results of the flat, triangular and circular stamp problems. Hence, the non-homogeneity constant γ introduce material gradations to the orthotropic coating. The symbols a and b indicate the coordinates of the leading and trailing ends of the inelastic stamp. c represents the centerline position of the circular stamp. The numerical results can be presented considering the normalized nonhomogeneity parameter γh and the normalized contact length $(b-a)/h$. On contrary to the flat stamp problem, in the cases of the triangular and circular stamps the contact length $(b-a)$ is strongly dependent on the normal contact force P . The normalized contact forces are evaluated by utilizing (2.104) for the triangular stamp and (2.114a) for the circular stamp. For the flat stamp, such kind of calculations is not needed since P and $(b-a)$ are independent in that case.

The first group of results are presented in Tables 4.1-4.2 and Figures 4.2–4.14, which are generated for a flat stamp. Another set of results, produced regarding a triangular stamp, are presented in Tables 4.3-4.7 and Figures 4.15–4.27. The third set are for a circular stamp and presented in Tables 4.8-4.17 and Figures 4.28–4.40. The fourth set of results that show the surface and interfacial behavior of orthotropic homogeneous coatings under contact loads, are given in Figures 4.42–4.52. All the results showing the effects of problem parameters on the normalized surface contact stresses are produced by using the developed analytical procedure. Note that the interfacial stresses for orthotropic homogeneous coatings given in Figures 4.49-4.52 are obtained by using FEA.

In all the parametric analyses of FGM coatings; the coating surface is taken as % 100 Alumina for which the engineering parameters are given in Table 2.1. The orthotropic stiffness constant $c_{66}(x)$ ($0 < x < \infty$) of a material corresponds to its shear modulus in plane strain assumption, for either the material is orthotropic or isotropic (see Equation 2.4). In this study, the continuity of stiffness constant $c_{66}(x)$ is satisfied all through the thickness as done in the study by Ben-Romdhane et al. [41]. This continuity is enabled using the following the procedure: Firstly the shear modulus at the coating-substrate interface is computed using the relation $c_{66}(h) = c_{660}e^{\gamma h}$ for a given normalized non-homogeneity constant γh of the coating. Then the shear modulus of the isotropic substrate is attributed as $\mu = c_{66}(h)$. After that, the elastic modulus E of the isotropic substrate is calculated by using the restriction $E = 2\mu(1+\nu)$ taking the poison's ratio of the substrate as a constant ($\nu = 0.31$).

Nickel is one of the most commonly used substrate material for Alumina coatings. Taking the preceding $c_{66}(x)$ continuity procedure into account, the substrate material is obtained as % 100 Nickel when the normalized non-homogeneity constant γh is attributed to 0.712. The engineering parameters of Nickel are given in Table 2.1. Thus all the FGM coating results presented in this study are produced for $\gamma h = 0.712$ except the cases showing the effect of non-homogeneity constant variations on the normalized contact stresses and the normalized contact forces. Note that when the non-homogeneity constant γh is taken as negative, the stiffness coefficients $c_{11}(x)$, $c_{12}(x)$, $c_{22}(x)$ are continuously decreasing through the coating thickness ($0 < x < h$) and increases sharply at the interface ($x = h$). However, when $\gamma h > 0$ the stiffness coefficients $c_{11}(x)$, $c_{12}(x)$, $c_{22}(x)$ are continuously increasing through the coating thickness ($0 < x < h$) and also increases at the interface ($x = h$). Therefore, we can infer that the gradation is much more feasible for $\gamma h > 0$ (see Figure 4.1). Hence all the parametric analyses generated for FGM coatings are produced for $\gamma h > 0$.

The contact analyses of orthotropic homogeneous coatings are enabled by attributing the normalized nonhomogeneity constant to zero in the analytical and computational procedures. In the presented results for the homogeneous orthotropic coating case, the homogenous coating and the substrate are taken as Alumina and Nickel, respectively. Their elastic material properties are available in Table 2.1. Additionally, there is no material property continuity defined at the interface between the coating and substrate since they are different homogeneous materials.

Note that the normalized contact stress $\sigma_{xx}(0, y)/(P/(b-a))$ and normalized lateral contact stress $\sigma_{yy}(0, y)/(P/(b-a))$ calculated by analytical technique are independent of the radius of the stamp R and the inclination angle of the stamp θ for the circular and triangular stamp problems, respectively. These normalized stresses are also independent of the magnitude of the contact length $(b-a)$ and the magnitude of the contact force P for all the stamp cases. Also note that the normalized contact force of the circular stamp $P/(\mu_{xy}(b-a))$ is dependent on the ratio $(b-a)/R$ (see Equations 2.114 and 2.123), although the normalized contact force of the triangular stamp $P/(\tan(\theta)\mu_{xy}(b-a))$ is independent to the contact length $(b-a)$ (see Equations 2.104-105).

4.1 Flat Stamp

The geometry of the flat stamp problem is shown in Figure 2.2. Figure 4.2 and Figure 4.3 show the results on the normalized contact stress $\sigma_{xx}(0, y)/(P/(b-a))$ and on the normalized lateral contact stress $\sigma_{yy}(0, y)/(P/(b-a))$, which are evaluated regarding an orthotropic graded coating which is exposed to contact tractions of an inelastic flat stamp. In these figures, the analytical and finite element methods are used to calculate the normalized contact stress results which are presented together to assess the accuracy and the compatibility of both techniques. The normalized stresses are plotted versus the normalized y-axis $(2y-(b+a))/(b-a)$ which is equal to -1 for $y=a$ and 1 for $y=b$.

The results are provided for two different normalized nonhomogeneity constants: $\gamma h = 0.1$ in Figure 4.2 and $\gamma h = 0.712$ in Figure 4.3. Note that when the normalized nonhomogeneity constant γh is 0.712, the substrate material becomes %100 Nickel. The fixed parameters in the evaluation of these results are; $(b-a)/h = 1.0$, $\eta = 0.3$. Also note that a positive value for γh implies that the stiffness constants of the coating increase in the thickness direction (positive x -direction). The coating becomes homogeneous when the normalized nonhomogeneity parameter γh is assigned to zero. It is observed from Figure 4.2 and Figure 4.3 that the analytical and computational methods provide very close results. The scaled deformed shape which is produced by using the FE solution of a flat stamp problem is presented by Figure 4.4. Referring to Figure 4.2 and Figure 4.3, we realize that the contact stress $\sigma_{xx}(0, y)/(P/(b-a))$ and the lateral contact stress $\sigma_{yy}(0, y)/(P/(b-a))$ possess singular behavior at the leading and trailing ends of the contact zone (at $y=b$ and $y=a$), due to the sharp edges of the flat stamp. The normalized contact and lateral contact stress curves generated are not symmetric about $y=0$ due to laterally acting frictional forces on the coating surface. Lateral contact stress is in tension as $y \rightarrow a^-$ and in compression as $y \rightarrow b^+$. After the evaluation of the contact stress $\sigma_{xx}(0, y)$, one can easily calculate the shear stress $\sigma_{xy}(0, y)$ by using the dry friction law as $\sigma_{xy}(0, y) = \eta \sigma_{xx}(0, y)$.

In the analytical method, the normalized stresses are evaluated through the truncated forms of series representation. As the truncation number N is increased, a stress result should converge to a definite magnitude. Hence, we present some tables in this Chapter to validate the convergence behavior of the analytical method. The related results are evaluated regarding the flat stamp and given in Table 4.1 and Table 4.2. The results are generated for two distinct normalized contact length values: $(b-a)/h = 0.4$ in Table 4.1 and $(b-a)/h = 1.0$ in Table 4.2. These tables present 12 cases in total. For each of these cases the normalized contact stress $\sigma_{xx}(0, y)/(P/(b-a))$ is evaluated by increasing the truncation number N six times. Note that N is the upper limit for the truncated form of the series representation given by (2.91). N also indicates the number of discretization

points utilized for (2.95). As observed in Table 4.1 and Table 4.2, the results quickly converge as N is raised from 1 to 14. For any combination of the problem parameters, three-digit convergence is obtained for $N = 10$. Thus, all the analytical results presented in this study are generated for $N = 10$.

Additionally, the influences of the problem parameters on the contact stresses are also presented for the flat stamp utilizing the developed analytical technique. Figure 4.5 shows the effect of the nonhomogeneity parameter γh on the normalized contact stress $\sigma_{xx}(0, y)/(P/(b-a))$ for $(b-a)/h = 1.0$ and $\eta = 0.3$. Due to the singular behavior of the contact stresses near the leading and trailing contact ends, the results produced for different normalized non-homogeneity parameters γh cannot be distinguished in these regions. However, the effect of the nonhomogeneity parameter is observable inside the contact region. Note that when γh increases from 0.0 to 1.0, the magnitude of the contact stress increases remarkably inside the contact region. Figure 4.6 shows the influences of the friction coefficient on the normalized contact stress $\sigma_{xx}(0, y)/(P/(b-a))$ for $(b-a)/h = 1.0$ and $\gamma h = 0.712$. The negative sign of the friction coefficient η implies that the lateral force Q acts in the negative y -direction. If this sign of the friction coefficient η is positive, then lateral force Q acts in the positive y -direction. Examining Figure 4.6, the contact stress reaches its maximum value on the region near the end point $y = b$, if $\eta > 0.0$ and on the region near the end point $y = a$, if $\eta < 0.0$. Figure 4.7 shows the effect of the normalized contact length $(b-a)/h$ on the normalized contact stress $\sigma_{xx}(0, y)/(P/(b-a))$ for $\eta = 0.3$ and $\gamma h = 0.712$. Note that the increase of the normalized contact length $(b-a)/h$ implies either the decreasing size of the coating thickness relative to a fixed contact length or the increasing size of the contact length relative to a fixed coating thickness. When $(b-a)/h$ is increased from 0.1 to 1.0, the magnitude of the contact stress increases inside the contact region. Figure 4.8 shows the effect of Elastic modulus ratio E_x/E_y on the normalized contact stress $\sigma_{xx}(0, y)/(P/(b-a))$ for $\eta = 0.3$, $(b-a)/h = 1.0$ and $\gamma h = 0.712$. In these plots, the engineering parameters of Alumina are used as in Table 2.1 such that only the parameter E_y is changed to

get the desired E_x/E_y ratio. After that, ν_{yz} and ν_{yx} are recalculated considering the restrictions given in (2.6). Also note that all the Poisson's ratio values should be between 0 and 0.5. Examining Figure 4.8, the normalized contact stress $\sigma_{xx}(0, y)/(P/(b-a))$ slants towards the positive y-direction slightly, when E_x/E_y is increased from 0.6 to 1.5. Figure 4.9 shows the effect of Elastic modulus ratio E_x/E_z on the normalized contact stress $\sigma_{xx}(0, y)/(P/(b-a))$ for $\eta=0.3$, $(b-a)/h=1.0$ and $\gamma h=0.712$. In these plots, the engineering parameters of Alumina are used as in Table 2.1 such that only the parameter E_z is changed to get the desired E_x/E_z ratio. Then ν_{yz} and ν_{zx} are recalculated obeying the restrictions given in (2.6). As observed in this figure, variation of the elastic modulus ratio E_x/E_z has no significant effect on the normalized contact stress $\sigma_{xx}(0, y)/(P/(b-a))$. The crack formation or initiation may occur on the ceramic based surfaces loaded by contact loads involving friction. These defects are commonly called as herringbone crackings [5] or partial-cone crackings [57] which results from the existence of the lateral contact stress $\sigma_{yy}(0, y)$ on the surface of the loaded medium. Therefore, the influences of problem parameters on the surface lateral contact stress $\sigma_{yy}(0, y)$ are illustrated in this study. Figure 4.10 shows the effect of nonhomogeneity parameter on the normalized lateral contact stress $\sigma_{yy}(0, y)/(P/(b-a))$ for $\eta=0.3$ and $(b-a)/h=1.0$. On contrary to the normal stress $\sigma_{xx}(0, y)$, the lateral contact stress $\sigma_{yy}(0, y)$ possesses non-zero distributions on the free surfaces ($y < a$, $y > b$). The effect of the non-homogeneity parameter on the lateral contact stress is not that significant near the trailing end of the contact. The magnitude of the compressive stresses decrease significantly as the nonhomogeneity constant γh is increased from 0.0 to 1.0. Figure 4.11 shows the effect of coefficient of friction η on the normalized lateral contact stress $\sigma_{yy}(0, y)/(P/(b-a))$ for $\gamma h=0.712$ and $(b-a)/h=1.0$. Examining Figure 4.11, the lateral contact stress increases significantly on and outside the contact zone, when the absolute value of the friction coefficient is increased. Some further analytical results are presented by considering the flat stamp in Figure 4.12 for $\eta=0.3$ and $\gamma h=0.712$, in order to examine the influences of the normalized contact length

$(b-a)/h$ on the lateral contact stress $\sigma_{yy}(0, y)/(P/(b-a))$. As can be seen in Figure 4.12, the lateral contact stress decreases slightly on and outside the contact zone as the normalized contact length $(b-a)/h$ is increased from 0.1 to 1.0. In other words, the magnitude of the lateral contact stress increases as the size of the coating thickness relative to the contact length increases. Figure 4.13 shows the influences of Elastic modulus ratio E_x/E_y on the normalized lateral contact stress $\sigma_{yy}(0, y)/(P/(b-a))$ for $\eta=0.3$ and $\gamma h=0.712$. As seen in Figure 4.13, the effect of elastic modulus ratio E_x/E_y on normalized lateral contact stress is very significant on and outside the contact zone. If E_x/E_y is increased from 0.6 to 1.5, it is observed that the magnitude of the lateral contact stress decreases significantly. Figure 4.14 shows the effect of Elastic modulus ratio E_x/E_z on the normalized lateral contact stress $\sigma_{yy}(0, y)/(P/(b-a))$ for $\eta=0.3$, $(b-a)/h=1.0$ and $\gamma h=0.712$. As observed in this figure, variation of the elastic modulus ratio E_x/E_z has no significant effect on the normalized lateral contact stress $\sigma_{yy}(0, y)/(P/(b-a))$.

4.2 Triangular Stamp

The results produced for an orthotropic FGM coating which is subjected to contact loads by an inelastic triangular stamp are given in Figures 4.15-4.27 and Tables 4.3-4.7. The view of the triangular stamp problem is presented in Figure 2.3. In the triangular stamp problem the contact length $(b-a)$ is strongly dependent on the normal contact force P . The normal contact force is analytically computed for a specified contact length by using (2.104). Tables 4.3-4.7 tabulates the normalized contact forces $P/(\mu_{xy} \tan(\theta)(b-a))$ evaluated utilizing the analytical method for different combinations of the friction coefficient η , the normalized non-homogeneity constant γh , the normalized contact length $(b-a)/h$, the elastic modulus ratio E_x/E_y and the elastic modulus ratio E_x/E_z . As observed from these Tables; when the normalized non-homogeneity constant γh is increased

from 0.1 to 1.0, the normalized contact force $P/(\mu_{xy} \tan(\theta)(b-a))$ increases significantly for any combination of the other problem parameters. When the friction coefficient η is raised from -0.6 to 0.6, the normalized contact force $P/(\mu_{xy} \tan(\theta)(b-a))$ also increases significantly regardless of the combination of the other problem parameters. When the normalized contact length $(b-a)/h$ is increased from 0.4 to 1.0, the normalized contact force $P/(\mu_{xy} \tan(\theta)(b-a))$ increases slightly in any case. It should be also emphasized that the effect of the variations of the normalized nonhomogeneity parameter γh on the normalized force $P/(\mu_{xy} \tan(\theta)(b-a))$ become much more significant, when the normalized contact length $(b-a)/h$ is increased. We can infer from these tables that when the elastic modulus ratios E_x/E_y and E_x/E_z are increased, then the normalized contact force $P/(\mu_{xy} \tan(\theta)(b-a))$ decreases considerably regardless of the change in other parameters. To be able to obtain accordant stress curves for triangular, flat and circular stamp problems, the curves for all the stamp profiles are normalized with respect to the normal force $P/(b-a)$. The comparisons of the normalized contact and the normalized lateral contact stresses evaluated utilizing the analytic and FE techniques are presented for two different nonhomogeneity constants γh in Figure 4.15 and Figure 4.16: $\gamma h = 0.1$ in Figure 4.15 and $\gamma h = 0.712$ in Figure 4.16. The fixed parameters in the computation of these normalized stresses are $(b-a)/h = 1.0$, $\eta = 0.3$. One can observe that the normalized contact stress becomes singular at point $y = a$ and zero at point $y = b$. The related behavior of the triangular stamp results from its sharp edge at $y = a$ and smooth edge at $y = b$. Due to the positive friction coefficient, the lateral stress around the trailing end ($y \rightarrow a^-$) is tensional and tends to infinity at $y = a$. The lateral contact stress around the leading end is compressive and nonsingular since the contact is smooth at $y = b$. Figure 4.15 and Figure 4.16 indicate that the analytic and computational techniques provide very close results. The scaled deformed shape of the contact region, which is produced by using the FE solution of a triangular stamp problem is provided in Figure 4.17. Figure 4.18 shows the behavior of the normalized contact stress $\sigma_{xx}(0, y)/(P/(b-a))$ with the change in the normalized

nonhomogeneity constant γh . Examining Figure 4.18, it can be observed that, the magnitude of the normalized contact stress increases inside the contact region of the triangular stamp as the nonhomogeneity constant is raised from 0.0 to 1.0. Figure 4.19 demonstrates the effects of friction coefficient on the normalized contact stress $\sigma_{xx}(0, y)/(P/(b-a))$. As seen in Figure 4.19, the normalized contact stress decreases significantly away from the sharp edge of the triangular stamp, as the coefficient of friction is raised from -0.6 to 0.6. Figure 4.20 shows the effect of the normalized contact length $(b-a)/h$ on the normalized contact stress $\sigma_{xx}(0, y)/(P/(b-a))$ for $\eta=0.3$ and $\gamma h=0.712$. When $(b-a)/h$ is raised from 0.1 to 1.0, the magnitude of the contact stress increases inside the contact region. Figure 4.21 shows the effect of Elastic modulus ratio E_x/E_y on the normalized contact stress $\sigma_{xx}(0, y)/(P/(b-a))$ for $\eta=0.3$ and $\gamma h=0.712$. It can be observed from Figure 4.22 that the change in elastic modulus ratio E_x/E_y has no significant effect on the normalized contact stress $\sigma_{xx}(0, y)/(P/(b-a))$. Figure 4.22 shows the effect of Elastic modulus ratio E_x/E_z on the normalized contact stress $\sigma_{xx}(0, y)/(P/(b-a))$ for $\eta=0.3$ and $\gamma h=0.712$. It can be observed from Figure 4.22 that the change in elastic modulus ratio E_x/E_z has no significant effect on the normalized contact stress $\sigma_{xx}(0, y)/(P/(b-a))$. Figure 4.23 illustrates the effect of normalized nonhomogeneity parameter γh on the normalized lateral contact stress $\sigma_{yy}(0, y)/(P/(b-a))$ for $(b-a)/h=1.0$ and $\eta=0.3$. Unlike the stress component $\sigma_{xx}(0, y)$, the lateral stress $\sigma_{yy}(0, y)$ is not zero in the region outside the contact zone ($y < a, y > b$). As can be observed in Figure 4.23 that when the nonhomogeneity constant increases from 0.0 to 1.0, the magnitude of the lateral compressive stress decreases on and outside the contact zone, although the effect is more significant on the contact zone. Figure 4.24 shows the effect of friction coefficient on the normalized lateral contact stress $\sigma_{yy}(0, y)/(P/(b-a))$ for $(b-a)/h=1.0$ and $\gamma h=0.712$. Note that the smooth contact at the end $y=b$ becomes the trailing end if the friction coefficient is negative, for which the trends of the lateral contact stress has sharp transitions at $y=b$. Examining Figure 4.24,

the effect of the friction coefficient on the lateral contact stress is very remarkable. The larger the absolute value of the friction coefficient is, the greater the normalized lateral contact stress near the trailing end we get. Figure 4.25 is provided to demonstrate the influences of the normalized contact length $(b-a)/h$ on the normalized lateral contact stress $\sigma_{yy}(0, y)/(P/(b-a))$ for $\eta=0.3$ and $\gamma h=0.712$. As seen in the figure, when the normalized contact length $(b-a)/h$ is increased from 0.1 to 1.0, the magnitude of the lateral contact stress decreases slightly on and outside the contact zone. Thus we can conclude that the size of the coating thickness relative to the contact length can be decreased to reduce the possibility of damage due to the herringbone cracks near the trailing end. Figure 4.26 shows the influences of elastic modulus ratio E_x/E_y on the normalized lateral contact stress $\sigma_{yy}(0, y)/(P/(b-a))$ for $\eta=0.3$ and $\gamma h=0.712$. As can be seen in this figure, the effect of elastic modulus ratio E_x/E_y on normalized lateral contact stress $\sigma_{yy}(0, y)/(P/(b-a))$ is very significant on and outside the contact zone. If E_x/E_y is increased from 0.6 to 1.5, it is observed that the magnitude of the lateral contact stress decreases remarkably. Hence, the option of increasing the ratio E_x/E_y can be used in the graded coating so as to prevent the risk of damage near the trailing end of the contact zone. Figure 4.27 shows the effect of Elastic modulus ratio E_x/E_z on the normalized lateral contact stress $\sigma_{yy}(0, y)/(P/(b-a))$ for $\eta=0.3$, $(b-a)/h=1.0$ and $\gamma h=0.712$. As observed in this figure, variation of the elastic modulus ratio E_x/E_z has no significant effect on the normalized lateral contact stress $\sigma_{yy}(0, y)/(P/(b-a))$.

4.3 Circular Stamp

The results produced for an orthotropic FGM coating which is subjected to contact loads by an inelastic circular stamp are given in Figures 4.28–4.40 and Tables 4.8–4.17. The view of the circular stamp problem is presented in Figure 2.4. In the circular stamp problem the contact length $(b-a)$ is strongly dependent on the normal contact force P , just as in the triangular stamp problem. Tables 4.8–4.12

tabulates the normalized contact forces $P/(\mu_{xy}(b-a))$ evaluated utilizing the analytical method for different combinations of the friction coefficient η , the normalized non-homogeneity constant γh , the normalized contact length $(b-a)/h$, the elastic modulus ratio E_x/E_y and the elastic modulus ratio E_x/E_z . The end point locations which are used throughout the computation of the normalized forces are $a/R=0$ and $b/R=0.02$. As observed from these Tables; when the normalized non-homogeneity constant γh is increased from 0.1 to 1.0, the normalized contact force $P/(\mu_{xy}(b-a))$ increases for any combination of the other problem parameters significantly. When the friction coefficient η is raised from 0.0 to 0.6, the normalized contact force $P/(\mu_{xy}(b-a))$ decreases slightly in any case. Similarly, when the normalized contact length $(b-a)/h$ is increased from 0.4 to 1.0, the normalized contact force $P/(\mu_{xy}(b-a))$ increases considerably regardless of the combination of the other problem parameters. It should be also emphasized that the effect of the variations of the normalized nonhomogeneity parameter γh on the normalized force $P/(\mu_{xy}(b-a))$ become much more significant, when the normalized contact length $(b-a)/h$ is increased. We can also infer from these tables that when the elastic modulus ratios E_x/E_y and E_x/E_z are increased, then the normalized contact force $P/(\mu_{xy}(b-a))$ decreases considerably for any case. Tables 4.13-4.17 tabulates the centerline position c/R of the circular stamp evaluated utilizing the analytic method for different combinations of the friction coefficient η , the normalized non-homogeneity constant γh , the normalized contact length $(b-a)/h$, the elastic modulus ratio E_x/E_y and the elastic modulus ratio E_x/E_z . The end point locations which are used throughout the computation of the normalized forces are $a/R=0$ and $b/R=0.02$. As observed from these Tables; when the normalized non-homogeneity constant γh is increased from 0.1 to 1.0, the centerline position c/R tends to approach the geometric centerline of the rigid circular stamp independently

to the combination of any other problem parameters. When the friction coefficient η is increased from 0.0 to 0.6, the centerline position c/R moves away from the geometric centerline of the stamp to the right significantly. This effect is also independent to the variation of any other problem parameters. The change in the normalized contact length $(b-a)/h$ does not seem to have considerable effect on the centerline position c/R for any combination of the problem parameters. It can be also inferred from these Tables that when the elastic modulus ratios E_x/E_y is increased, then the centerline position c tends to move to the right considerably. When the elastic modulus ratios E_x/E_z is increased, then the centerline position c/R remains almost stationary regardless of the change in other parameters. The comparisons of the normalized contact and the normalized lateral contact stresses evaluated regarding the analytic and FE techniques are given for two different nonhomogeneity constants γh in Figure 4.29 and Figure 4.30: $\gamma h = 0.1$ in Figure 4.29 and $\gamma h = 0.712$ in Figure 4.30. The fixed parameters in the computation of these normalized stresses are $(b-a)/h = 1.0$, $\eta = 0.3$. One can observe that the normalized contact stress is zero at the leading and the trailing ends $y = a$ and $y = b$. That is due to the fact that the stamp edges are smooth the leading and the trailing ends $y = a$ and $y = b$. Due to the positive friction coefficient, the lateral contact stress around the trailing end ($y \rightarrow a^-$) is tensional nonsingular due to smooth contact. The lateral contact stress around the leading end is compressive and also nonsingular at $y = b$. Figure 4.29 and Figure 4.30 indicate that the analytic and computational techniques provide very close results. The scaled deformed shape of the contact region, which is produced by using the FE solution of a circular stamp problem is provided in in Figure 4.28. Figure 4.31 shows the behavior of the normalized contact stress $\sigma_{xx}(0, y)/(P/(b-a))$ with the change in the normalized nonhomogeneity constant γh . Examining Figure 4.31, it can be observed that, the magnitude of the normalized contact stress increases inside the contact region of the circular stamp as the nonhomogeneity constant is raised from 0.0 to 1.0. Figure 4.32 demonstrates the effects of friction coefficient on the normalized contact stress $\sigma_{xx}(0, y)/(P/(b-a))$. As seen in Figure 4.32, the

normalized contact stress slant towards the positive y direction significantly, as the friction coefficient is decreased from 0.6 to -0.6. Figure 4.33 shows the effect of the normalized contact length $(b-a)/h$ on the normalized contact stress $\sigma_{xx}(0, y)/(P/(b-a))$ for $\eta=0.3$ and $\gamma h=0.712$. When $(b-a)/h$ is raised from 0.1 to 1.0, the magnitude of the contact stress increases in the contact region slightly. Figure 4.34 shows the effect of Elastic modulus ratio E_x/E_y on the normalized contact stress $\sigma_{xx}(0, y)/(P/(b-a))$ for $\eta=0.3$ and $\gamma h=0.712$. It can be observed from Figure 4.34 that as the elastic modulus ratio E_x/E_y is decreased from 1.5 to 0.6, the normalized contact stress $\sigma_{xx}(0, y)/(P/(b-a))$ slants towards positive y direction slightly. Figure 4.35 shows the effect of Elastic modulus ratio E_x/E_z on the normalized contact stress $\sigma_{xx}(0, y)/(P/(b-a))$ for $\eta=0.3$ and $\gamma h=0.712$. It can be observed from Figure 4.35 that the change in elastic modulus ratio E_x/E_z has no significant effect on the normalized contact stress $\sigma_{xx}(0, y)/(P/(b-a))$. Figure 4.36 illustrates the effect of normalized nonhomogeneity parameter γh on the normalized lateral contact stress $\sigma_{yy}(0, y)/(P/(b-a))$ for $(b-a)/h=1.0$ and $\eta=0.3$. On contrary to the normal stress $\sigma_{xx}(0, y)$, the lateral contact stress $\sigma_{yy}(0, y)$ possesses non-zero distributions on the free surfaces ($y < a$, $y > b$). As can be observed in Figure 4.36, the variation of normalized nonhomogeneity constant γh possesses significant effect on the lateral contact stresses on and outside the contact zone. When the nonhomogeneity constant is increased from 0.0 to 1.0, the magnitude of the lateral compressive stress decreases. Figure 4.37 shows the effect of friction coefficient η on the normalized lateral contact stress $\sigma_{yy}(0, y)/(P/(b-a))$ for $(b-a)/h=1.0$ and $\gamma h=0.712$. Note that when the friction coefficient η is positive, the contact end at $y=a$ becomes the trailing end of the contact and the normalized lateral contact stress $\sigma_{yy}(0, y)/(P/(b-a))$ has sharp transitions at that point. However, when the friction coefficient is negative, the contact end at $y=a$ becomes the leading end of the contact and the normalized lateral stress $\sigma_{yy}(0, y)/(P/(b-a))$ has smooth transitions at that point. Examining

Figure 4.37, the effect of the friction coefficient η on the lateral contact stress is very remarkable. The larger the absolute value of the friction coefficient is, the greater the normalized lateral contact stress around the trailing and the leading ends. Figure 4.38 is provided to demonstrate the influences of the normalized contact length $(b-a)/h$ on the normalized lateral contact stress $\sigma_{yy}(0, y)/(P/(b-a))$ for $\eta=0.3$ and $\gamma h=0.712$. As seen in the figure, when the normalized contact length $(b-a)/h$ is increased from 0.1 to 1.0, the magnitude of the lateral contact stress decreases slightly on and outside the contact zone. Thus we can conclude that the size of the coating thickness relative to the contact length can be decreased to reduce the possibility of damage due to the herringbone cracks near the trailing end. Figure 4.39 shows the influences of elastic modulus ratio E_x/E_y on the normalized lateral contact stress $\sigma_{yy}(0, y)/(P/(b-a))$ for $\eta=0.3$ and $\gamma h=0.712$. As can be seen in this figure, the effect of elastic modulus ratio E_x/E_y on normalized lateral contact stress $\sigma_{yy}(0, y)/(P/(b-a))$ is very significant on and outside the contact zone. If E_x/E_y is increased from 0.6 to 1.5, it is observed that the magnitude of the lateral contact stress decreases remarkably. Hence, the option of increasing the ratio E_x/E_y can be used in the graded coating so as to prevent the risk of damage around the trailing end of the contact region. Figure 4.40 shows the effect of Elastic modulus ratio E_x/E_z on the normalized lateral contact stress $\sigma_{yy}(0, y)/(P/(b-a))$ for $\eta=0.3$, $(b-a)/h=1.0$ and $\gamma h=0.712$. As observed in this figure, variation of the elastic modulus ratio E_x/E_z has no significant effect on the normalized lateral contact stress $\sigma_{yy}(0, y)/(P/(b-a))$.

4.4 Homogeneous coating

The surface and interfacial contact stresses of an orthotropic homogeneous coating under the action of complete contact loadings are given in Figures 4.42-4.52. The view of the circular stamp problem is presented in Figure 4.41. The comparisons of the normalized contact and the lateral contact stresses evaluated utilizing the

analytic and FE techniques are presented for various problem parameters in Figures 4.42-4.44: $(b-a)/h=1.0$ and $E_x/E_y=1.3$ (Alumina) in Figure 4.42. $(b-a)/h=0.4$ and $E_x/E_y=1.3$ (Alumina) in Figure 4.43. $(b-a)/h=1.0$, $E_x/E_y=1.5$ in Figure 4.44. It can be inferred from these figures that the results of analytical and computational methods agree with each other for various problem parameters, which is the indication of the accuracy for both methods. Some detailed results showing the influences of problem parameters on surface contact stresses are also given. Figure 4.45 demonstrates the effects of friction coefficient η on the normalized contact stress $\sigma_{xx}(0, y)/(P/(b-a))$ and on the lateral contact stress $\sigma_{yy}(0, y)/(P/(b-a))$. Observing Figure 4.45a the contact stress $\sigma_{xx}(0, y)/(P/(b-a))$ slants toward the positive y-direction, as the friction coefficient η is raised from 0 to 0.45. Figure 4.45b reveals that the magnitude of the lateral contact stress $\sigma_{yy}(0, y)/(P/(b-a))$ elevates as the friction coefficient η is raised from 0 to 0.6. Figure 4.46 illustrates the effects of the normalized contact length $(b-a)/h$ on the normalized contact stress $\sigma_{xx}(0, y)/(P/(b-a))$ and on the lateral contact stress $\sigma_{yy}(0, y)/(P/(b-a))$. One can infer from Figure 4.46 that the variation of the normalized contact length $(b-a)/h$ has no effect on the contact stresses. Figure 4.47 shows the effects the variations in the elastic modulus ratio E_x/E_y on the normalized contact stress $\sigma_{xx}(0, y)/(P/(b-a))$ and the lateral contact stress $\sigma_{yy}(0, y)/(P/(b-a))$. Observing Figure 4.47a the contact stress $\sigma_{xx}(0, y)/(P/(b-a))$ slants toward the positive y-direction, as the elastic modulus ratio E_x/E_y is increased from 0.6 to 1.5. Figure 4.47b reveals that the magnitude of the lateral contact stress $\sigma_{yy}(0, y)/(P/(b-a))$ decreases significantly as the elastic modulus ratio E_x/E_y is increased from 0.6 to 1.5. Thus the option of selecting orthotropic materials having higher E_x/E_y ratio can be assessed to prevent surface crackings. Figure 4.48 reveals the influences of the elastic modulus ratio E_x/E_z on the normalized contact stress $\sigma_{xx}(0, y)/(P/(b-a))$ and on the lateral contact stress $\sigma_{yy}(0, y)/(P/(b-a))$. It can

be inferred from this figure that the variation of the elastic modulus ratio E_x/E_z has no significant influence on the contact stresses. Figure 4.49 demonstrates the effects of friction coefficient on the normalized interfacial contact stress $\sigma_{xx}(h, y)/(P/(b-a))$ and on the interfacial shear stress $\sigma_{xy}(h, y)/(P/(b-a))$. Examining Figure 4.49a, the magnitude of the contact stress $\sigma_{xx}(h, y)/(P/(b-a))$ increases remarkably, as the friction coefficient η is raised from 0 to 0.6. Figure 4.49b illustrates that the magnitude of the interfacial shear stress $\sigma_{xy}(h, y)/(P/(b-a))$ increases significantly as the friction coefficient η is raised from 0 to 0.6. Figure 4.50 reveals the effect of the normalized contact length $(b-a)/h$ on the normalized interfacial contact stress $\sigma_{xx}(h, y)/(P/(b-a))$ and on the interfacial shear stress $\sigma_{xy}(h, y)/(P/(b-a))$. Observing Figure 4.50, the magnitude of the interfacial contact stresses $\sigma_{xx}(h, y)/(P/(b-a))$ and $\sigma_{xy}(h, y)/(P/(b-a))$ increase remarkably, as the normalized contact length $(b-a)/h$ is raised from 0.4 to 0.7. In Figure 4.51, the influences of the elastic modulus ratio E_x/E_y on the normalized interfacial contact stress $\sigma_{xx}(h, y)/(P/(b-a))$ and on the interfacial shear stress $\sigma_{xy}(h, y)/(P/(b-a))$ are plotted. As seen in Figure 4.51, the magnitude of the interfacial contact stresses $\sigma_{xx}(h, y)/(P/(b-a))$ and $\sigma_{xy}(h, y)/(P/(b-a))$ increase remarkably, as the elastic modulus ratio E_x/E_y is increased from 0.6 to 1.5. Figure 4.52 illustrates the influences of the elastic modulus ratio E_x/E_z on the normalized interfacial contact stress $\sigma_{xx}(h, y)/(P/(b-a))$ and on the interfacial shear stress $\sigma_{xy}(h, y)/(P/(b-a))$. It can be inferred from this figure that the variation of the elastic modulus ratio E_x/E_z has no significant influence on the interfacial contact stresses.

4.5 Tables

Table 4.1: Convergence of the normalized contact stresses evaluated for various values of γh , N and r regarding the flat stamp, $\eta = 0.3$, $(b - a)/h = 0.4$, $r = (2y - (b + a))/(b - a)$.

| | N | $\frac{\sigma_{xx}(0, y)}{P/(b - a)}$ | | |
|------------|-----|---------------------------------------|------------------|------------------|
| | | $\gamma h = 0.1$ | $\gamma h = 0.6$ | $\gamma h = 1.0$ |
| $r = -0.6$ | 1 | -0.828 | -0.821 | -0.815 |
| | 2 | -0.831 | -0.838 | -0.843 |
| | 4 | -0.832 | -0.845 | -0.853 |
| | 6 | -0.832 | -0.843 | -0.850 |
| | 10 | -0.832 | -0.843 | -0.850 |
| | 14 | -0.832 | -0.843 | -0.850 |
| $r = 0.6$ | 1 | -0.755 | -0.763 | -0.770 |
| | 2 | -0.756 | -0.774 | -0.786 |
| | 4 | -0.757 | -0.776 | -0.790 |
| | 6 | -0.757 | -0.775 | -0.789 |
| | 10 | -0.757 | -0.775 | -0.789 |
| | 14 | -0.757 | -0.775 | -0.789 |

Table 4.2: Convergence of the normalized contact stresses evaluated for various values of γh , N and r regarding the flat stamp, $\eta=0.3$, $(b-a)/h=1.0$, $r = (2y - (b+a))/(b-a)$.

| | N | $\frac{\sigma_{xx}(0, y)}{P/(b-a)}$ | | |
|------------|-----|-------------------------------------|----------------|----------------|
| | | $\gamma h=0.1$ | $\gamma h=0.6$ | $\gamma h=1.0$ |
| $r = -0.6$ | 1 | -0.828 | -0.820 | -0.814 |
| | 2 | -0.831 | -0.848 | -0.859 |
| | 4 | -0.835 | -0.865 | -0.882 |
| | 6 | -0.834 | -0.861 | -0.876 |
| | 10 | -0.834 | -0.861 | -0.876 |
| | 14 | -0.834 | -0.861 | -0.876 |
| $r = 0.6$ | 1 | -0.755 | -0.764 | -0.771 |
| | 2 | -0.758 | -0.783 | -0.801 |
| | 4 | -0.759 | -0.789 | -0.810 |
| | 6 | -0.759 | -0.787 | -0.806 |
| | 10 | -0.759 | -0.787 | -0.807 |
| | 14 | -0.759 | -0.787 | -0.807 |

Table 4.3: Normalized forces $P/(\mu_{xy} \tan(\theta)(b-a))$ evaluated for various magnitudes of the friction coefficient η , the normalized non-homogeneity constant γh and the normalized contact length $(b-a)/h$ regarding the triangular stamp for which the coating surface is Alumina

| | | P | | | | |
|-----------------|------|------------------------------|------------------|------------------|------------------|------------------|
| | | $\mu_{xy} \tan(\theta)(b-a)$ | | | | |
| | | η | $\gamma h = 0.1$ | $\gamma h = 0.4$ | $\gamma h = 0.7$ | $\gamma h = 1.0$ |
| $(b-a)/h = 0.4$ | -0.6 | 2.034 | 2.222 | 2.416 | 2.615 | |
| | -0.3 | 2.193 | 2.383 | 2.578 | 2.776 | |
| | 0.0 | 2.354 | 2.543 | 2.735 | 2.929 | |
| | 0.3 | 2.513 | 2.698 | 2.883 | 3.070 | |
| | 0.6 | 2.668 | 2.843 | 3.019 | 3.195 | |
| $(b-a)/h = 0.7$ | -0.6 | 2.054 | 2.335 | 2.635 | 2.954 | |
| | -0.3 | 2.213 | 2.504 | 2.813 | 3.136 | |
| | 0.0 | 2.375 | 2.674 | 2.987 | 3.312 | |
| | 0.3 | 2.534 | 2.838 | 3.153 | 3.476 | |
| | 0.6 | 2.688 | 2.994 | 3.308 | 3.627 | |
| $(b-a)/h = 1.0$ | -0.6 | 2.066 | 2.414 | 2.799 | 3.219 | |
| | -0.3 | 2.224 | 2.590 | 2.991 | 3.424 | |
| | 0.0 | 2.384 | 2.767 | 3.182 | 3.624 | |
| | 0.3 | 2.542 | 2.940 | 3.366 | 3.814 | |
| | 0.6 | 2.693 | 3.105 | 3.541 | 3.996 | |

Table 4.4: Normalized forces $P/(\mu_{xy} \tan(\theta)(b-a))$ evaluated for various magnitudes of the friction coefficient η , the normalized non-homogeneity parameter γh and the normalized contact length $(b-a)/h$ regarding the triangular stamp, $E_x/E_y=0.6$.

| | | P | | | |
|-----------------|---------|------------------------------|------------------|------------------|------------------|
| | | $\mu_{xy} \tan(\theta)(b-a)$ | | | |
| | | $\gamma h = 0.1$ | $\gamma h = 0.4$ | $\gamma h = 0.7$ | $\gamma h = 1.0$ |
| $(b-a)/h = 0.4$ | -0.60 | 2.343 | 2.549 | 2.761 | 2.977 |
| | -0.30 | 2.448 | 2.650 | 2.857 | 3.066 |
| | 0.00 | 2.554 | 2.751 | 2.950 | 3.151 |
| | 0.30 | 2.660 | 2.849 | 3.040 | 3.232 |
| | 0.60 | 2.766 | 2.945 | 3.125 | 3.306 |
| $(b-a)/h = 0.7$ | -0.60 | 2.356 | 2.668 | 3.002 | 3.354 |
| | -0.30 | 2.463 | 2.777 | 3.108 | 3.455 |
| | 0.00 | 2.572 | 2.885 | 3.213 | 3.553 |
| | 0.30 | 2.681 | 2.992 | 3.315 | 3.648 |
| | 0.60 | 2.790 | 3.098 | 3.414 | 3.736 |
| $(b-a)/h = 1.0$ | -0.60 | 2.359 | 2.751 | 3.182 | 3.652 |
| | -0.30 | 2.468 | 2.866 | 3.301 | 3.770 |
| | 0.00 | 2.578 | 2.983 | 3.420 | 3.887 |
| | 0.30 | 2.689 | 3.099 | 3.538 | 4.001 |
| | 0.60 | 2.800 | 3.224 | 3.653 | 4.111 |

Table 4.5: Normalized forces $P/(\mu_{xy} \tan(\theta)(b-a))$ evaluated for various magnitudes of the friction coefficient η , the normalized non-homogeneity parameter γh and the normalized contact length $(b-a)/h$ regarding the triangular stamp, $E_x/E_y = 1.5$.

| | | P | | | | |
|-----------------|--|------------------------------|------------------|------------------|------------------|------------------|
| | | $\mu_{xy} \tan(\theta)(b-a)$ | | | | |
| | | η | $\gamma h = 0.1$ | $\gamma h = 0.4$ | $\gamma h = 0.7$ | $\gamma h = 1.0$ |
| $(b-a)/h = 0.4$ | | -0.60 | 1.970 | 2.155 | 2.345 | 2.540 |
| | | -0.30 | 2.139 | 2.327 | 2.519 | 2.715 |
| | | 0.00 | 2.311 | 2.499 | 2.689 | 2.882 |
| | | 0.30 | 2.481 | 2.664 | 2.849 | 3.034 |
| | | 0.60 | 2.643 | 2.818 | 2.992 | 3.167 |
| $(b-a)/h = 0.7$ | | -0.60 | 1.993 | 2.267 | 2.560 | 2.873 |
| | | -0.30 | 2.162 | 2.448 | 2.751 | 3.071 |
| | | 0.00 | 2.333 | 2.629 | 2.939 | 3.262 |
| | | 0.30 | 2.502 | 2.804 | 3.116 | 3.438 |
| | | 0.60 | 2.663 | 2.968 | 3.280 | 3.597 |
| $(b-a)/h = 1.0$ | | -0.60 | 2.007 | 2.347 | 2.722 | 3.133 |
| | | -0.30 | 2.175 | 2.534 | 2.928 | 3.354 |
| | | 0.00 | 2.344 | 2.723 | 3.132 | 3.570 |
| | | 0.30 | 2.510 | 2.905 | 3.327 | 3.772 |
| | | 0.60 | 2.666 | 3.076 | 3.510 | 3.963 |

Table 4.6: Normalized forces $P/(\mu_{xy} \tan(\theta)(b-a))$ evaluated for various magnitudes of the friction coefficient η , the normalized non-homogeneity parameter γh and the normalized contact length $(b-a)/h$ regarding the triangular stamp, $E_x/E_z = 0.6$.

| | | P | | | |
|-----------------|---------|------------------------------|------------------|------------------|------------------|
| | | $\mu_{xy} \tan(\theta)(b-a)$ | | | |
| | | $\gamma h = 0.1$ | $\gamma h = 0.4$ | $\gamma h = 0.7$ | $\gamma h = 1.0$ |
| $(b-a)/h = 0.4$ | -0.60 | 2.116 | 2.319 | 2.528 | 2.741 |
| | -0.30 | 2.283 | 2.488 | 2.698 | 2.910 |
| | 0.00 | 2.454 | 2.658 | 2.864 | 3.072 |
| | 0.30 | 2.623 | 2.822 | 3.021 | 3.222 |
| | 0.60 | 2.788 | 2.978 | 3.166 | 3.355 |
| $(b-a)/h = 0.7$ | -0.60 | 2.130 | 2.433 | 2.756 | 3.097 |
| | -0.30 | 2.298 | 2.613 | 2.944 | 3.292 |
| | 0.00 | 2.470 | 2.794 | 3.131 | 3.481 |
| | 0.30 | 2.641 | 2.971 | 3.310 | 3.659 |
| | 0.60 | 2.807 | 3.140 | 3.479 | 3.826 |
| $(b-a)/h = 1.0$ | -0.60 | 2.133 | 2.505 | 2.914 | 3.361 |
| | -0.30 | 2.300 | 2.692 | 3.119 | 3.578 |
| | 0.00 | 2.469 | 2.880 | 3.323 | 3.793 |
| | 0.30 | 2.637 | 3.066 | 3.521 | 3.998 |
| | 0.60 | 2.799 | 3.245 | 3.712 | 4.196 |

Table 4.7: Normalized forces $P/(\mu_{xy} \tan(\theta)(b-a))$ evaluated for various magnitudes of the friction coefficient η , the normalized non-homogeneity parameter γh and the normalized contact length $(b-a)/h$ regarding the triangular stamp, $E_x/E_z = 3.0$.

| | η | P | | | |
|-----------------|--------|------------------------------|------------------|------------------|------------------|
| | | $\mu_{xy} \tan(\theta)(b-a)$ | | | |
| | | $\gamma h = 0.1$ | $\gamma h = 0.4$ | $\gamma h = 0.7$ | $\gamma h = 1.0$ |
| $(b-a)/h = 0.4$ | -0.60 | 2.004 | 2.187 | 2.375 | 2.567 |
| | -0.30 | 2.158 | 2.342 | 2.531 | 2.772 |
| | 0.00 | 2.313 | 2.497 | 2.682 | 2.870 |
| | 0.30 | 2.467 | 2.645 | 2.825 | 3.005 |
| | 0.60 | 2.615 | 2.785 | 2.955 | 3.126 |
| $(b-a)/h = 0.7$ | -0.60 | 2.027 | 2.300 | 2.592 | 2.901 |
| | -0.30 | 2.181 | 2.463 | 2.763 | 3.076 |
| | 0.00 | 2.336 | 2.626 | 2.930 | 3.245 |
| | 0.30 | 2.490 | 2.784 | 3.089 | 3.401 |
| | 0.60 | 2.637 | 2.933 | 3.237 | 3.545 |
| $(b-a)/h = 1.0$ | -0.60 | 2.042 | 2.382 | 2.757 | 3.166 |
| | -0.30 | 2.195 | 2.552 | 2.942 | 3.362 |
| | 0.00 | 2.350 | 2.722 | 3.124 | 3.553 |
| | 0.30 | 2.501 | 2.887 | 3.300 | 3.734 |
| | 0.60 | 2.646 | 3.045 | 3.467 | 3.907 |

Table 4.8: Normalized forces $P/(\mu_{xy}(b-a))$ evaluated for various magnitudes of the friction coefficient η , the normalized non-homogeneity parameter γh and the normalized contact length $(b-a)/h$ regarding the circular stamp, for which the coating surface is Alumina, $a/R=0$, $b/R=0.02$.

| | η | $\frac{P}{\mu_{xy}(b-a)}$ | | | |
|-----------------|--------|---------------------------|------------------|------------------|------------------|
| | | $\gamma h = 0.1$ | $\gamma h = 0.4$ | $\gamma h = 0.7$ | $\gamma h = 1.0$ |
| $(b-a)/h = 0.4$ | 0.00 | 0.01169 | 0.01235 | 0.01300 | 0.01366 |
| | 0.15 | 0.01168 | 0.01233 | 0.01299 | 0.01365 |
| | 0.30 | 0.01163 | 0.01229 | 0.01294 | 0.01360 |
| | 0.45 | 0.01156 | 0.01221 | 0.01286 | 0.01352 |
| | 0.60 | 0.01146 | 0.01211 | 0.01276 | 0.01341 |
| $(b-a)/h = 0.7$ | 0.00 | 0.01179 | 0.01285 | 0.01394 | 0.01506 |
| | 0.15 | 0.01177 | 0.01283 | 0.01393 | 0.01504 |
| | 0.30 | 0.01173 | 0.01279 | 0.01388 | 0.01499 |
| | 0.45 | 0.01166 | 0.01271 | 0.01380 | 0.01491 |
| | 0.60 | 0.01156 | 0.01261 | 0.01368 | 0.01479 |
| $(b-a)/h = 1.0$ | 0.00 | 0.01185 | 0.01325 | 0.01473 | 0.01628 |
| | 0.15 | 0.01183 | 0.01324 | 0.01472 | 0.01626 |
| | 0.30 | 0.01179 | 0.01319 | 0.01466 | 0.01621 |
| | 0.45 | 0.01172 | 0.01311 | 0.01458 | 0.01612 |
| | 0.60 | 0.01162 | 0.01300 | 0.01447 | 0.01600 |

Table 4.9: Normalized forces $P/(\mu_{xy}(b-a))$ evaluated for various magnitudes of the friction coefficient η , the normalized non-homogeneity parameter γh and the normalized contact length $(b-a)/h$ regarding the circular stamp, $a/R=0$, $b/R=0.02$, $E_x/E_y=0.6$.

| | | $\frac{P}{\mu_{xy}(b-a)}$ | | | |
|-----------------|------|---------------------------|------------------|------------------|------------------|
| η | | $\gamma h = 0.1$ | $\gamma h = 0.4$ | $\gamma h = 0.7$ | $\gamma h = 1.0$ |
| $(b-a)/h = 0.4$ | 0.00 | 0.01270 | 0.01337 | 0.01405 | 0.01474 |
| | 0.15 | 0.01269 | 0.01337 | 0.01405 | 0.01473 |
| | 0.30 | 0.01267 | 0.01335 | 0.01403 | 0.01471 |
| | 0.45 | 0.01265 | 0.01332 | 0.01400 | 0.01468 |
| | 0.60 | 0.01261 | 0.01329 | 0.01396 | 0.01464 |
| $(b-a)/h = 1.0$ | 0.00 | 0.01283 | 0.01431 | 0.01586 | 0.01748 |
| | 0.15 | 0.01283 | 0.01430 | 0.01585 | 0.01747 |
| | 0.30 | 0.01281 | 0.01428 | 0.01583 | 0.01745 |
| | 0.45 | 0.01279 | 0.01426 | 0.01581 | 0.01742 |
| | 0.60 | 0.01275 | 0.01422 | 0.01577 | 0.01738 |

Table 4.10: Normalized forces $P/(\mu_{xy}(b-a))$ evaluated for various values of the friction coefficient η , the normalized non-homogeneity parameter γh and the normalized contact length $(b-a)/h$ regarding the circular stamp, $a/R=0$, $b/R=0.02$, $E_x/E_y=1.5$.

| | η | $\frac{P}{\mu_{xy}(b-a)}$ | | | |
|-----------------|--------|---------------------------|------------------|------------------|------------------|
| | | $\gamma h = 0.1$ | $\gamma h = 0.4$ | $\gamma h = 0.7$ | $\gamma h = 1.0$ |
| $(b-a)/h = 0.4$ | 0.00 | 0.01150 | 0.01213 | 0.01278 | 0.01343 |
| | 0.15 | 0.01146 | 0.01211 | 0.01276 | 0.01341 |
| | 0.30 | 0.01141 | 0.01206 | 0.01270 | 0.01336 |
| | 0.45 | 0.01133 | 0.01197 | 0.01261 | 0.01326 |
| | 0.60 | 0.01121 | 0.01185 | 0.01249 | 0.01313 |
| $(b-a)/h = 1.0$ | 0.00 | 0.01164 | 0.01303 | 0.01449 | 0.01602 |
| | 0.15 | 0.01162 | 0.01301 | 0.01447 | 0.01600 |
| | 0.30 | 0.01157 | 0.01295 | 0.01441 | 0.01594 |
| | 0.45 | 0.01149 | 0.01286 | 0.01431 | 0.01583 |
| | 0.60 | 0.01137 | 0.01274 | 0.01418 | 0.01569 |

Table 4.11: Normalized forces $P/(\mu_{xy}(b-a))$ evaluated for various magnitudes of the friction coefficient η , the normalized non-homogeneity parameter γh and the normalized contact length $(b-a)/h$ regarding the circular stamp, $a/R=0$, $b/R=0.02$, $E_x/E_z = 0.6$.

| | | $\frac{P}{\mu_{xy}(b-a)}$ | | | |
|-----------------|--------|---------------------------|------------------|------------------|------------------|
| | η | | | | |
| | | $\gamma h = 0.1$ | $\gamma h = 0.4$ | $\gamma h = 0.7$ | $\gamma h = 1.0$ |
| $(b-a)/h = 0.4$ | 0.00 | 0.01220 | 0.01290 | 0.01361 | 0.01432 |
| | 0.15 | 0.01218 | 0.01289 | 0.01359 | 0.01430 |
| | 0.30 | 0.01214 | 0.01284 | 0.01354 | 0.01425 |
| | 0.45 | 0.01206 | 0.01276 | 0.01346 | 0.01417 |
| | 0.60 | 0.01196 | 0.01265 | 0.01335 | 0.01405 |
| $(b-a)/h = 1.0$ | 0.00 | 0.01232 | 0.01382 | 0.01540 | 0.01707 |
| | 0.15 | 0.01230 | 0.01380 | 0.01539 | 0.01705 |
| | 0.30 | 0.01226 | 0.01375 | 0.01534 | 0.01699 |
| | 0.45 | 0.01218 | 0.01367 | 0.01525 | 0.01690 |
| | 0.60 | 0.01208 | 0.01356 | 0.01513 | 0.01677 |

Table 4.12: Normalized forces $P/(\mu_{xy}(b-a))$ evaluated for various magnitudes of the coefficient of friction η , the normalized non-homogeneity parameter γh and the normalized contact length $(b-a)/h$ regarding the circular stamp, $a/R=0$, $b/R=0.02$, $E_x/E_z=3.0$.

| | η | $\frac{P}{\mu_{xy}(b-a)}$ | | | |
|---------------|--------|---------------------------|----------------|----------------|----------------|
| | | $\gamma h=0.1$ | $\gamma h=0.4$ | $\gamma h=0.7$ | $\gamma h=1.0$ |
| $(b-a)/h=0.4$ | 0.00 | 0.01149 | 0.01212 | 0.01276 | 0.01339 |
| | 0.15 | 0.01147 | 0.01211 | 0.01274 | 0.01338 |
| | 0.30 | 0.01143 | 0.01206 | 0.01270 | 0.01333 |
| | 0.45 | 0.01136 | 0.01199 | 0.01262 | 0.01325 |
| | 0.60 | 0.01127 | 0.01189 | 0.01252 | 0.01315 |
| $(b-a)/h=1.0$ | 0.00 | 0.01166 | 0.01302 | 0.01445 | 0.01594 |
| | 0.15 | 0.01164 | 0.01300 | 0.01444 | 0.01593 |
| | 0.30 | 0.01160 | 0.01296 | 0.01439 | 0.01588 |
| | 0.45 | 0.01153 | 0.01288 | 0.01431 | 0.01580 |
| | 0.60 | 0.01144 | 0.01278 | 0.01420 | 0.01568 |

Table 4.13: Centerline position c/R of the circular stamp problem for various magnitudes of the friction coefficient η , the normalized non-homogeneity parameter γh and normalized contact length $(b-a)/h$, $a/R=0$, $b/R=0.02$, for which the coating surface is Alumina.

| | η | c/R | | | |
|-----------------|--------|------------------|------------------|------------------|------------------|
| | | $\gamma h = 0.1$ | $\gamma h = 0.4$ | $\gamma h = 0.7$ | $\gamma h = 1.0$ |
| $(b-a)/h = 0.4$ | 0.00 | 0.01000 | 0.01000 | 0.01000 | 0.01000 |
| | 0.15 | 0.01035 | 0.01032 | 0.01030 | 0.01028 |
| | 0.30 | 0.01070 | 0.01064 | 0.01059 | 0.01055 |
| | 0.45 | 0.01103 | 0.01095 | 0.01088 | 0.01082 |
| | 0.60 | 0.01136 | 0.01126 | 0.01117 | 0.01109 |
| $(b-a)/h = 0.7$ | 0.00 | 0.01000 | 0.01000 | 0.01000 | 0.01000 |
| | 0.15 | 0.01034 | 0.01032 | 0.01029 | 0.01027 |
| | 0.30 | 0.01068 | 0.01063 | 0.01058 | 0.01053 |
| | 0.45 | 0.01102 | 0.01094 | 0.01087 | 0.01079 |
| | 0.60 | 0.01135 | 0.01125 | 0.01115 | 0.01105 |
| $(b-a)/h = 1.0$ | 0.00 | 0.01000 | 0.01000 | 0.01000 | 0.01000 |
| | 0.15 | 0.01034 | 0.01032 | 0.01029 | 0.01027 |
| | 0.30 | 0.01068 | 0.01063 | 0.01058 | 0.01053 |
| | 0.45 | 0.01102 | 0.01094 | 0.01087 | 0.01079 |
| | 0.60 | 0.01135 | 0.01125 | 0.01115 | 0.01105 |

Table 4.14: Centerline position c/R of the circular stamp problem for various magnitudes of friction coefficient η , the normalized non-homogeneity parameter γh and normalized contact length $(b-a)/h$, $a/R=0$, $b/R=0.02$, $E_x/E_y=0.6$.

| | η | c/R | | | |
|-----------------|--------|------------------|------------------|------------------|------------------|
| | | $\gamma h = 0.1$ | $\gamma h = 0.4$ | $\gamma h = 0.7$ | $\gamma h = 1.0$ |
| $(b-a)/h = 0.4$ | 0.00 | 0.01000 | 0.01000 | 0.01000 | 0.01000 |
| | 0.15 | 0.01021 | 0.01019 | 0.01017 | 0.01015 |
| | 0.30 | 0.01041 | 0.01037 | 0.01034 | 0.01030 |
| | 0.45 | 0.01062 | 0.01056 | 0.01050 | 0.01045 |
| | 0.60 | 0.01082 | 0.01074 | 0.01067 | 0.01060 |
| $(b-a)/h = 1.0$ | 0.00 | 0.01000 | 0.01000 | 0.01000 | 0.01000 |
| | 0.15 | 0.01021 | 0.01019 | 0.01017 | 0.01015 |
| | 0.30 | 0.01042 | 0.01037 | 0.01033 | 0.01029 |
| | 0.45 | 0.01063 | 0.01056 | 0.01049 | 0.01043 |
| | 0.60 | 0.01084 | 0.01074 | 0.01066 | 0.01057 |

Table 4.15: Centerline position c/R of the circular stamp problem for various magnitudes of the friction coefficient η , the normalized non-homogeneity parameter γh and normalized contact length $(b-a)/h$, $a/R=0$, $b/R=0.02$, $E_x/E_y=1.5$.

| | η | c/R | | | |
|-----------------|--------|------------------|------------------|------------------|------------------|
| | | $\gamma h = 0.1$ | $\gamma h = 0.4$ | $\gamma h = 0.7$ | $\gamma h = 1.0$ |
| $(b-a)/h = 0.4$ | 0.00 | 0.01000 | 0.01000 | 0.01000 | 0.01000 |
| | 0.15 | 0.01038 | 0.01035 | 0.01033 | 0.01030 |
| | 0.30 | 0.01075 | 0.01070 | 0.01065 | 0.01061 |
| | 0.45 | 0.01112 | 0.01104 | 0.01097 | 0.01090 |
| | 0.60 | 0.01148 | 0.01138 | 0.01128 | 0.01119 |
| $(b-a)/h = 1.0$ | 0.00 | 0.01000 | 0.01000 | 0.01000 | 0.01000 |
| | 0.15 | 0.01037 | 0.01034 | 0.01032 | 0.01029 |
| | 0.30 | 0.01074 | 0.01069 | 0.01063 | 0.01058 |
| | 0.45 | 0.01110 | 0.01102 | 0.01095 | 0.01087 |
| | 0.60 | 0.01145 | 0.01135 | 0.01125 | 0.01115 |

Table 4.16: Centerline position c/R of the circular stamp problem for various magnitudes of the friction coefficient η , the normalized non-homogeneity parameter γh and normalized contact length $(b-a)/h$, $a/R=0$, $b/R=0.02$, $E_x/E_z = 0.6$.

| | η | c/R | | | |
|-----------------|--------|------------------|------------------|------------------|------------------|
| | | $\gamma h = 0.1$ | $\gamma h = 0.4$ | $\gamma h = 0.7$ | $\gamma h = 1.0$ |
| $(b-a)/h = 0.4$ | 0.00 | 0.01000 | 0.01000 | 0.01000 | 0.01000 |
| | 0.15 | 0.01035 | 0.01032 | 0.01030 | 0.01028 |
| | 0.30 | 0.01070 | 0.01064 | 0.01060 | 0.01055 |
| | 0.45 | 0.01104 | 0.01096 | 0.01089 | 0.01082 |
| | 0.60 | 0.01137 | 0.01127 | 0.01118 | 0.01109 |
| $(b-a)/h = 1.0$ | 0.00 | 0.01000 | 0.01000 | 0.01000 | 0.01000 |
| | 0.15 | 0.01035 | 0.01032 | 0.01030 | 0.01028 |
| | 0.30 | 0.01069 | 0.01064 | 0.01060 | 0.01054 |
| | 0.45 | 0.01103 | 0.01096 | 0.01088 | 0.01080 |
| | 0.60 | 0.01137 | 0.01127 | 0.01117 | 0.01107 |

Table 4.17: Centerline position c/R of the circular stamp problem for various magnitudes of the friction coefficient η , the normalized non-homogeneity parameter γh and normalized contact length $(b-a)/h$, $a/R=0$, $b/R=0.02$, $E_x/E_z = 3.0$.

| | | c/R | | | |
|-----------------|------|------------------|------------------|------------------|------------------|
| η | | | | | |
| | | $\gamma h = 0.1$ | $\gamma h = 0.4$ | $\gamma h = 0.7$ | $\gamma h = 1.0$ |
| $(b-a)/h = 0.4$ | 0.00 | 0.01000 | 0.01000 | 0.01000 | 0.01000 |
| | 0.15 | 0.01034 | 0.01032 | 0.01029 | 0.01027 |
| | 0.30 | 0.01068 | 0.01063 | 0.01058 | 0.01054 |
| | 0.45 | 0.01101 | 0.01094 | 0.01087 | 0.01081 |
| | 0.60 | 0.01134 | 0.01124 | 0.01116 | 0.01107 |
| $(b-a)/h = 1.0$ | 0.00 | 0.01000 | 0.01000 | 0.01000 | 0.01000 |
| | 0.15 | 0.01034 | 0.01031 | 0.01029 | 0.01026 |
| | 0.30 | 0.01067 | 0.01062 | 0.01057 | 0.01052 |
| | 0.45 | 0.01100 | 0.01092 | 0.01085 | 0.01078 |
| | 0.60 | 0.01132 | 0.01122 | 0.01113 | 0.01103 |

4.6 Figures

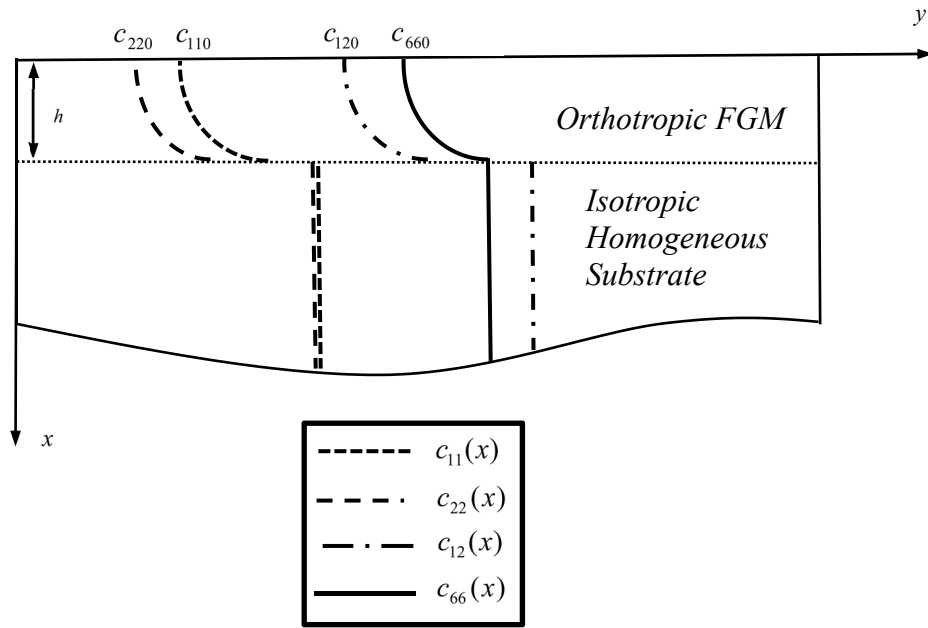


Figure 4.1: Gradation of orthotropic stiffness constants for $\gamma h > 0.0$.

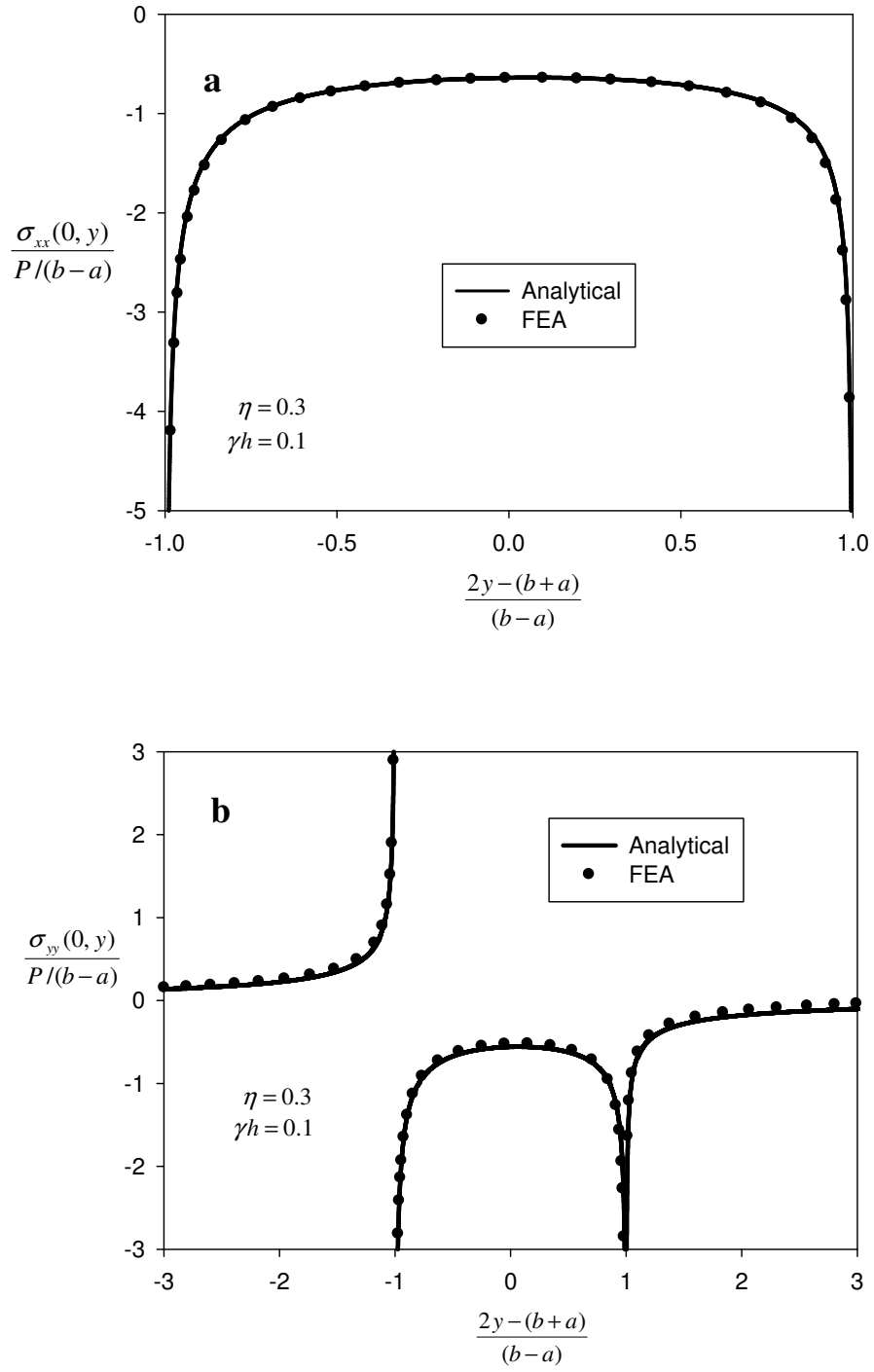


Figure 4.2: Comparison plots of the normalized stresses evaluated by the analytical and computational procedures for a flat stamp problem, $(b-a)/h = 1.0$, $\eta = 0.3$, $\gamma h = 0.1$. a) Normalized contact stress, b) Normalized lateral contact stress.

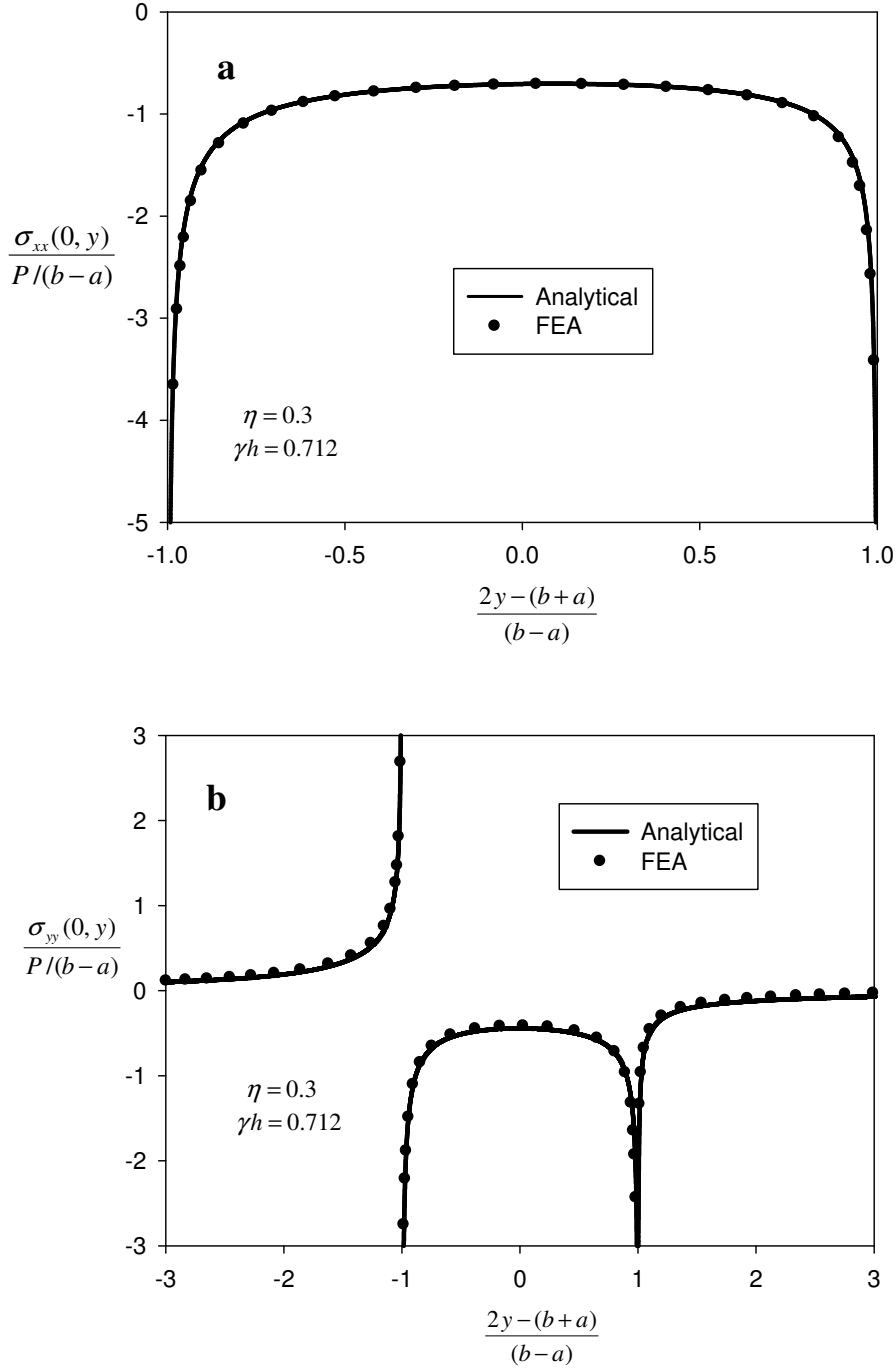


Figure 4.3: Comparison plots of the normalized stresses evaluated by the analytical and computational procedures for a flat stamp problem, $(b-a)/h = 1.0$, $\eta = 0.3$, $\gamma h = 0.712$. a) Normalized contact stress, b) Normalized lateral contact stress.

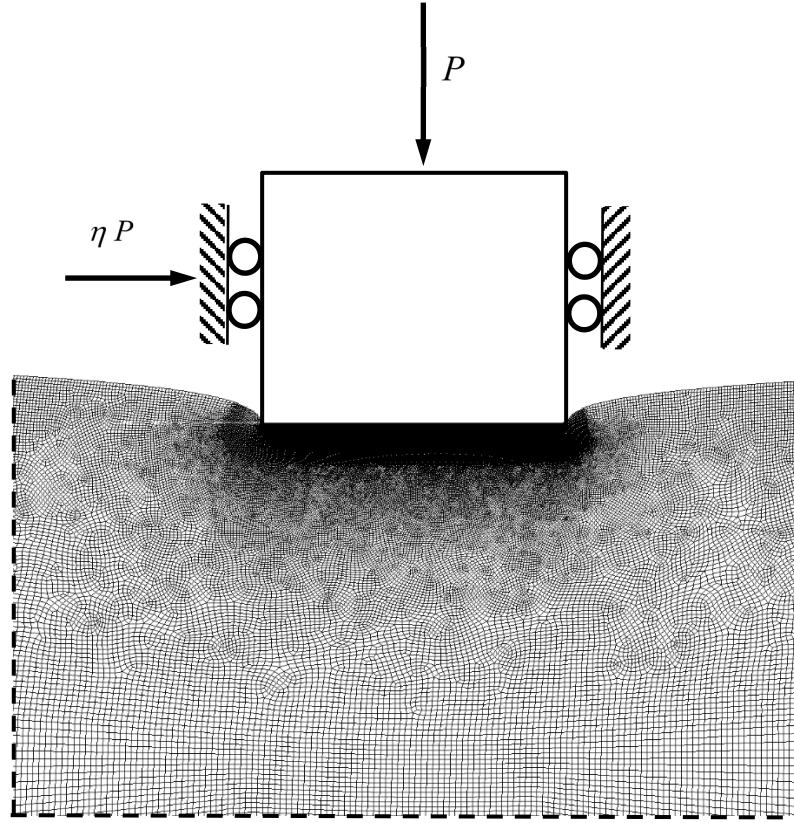


Figure 4.4: Scaled deformed shape of the contact region, which is produced by using the FE solution of a flat stamp problem, $(b - a)/h = 1.0$, $\eta = 0.3$, $\gamma h = 0.712$.

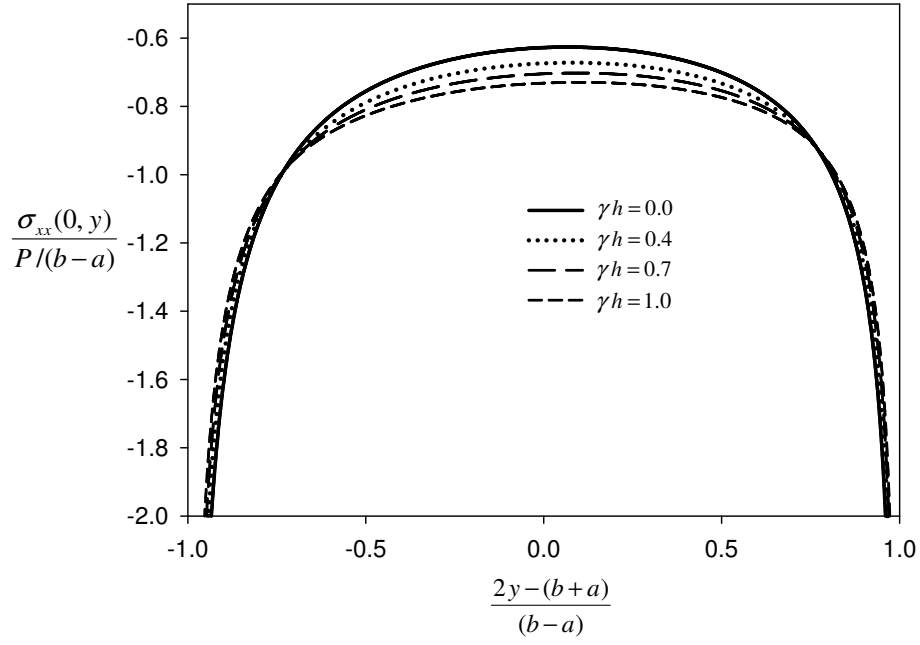


Figure 4.5: Effect of normalized non-homogeneity parameter γh variations on the normalized contact stress for a flat stamp problem, $(b - a)/h = 1.0$, $\eta = 0.3$.

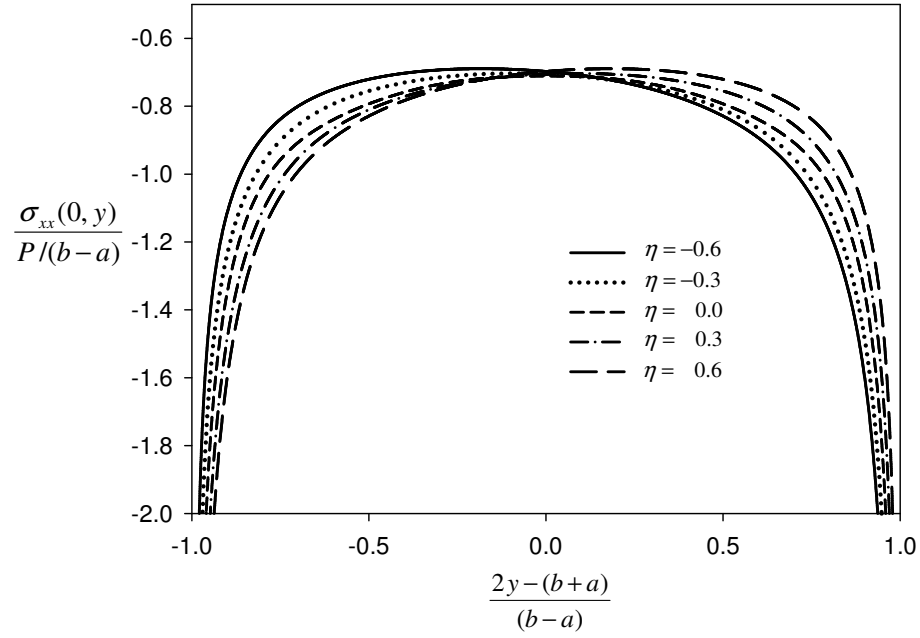


Figure 4.6: Effect of friction coefficient η variations on the normalized contact stress for a flat stamp problem, $(b - a)/h = 1.0$, $\gamma h = 0.712$.

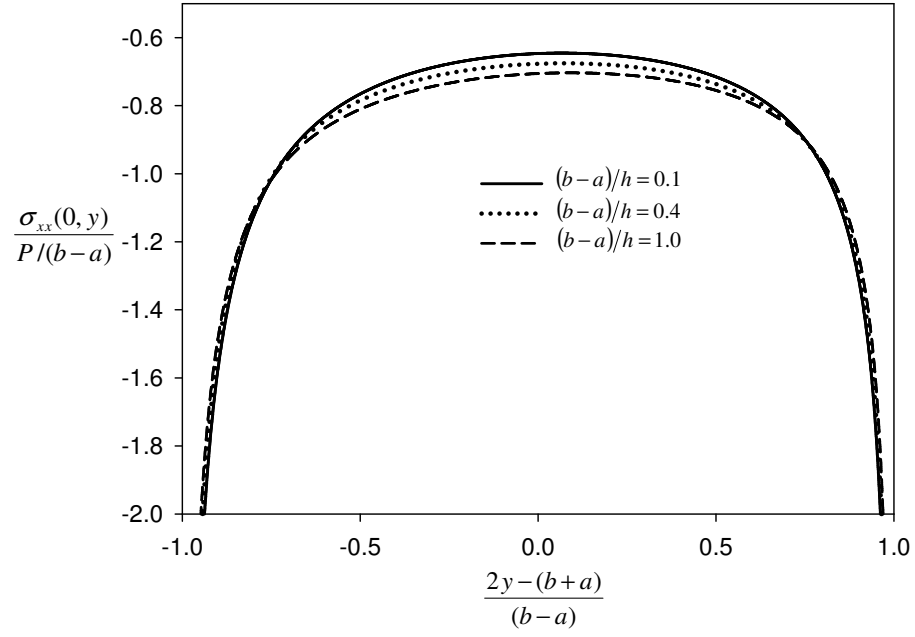


Figure 4.7: Effect of normalized contact length $(b-a)/h$ variations on the normalized contact stress for a flat stamp problem, $\eta = 0.3$, $\gamma h = 0.712$.

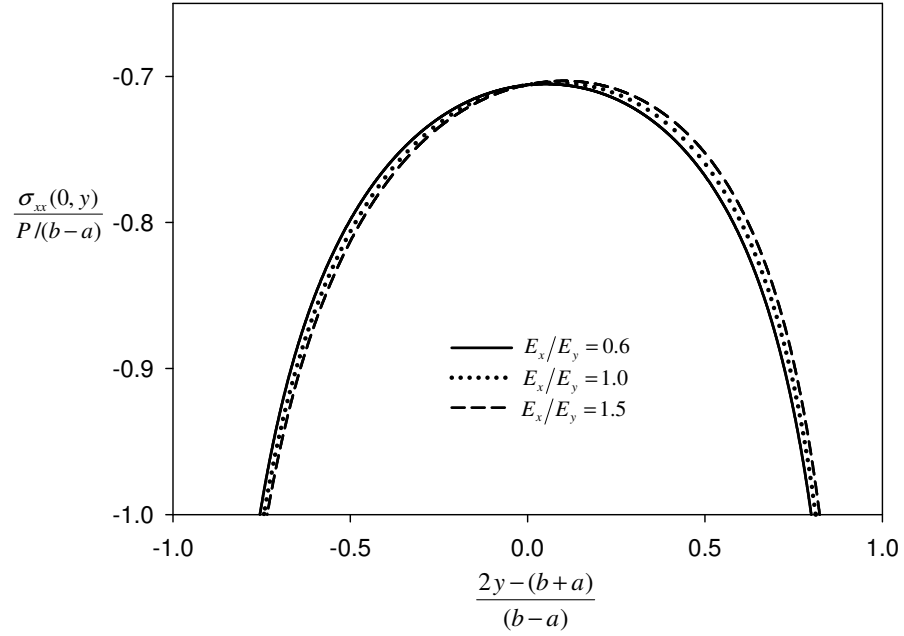


Figure 4.8: Effect of elastic modulus ratio E_x/E_y variations on the normalized contact stress for a flat stamp problem, $(b-a)/h = 1.0$, $\eta = 0.3$, $\gamma h = 0.712$.

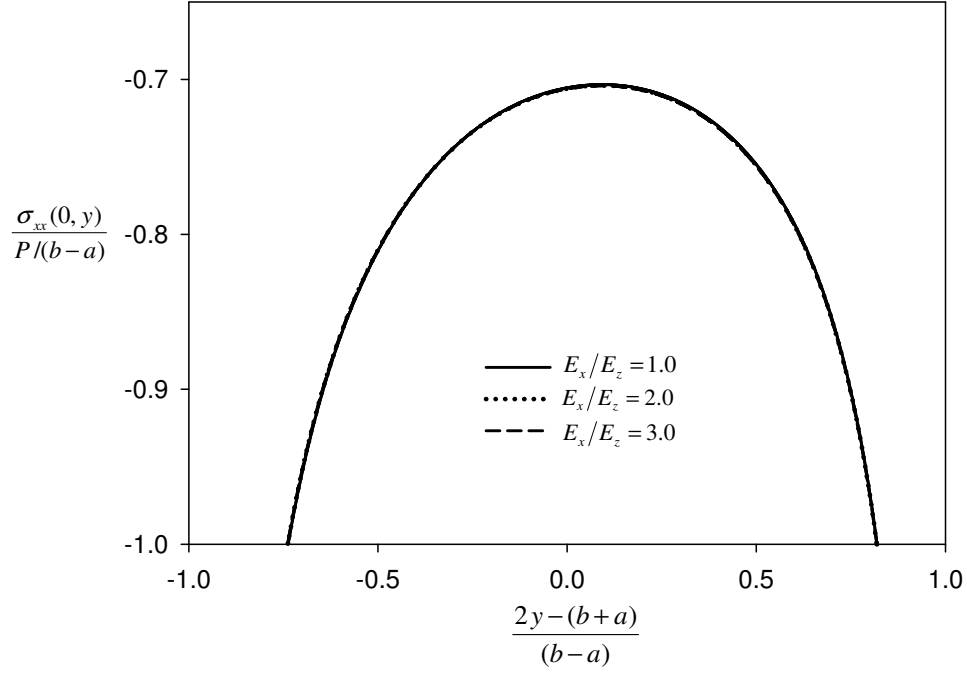


Figure 4.9: Effect of elastic modulus ratio E_x/E_z variations on the normalized contact stress for a flat stamp problem, $(b-a)/h = 1.0$, $\eta = 0.3$, $\gamma h = 0.712$.

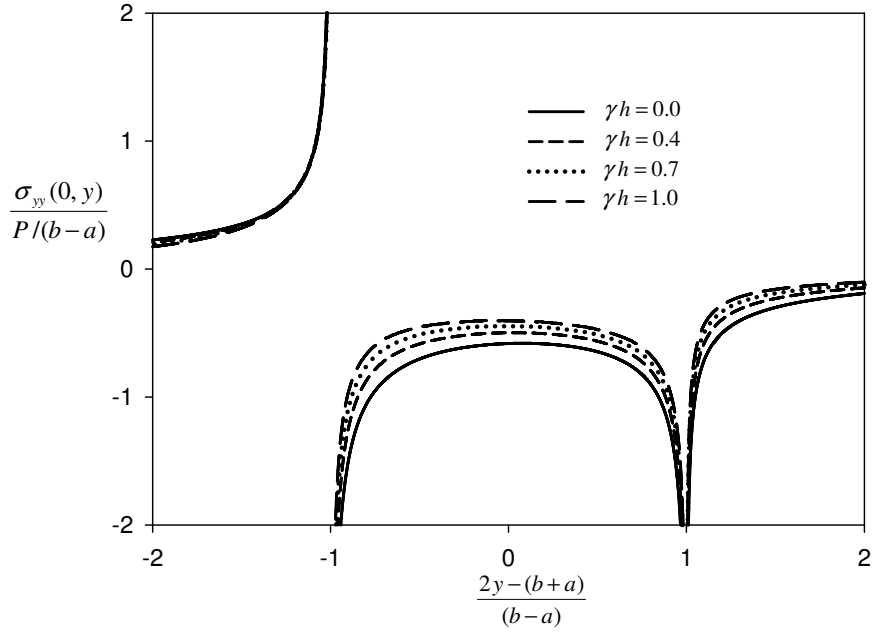


Figure 4.10: Effect of normalized non-homogeneity parameter γh variations on the normalized lateral contact stress for a flat stamp problem, $(b - a)/h = 1.0$, $\eta = 0.3$.

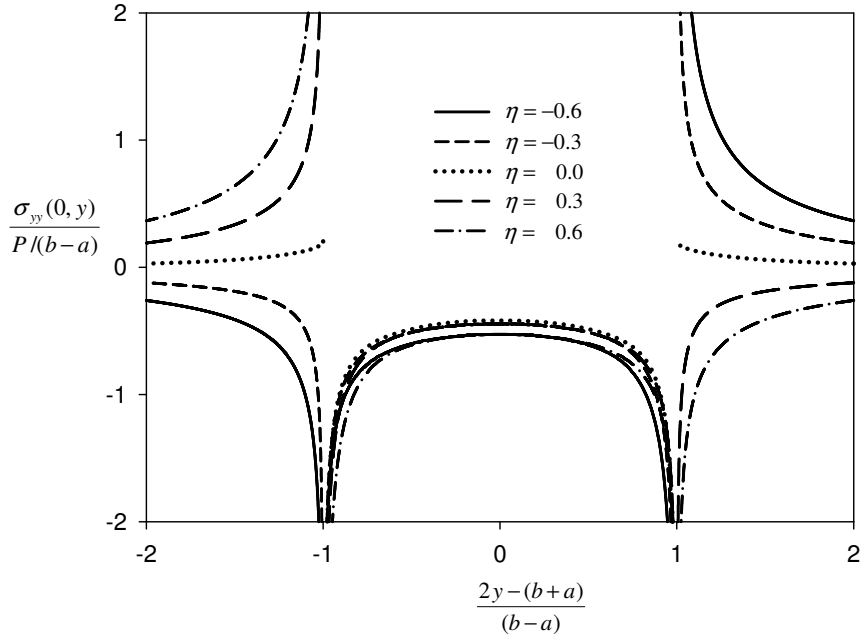


Figure 4.11: Effect of friction coefficient η variations on the normalized lateral contact stress for a flat stamp problem, $(b - a)/h = 1.0$, $\gamma h = 0.712$.

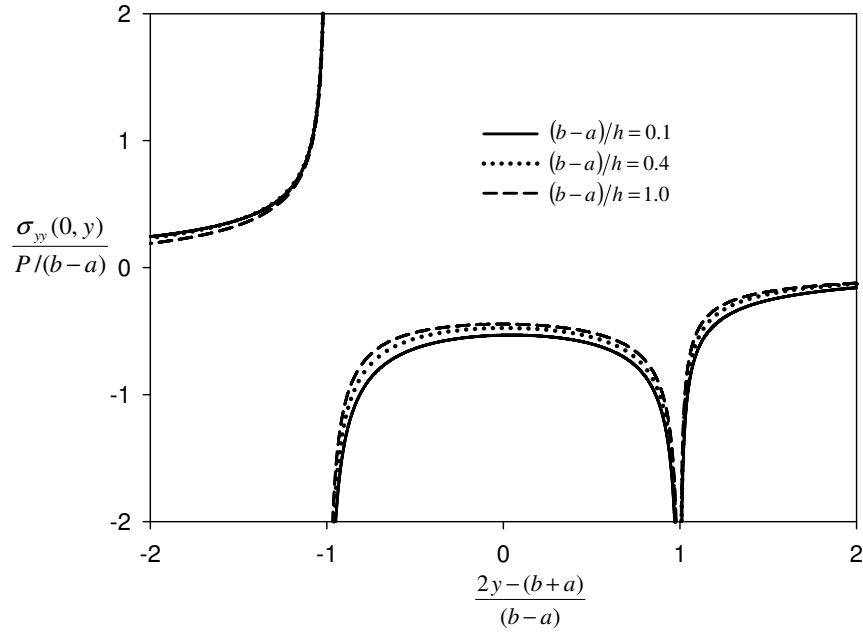


Figure 4.12: Effect of normalized contact length $(b-a)/h$ variations on the normalized lateral contact stress for a flat stamp problem, $\eta = 0.3$, $\gamma h = 0.712$.

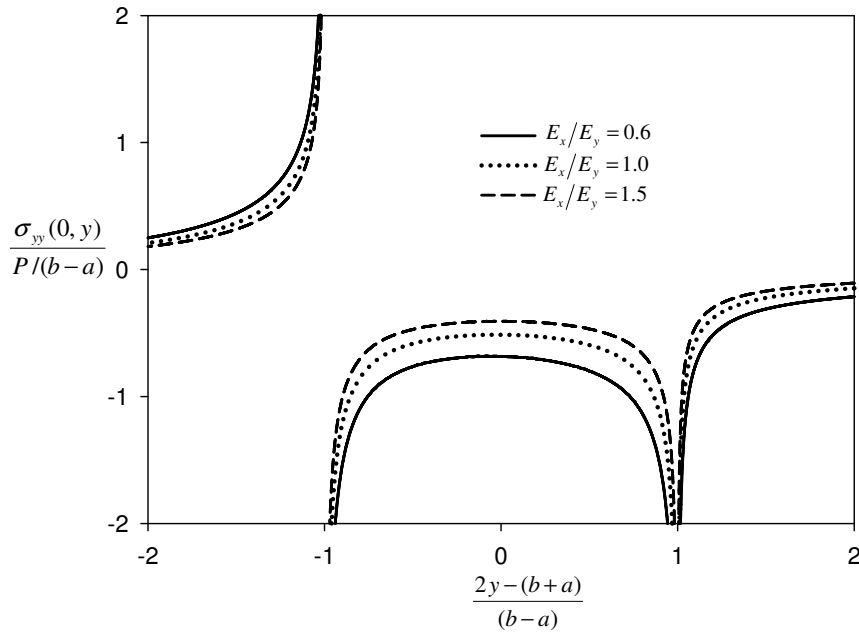


Figure 4.13: Effect of elastic modulus ratio E_x/E_y variations on the normalized lateral contact stress for a flat stamp problem, $(b-a)/h = 1.0$, $\eta = 0.3$, $\gamma h = 0.712$.

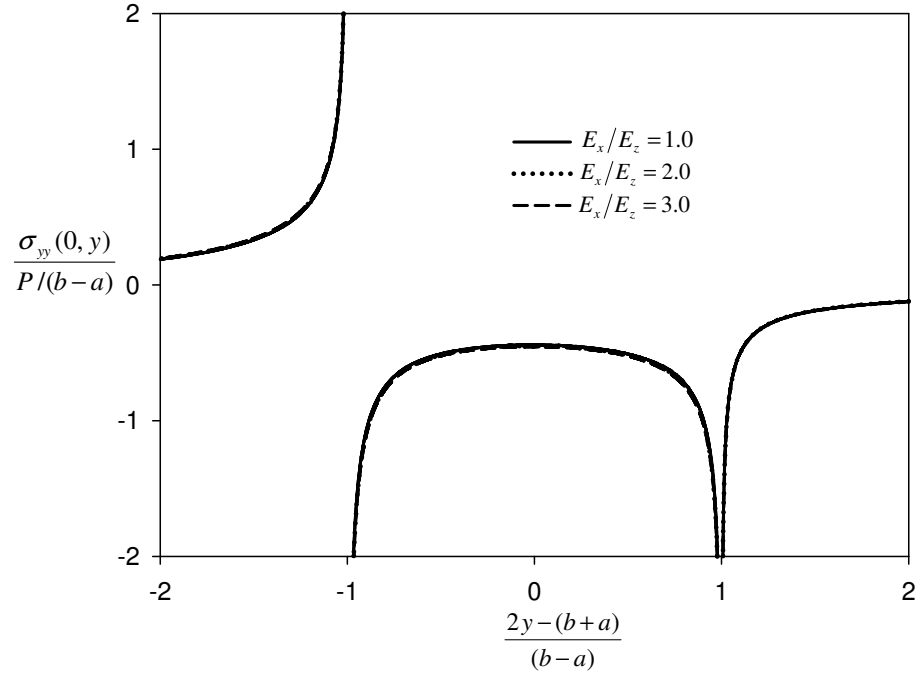


Figure 4.14: Effect of elastic modulus ratio E_x/E_z variations on the normalized lateral contact stress for a flat stamp problem, $(b-a)/h=1.0$, $\eta = 0.3$, $\gamma h=0.712$.

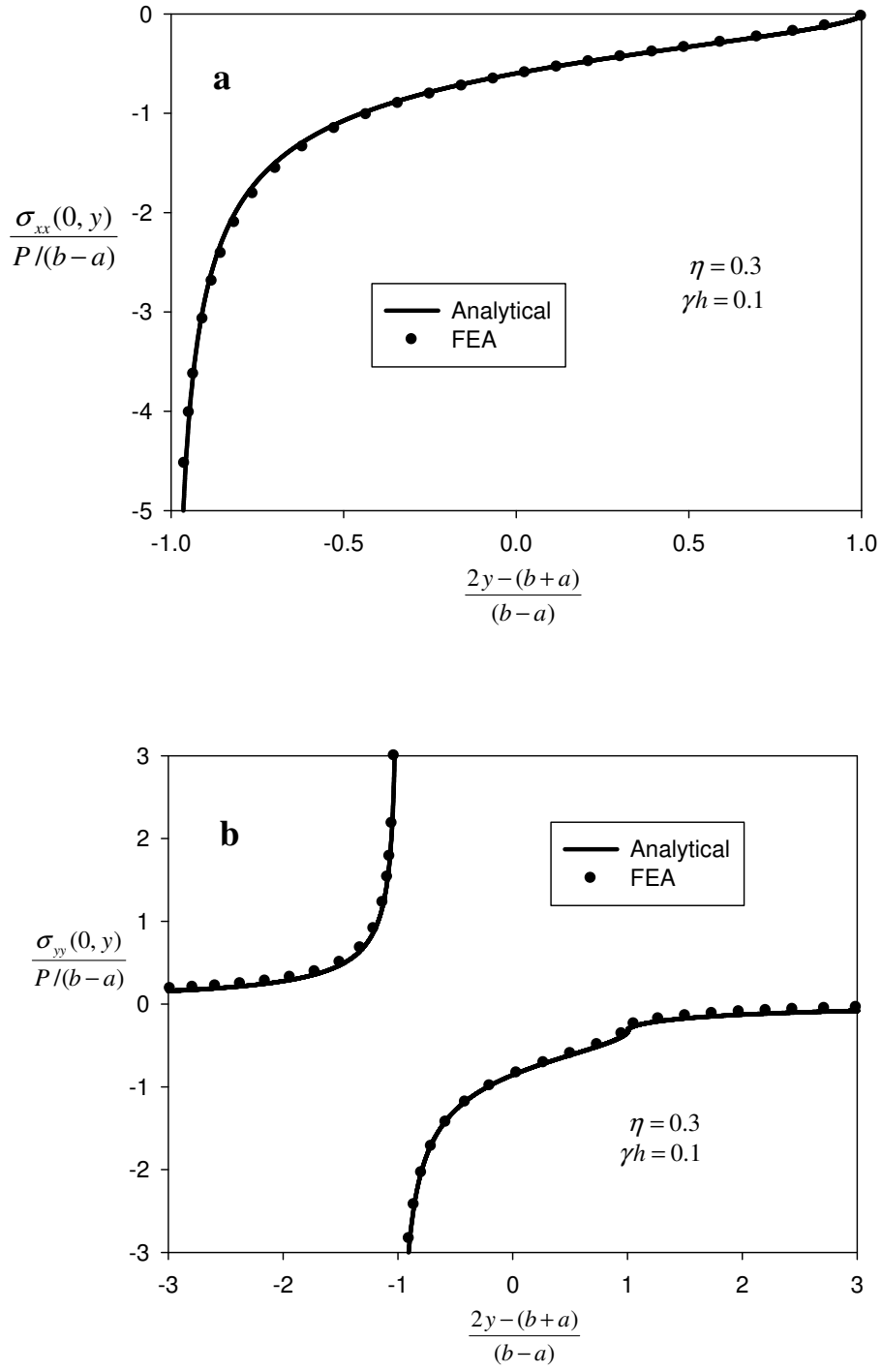


Figure 4.15: Comparison plots of the normalized stresses evaluated by the analytical and computational procedures for a triangular stamp problem, $(b-a)/h=1.0$, $\eta=0.3$, $\gamma h=0.1$. a) Normalized contact stress, b) Normalized lateral contact stress.

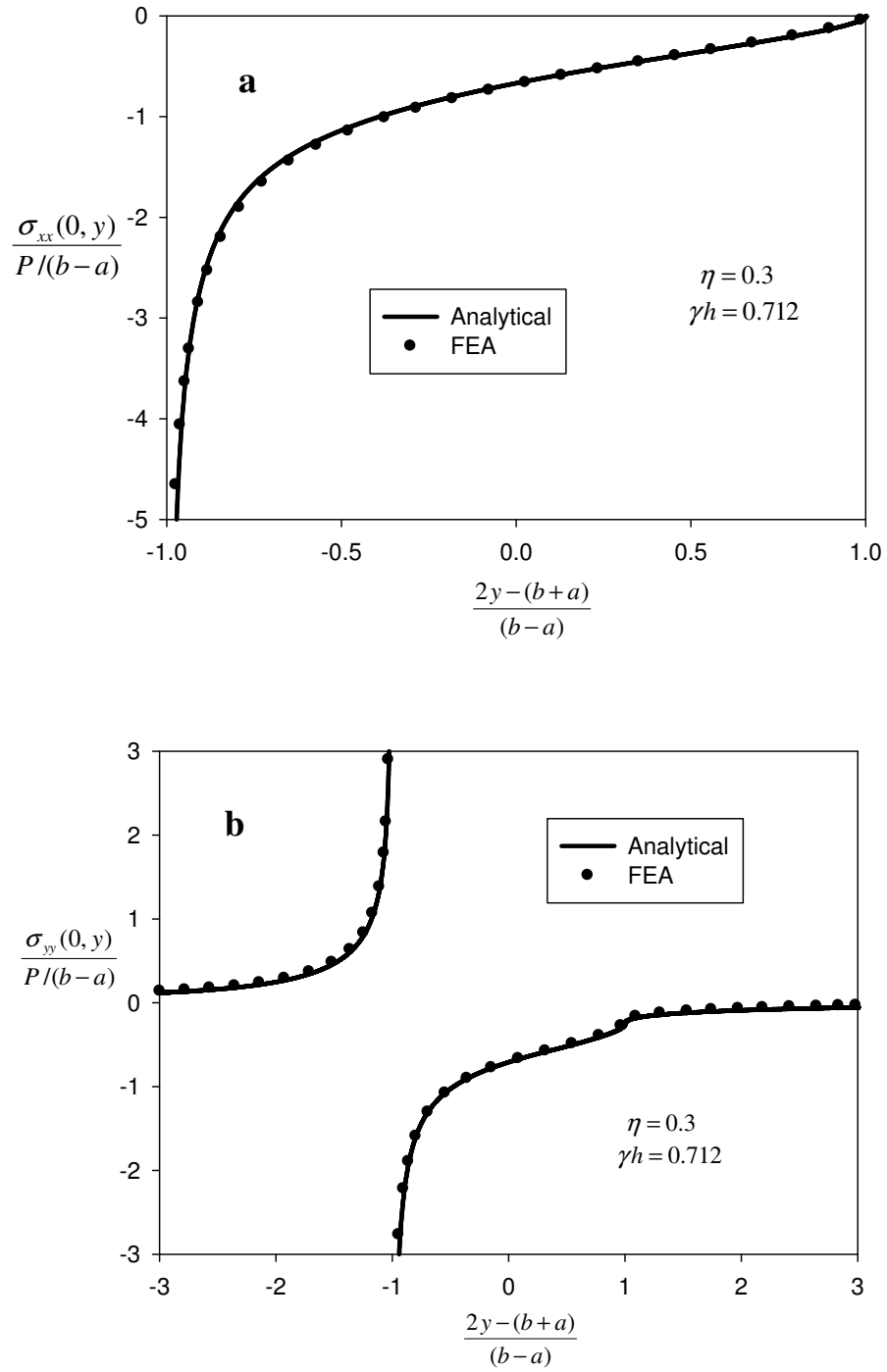


Figure 4.16: Comparison plots of the normalized stresses evaluated by the analytical and computational procedures for a triangular stamp problem, $(b-a)/h = 1.0$, $\eta = 0.3$, $\gamma h = 0.712$. a) Normalized contact stress, b) Normalized lateral contact stress.

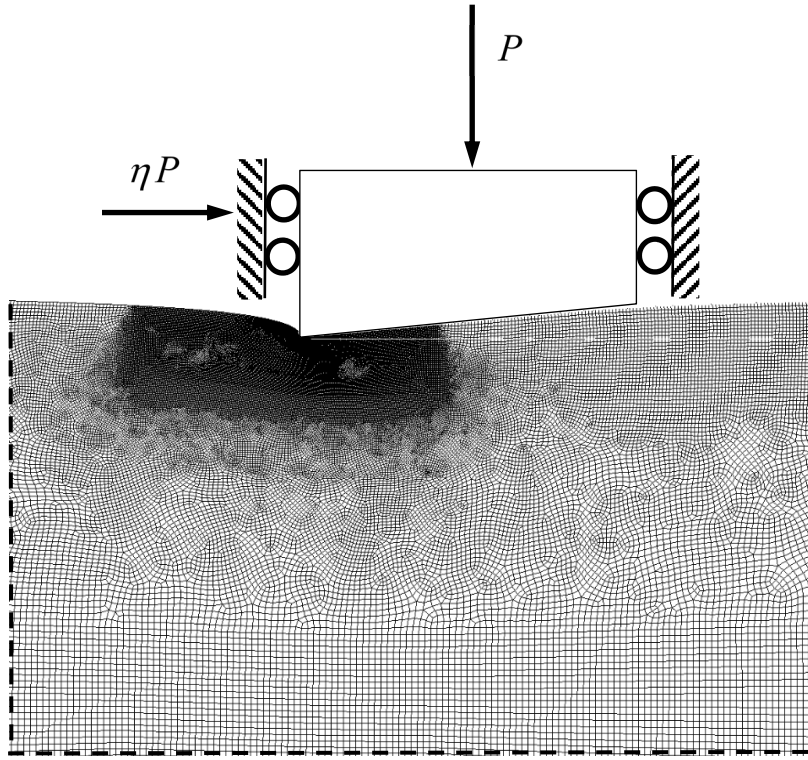


Figure 4.17: Scaled deformed shape of the contact region, which is produced by using the FE solution of a triangular stamp problem, $\eta=0.3$, $\gamma h=0.712$, $(b-a)/h=1.0$.

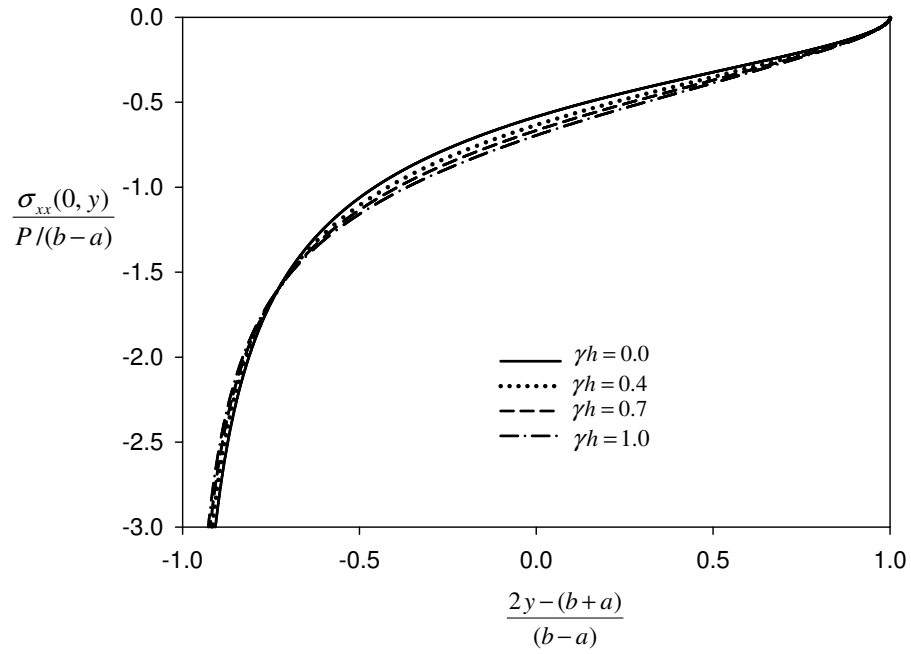


Figure 4.18: Effect of normalized non-homogeneity parameter γh variations on the normalized contact stress for a triangular stamp problem, $(b-a)/h=1.0$, $\eta=0.3$.

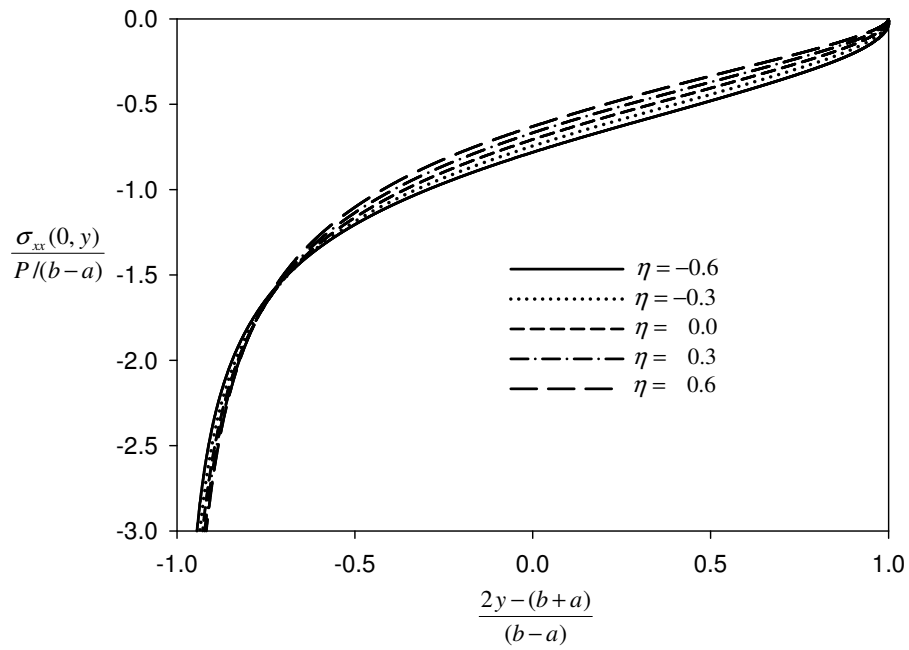


Figure 4.19: Effect of friction coefficient η variations on the normalized contact stress for a triangular stamp problem, $(b-a)/h=1.0$, $\gamma h=0.712$.

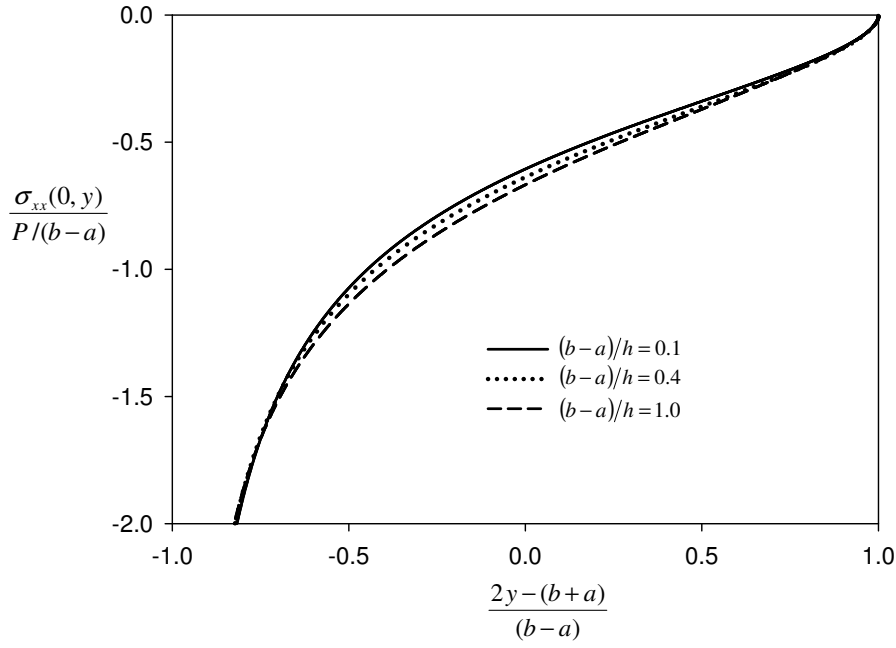


Figure 4.20: Effect of normalized contact length $(b-a)/h$ variations on the normalized contact stress for a triangular stamp problem, $\eta = 0.3$, $\gamma h = 0.712$.

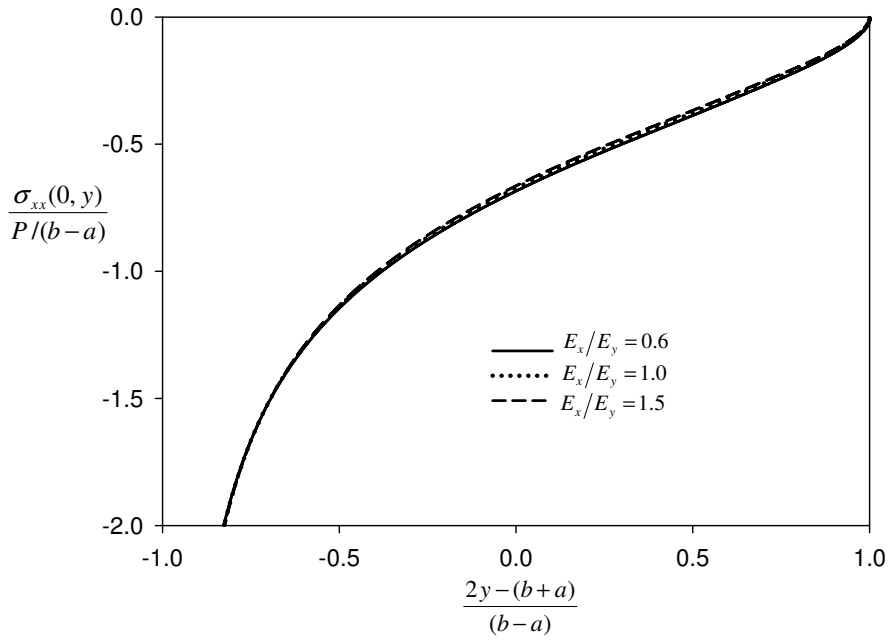


Figure 4.21: Effect of elastic modulus ratio E_x/E_y variations on the normalized contact stress for a triangular stamp problem, $(b-a)/h = 1.0$, $\eta = 0.3$, $\gamma h = 0.712$.

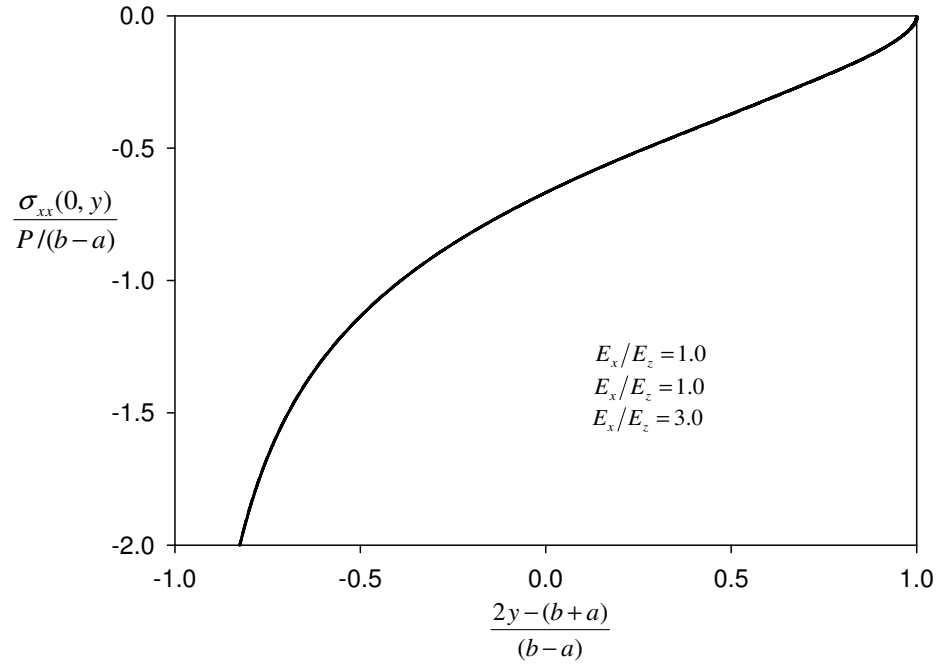


Figure 4.22: Effect of elastic modulus ratio E_x/E_z variations on the normalized contact stress for a triangular stamp problem, $(b-a)/h = 1.0$, $\eta = 0.3$, $\gamma h = 0.712$.

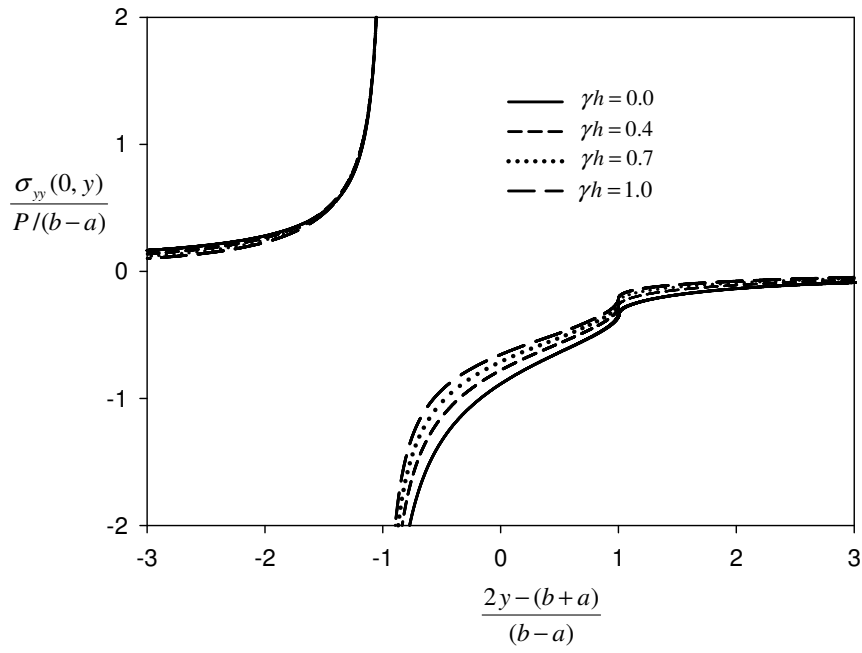


Figure 4.23: Effect of normalized non-homogeneity parameter γh variations on the normalized lateral contact stress for a triangular stamp problem, $(b-a)/h = 1.0$, $\eta = 0.3$.

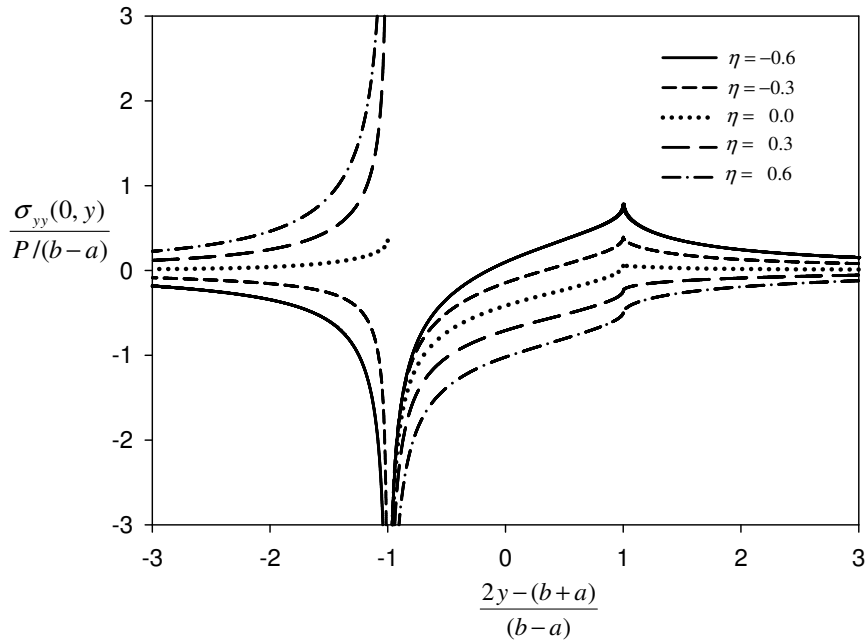


Figure 4.24: Effect of friction coefficient η variations on the normalized lateral contact stress for a triangular stamp problem, $(b-a)/h = 1.0$, $\gamma h = 0.712$.

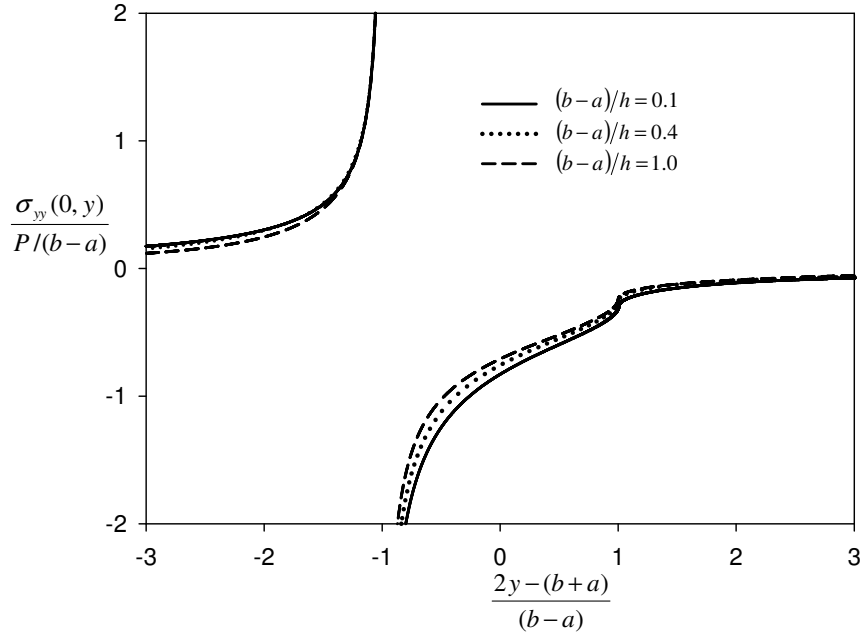


Figure 4.25: Effect of normalized contact length $(b-a)/h$ variations on the normalized lateral contact stress for a triangular stamp problem, $\eta = 0.3$, $\gamma h = 0.712$.

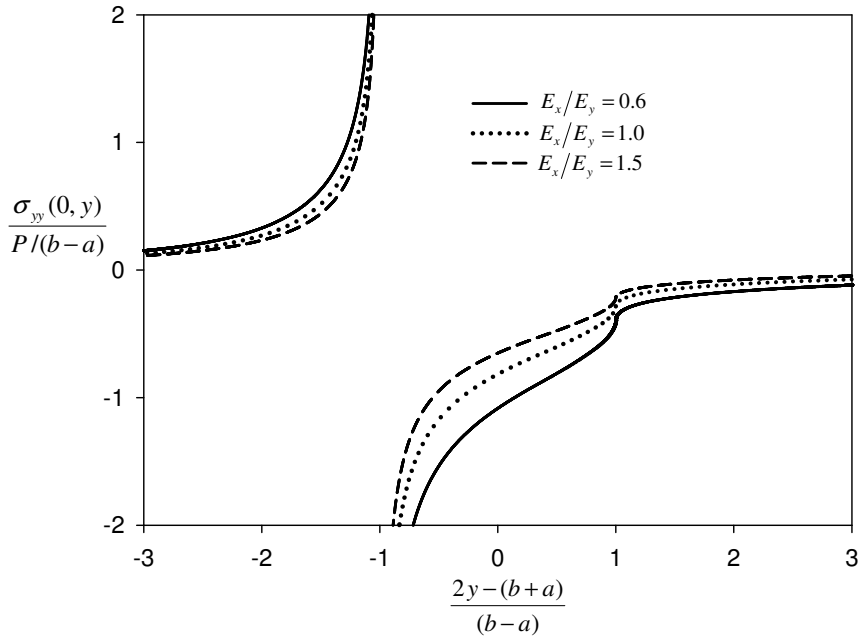


Figure 4.26: Effect of elastic modulus ratio E_x/E_y variations on the normalized lateral contact stress for a triangular stamp problem, $(b-a)/h = 1.0$, $\eta = 0.3$, $\gamma h = 0.712$.

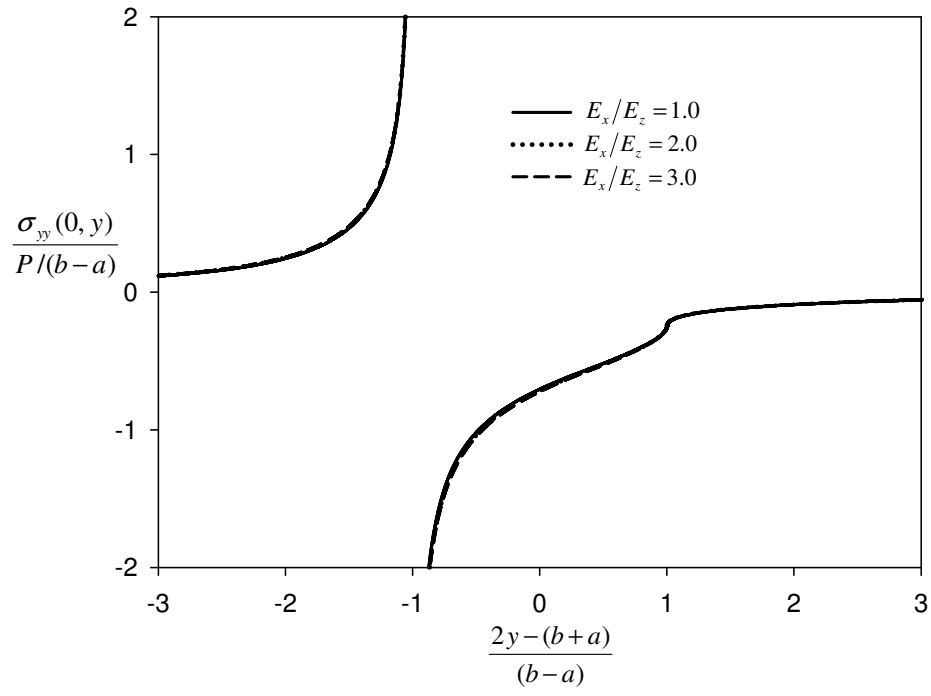


Figure 4.27: Effect of elastic modulus ratio E_x/E_z variations on the normalized lateral contact stress for a triangular stamp problem, $(b-a)/h=1.0$, $\eta=0.3$, $\gamma h=0.712$.

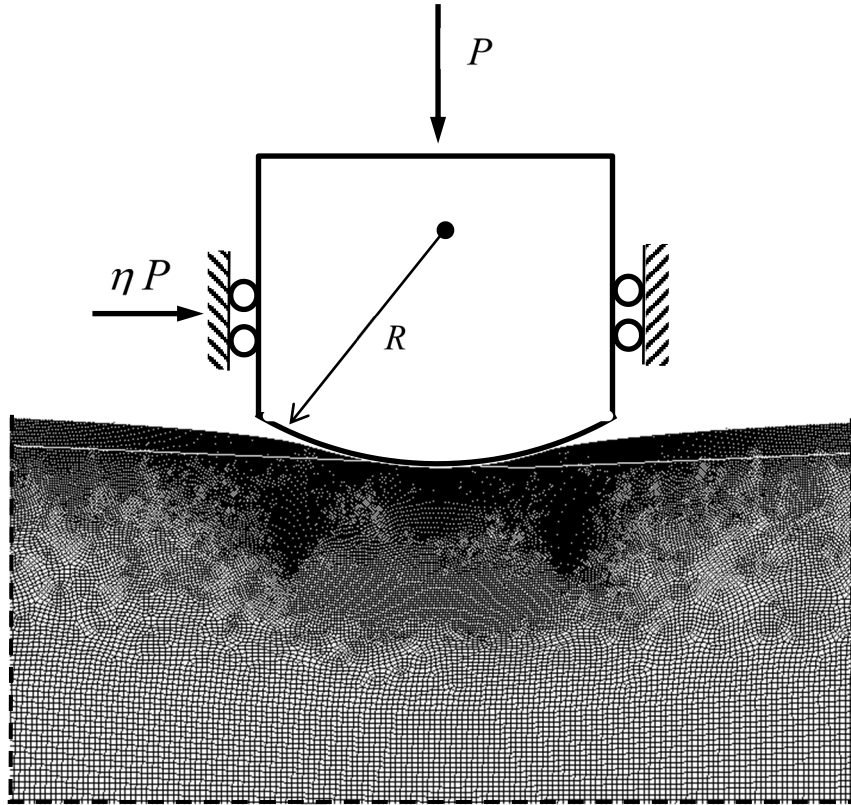


Figure 4.28: Scaled deformed shape of the contact region, which is produced by using the FE solution of a circular stamp problem, $\eta=0.3$, $\gamma h=0.712$, $(b-a)/h=1.0$.

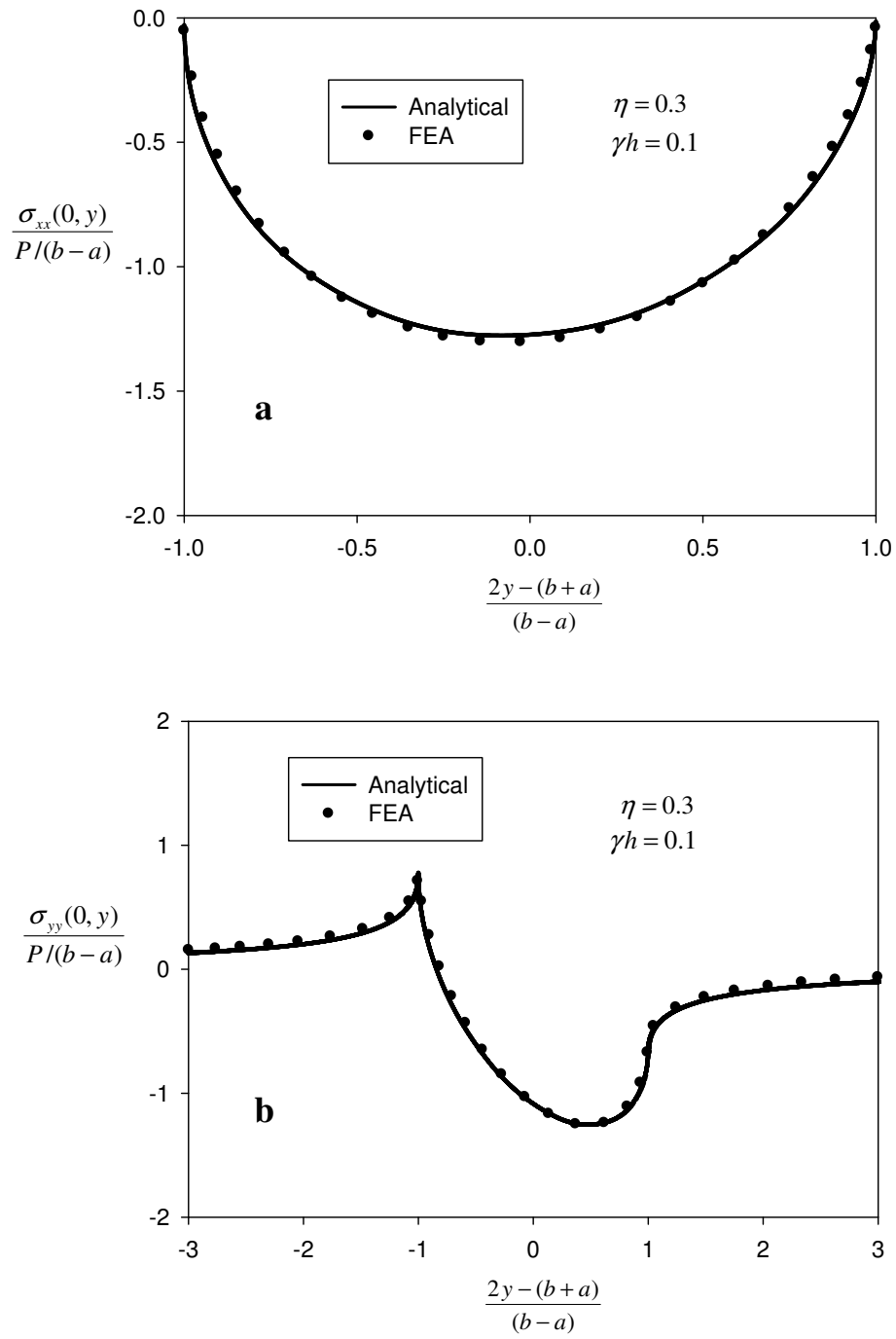


Figure 4.29: Comparison plots of the normalized stresses evaluated by the analytical and computational procedures for a circular stamp problem, $(b-a)/h = 1.0$, $\eta = 0.3$, $\gamma h = 0.1$. a) Normalized contact stress, b) Normalized lateral contact stress.

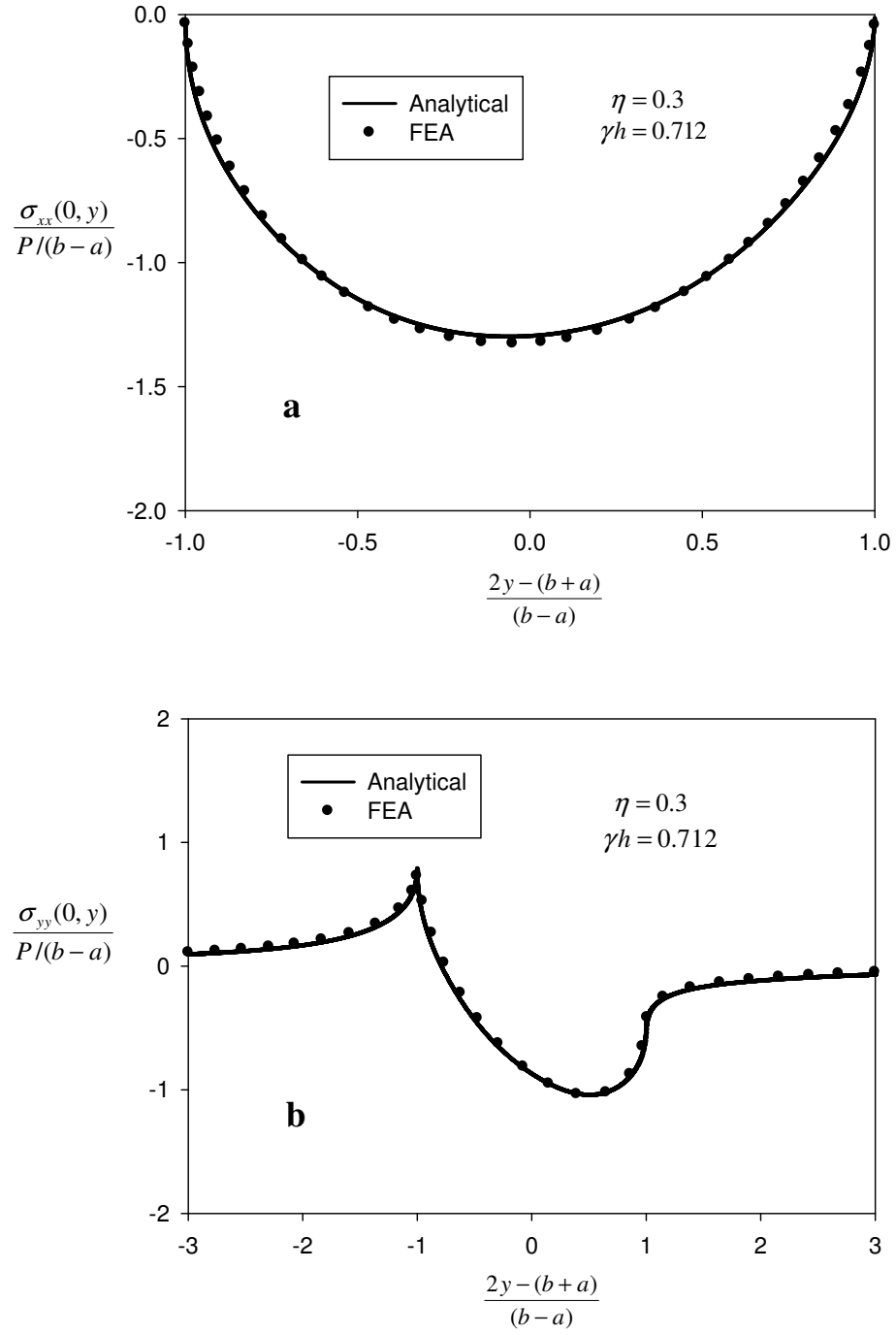


Figure 4.30: Comparison plots of the normalized stresses evaluated by the analytical and computational procedures for a circular stamp problem, $(b-a)/h = 1.0$, $\eta = 0.3$, $\gamma h = 0.712$. a) Normalized contact stress, b) Normalized lateral contact stress.

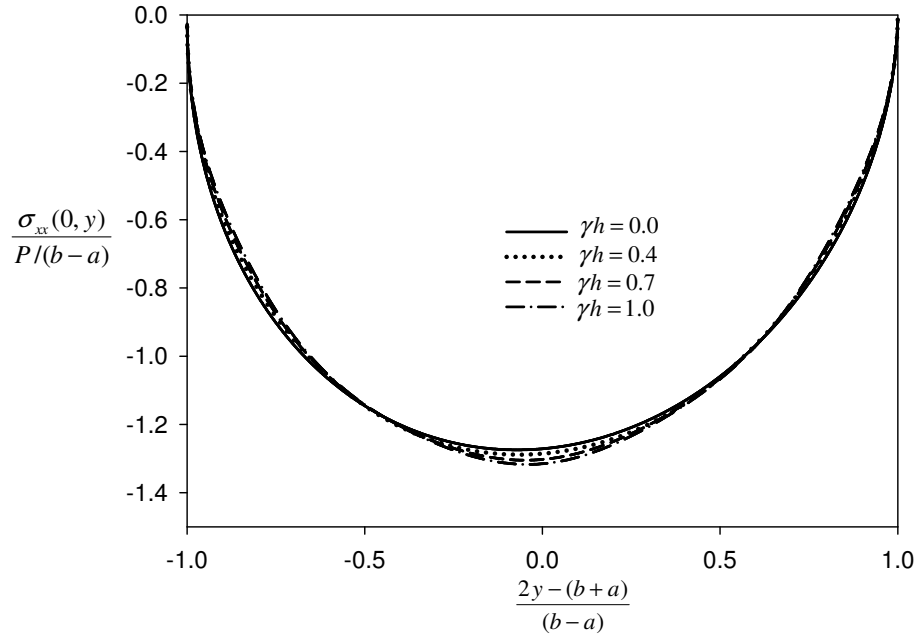


Figure 4.31: Effect of normalized non-homogeneity parameter γh variations on the normalized contact stress for a circular stamp problem, $(b-a)/h = 1.0$, $\eta = 0.3$.

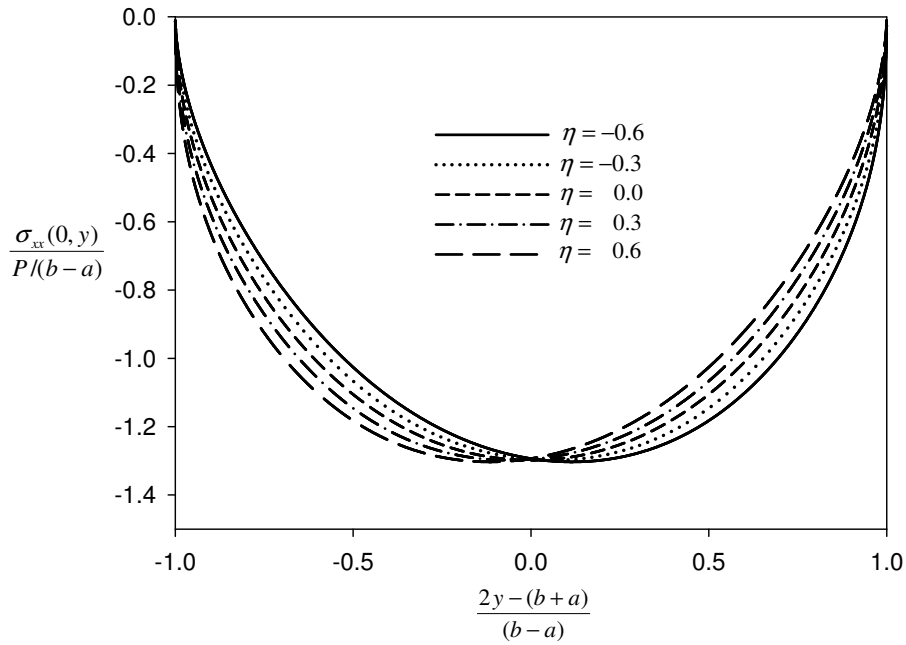


Figure 4.32: Effect of friction coefficient η variations on the normalized contact stress for a circular stamp problem, $(b-a)/h = 1.0$, $\gamma h = 0.712$.

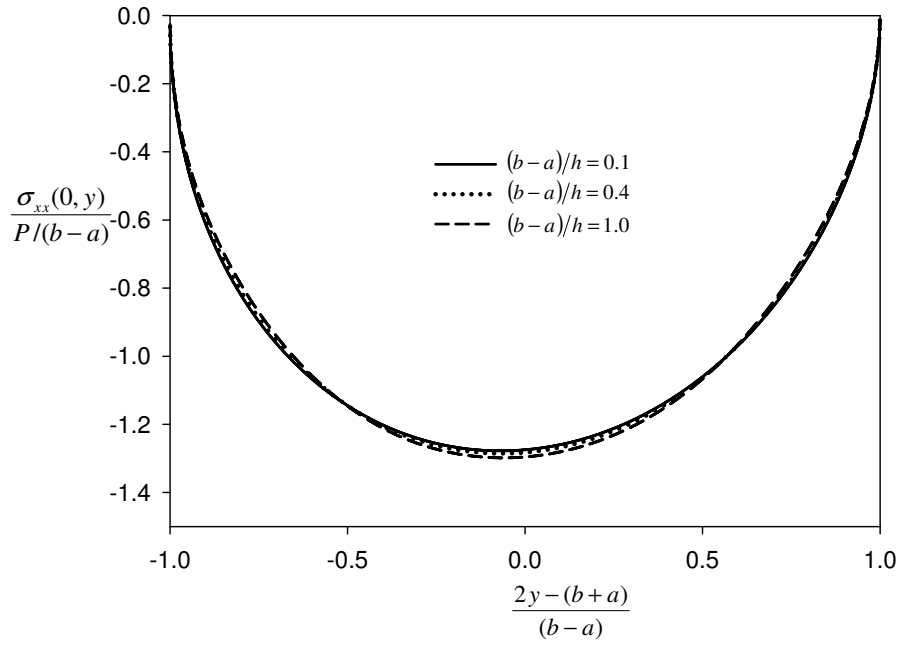


Figure 4.33: Effect of normalized contact length $(b-a)/h$ variations on the normalized contact stress for a circular stamp problem, $\eta = 0.3$, $\gamma h = 0.712$.

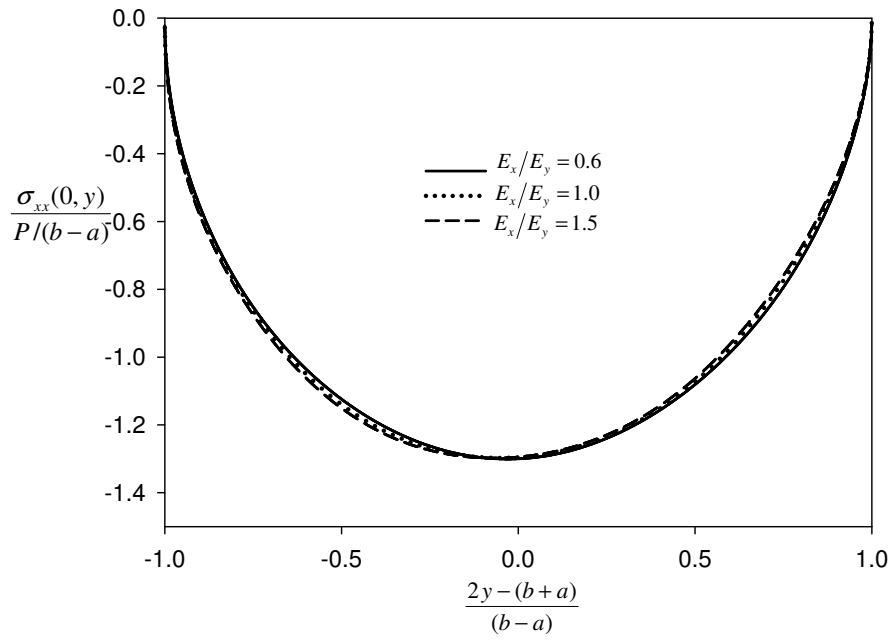


Figure 4.34: Effect of elastic modulus ratio E_x/E_y variations on the normalized contact stress for a circular stamp problem, $(b-a)/h = 1.0$, $\eta = 0.3$, $\gamma h = 0.712$.

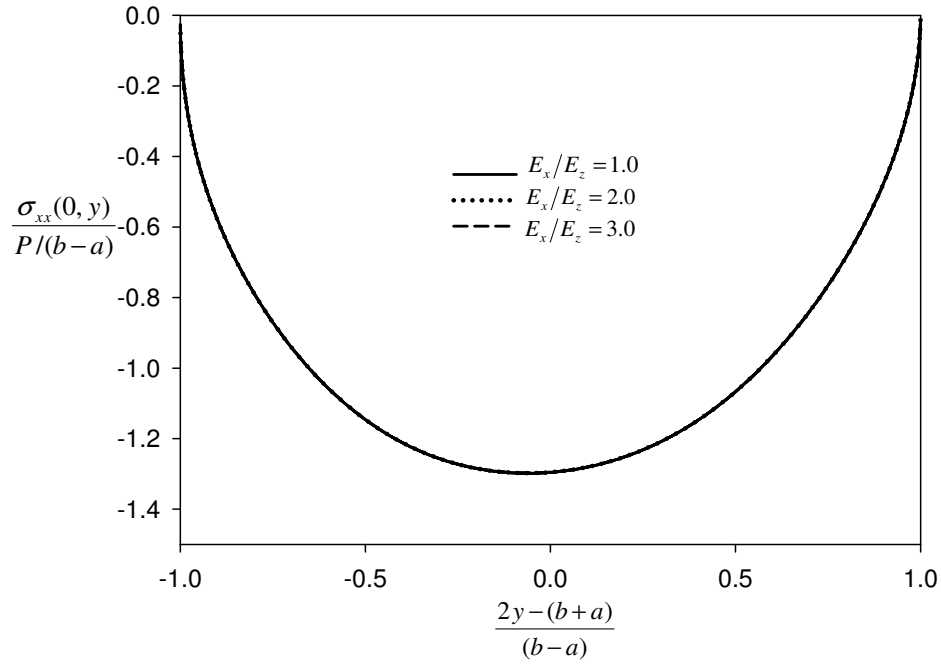


Figure 4.35: Effect of elastic modulus ratio E_x/E_z variations on the normalized lateral contact stress for a circular stamp problem, $(b-a)/h=1.0$, $\eta=0.3$, $\gamma h=0.712$.

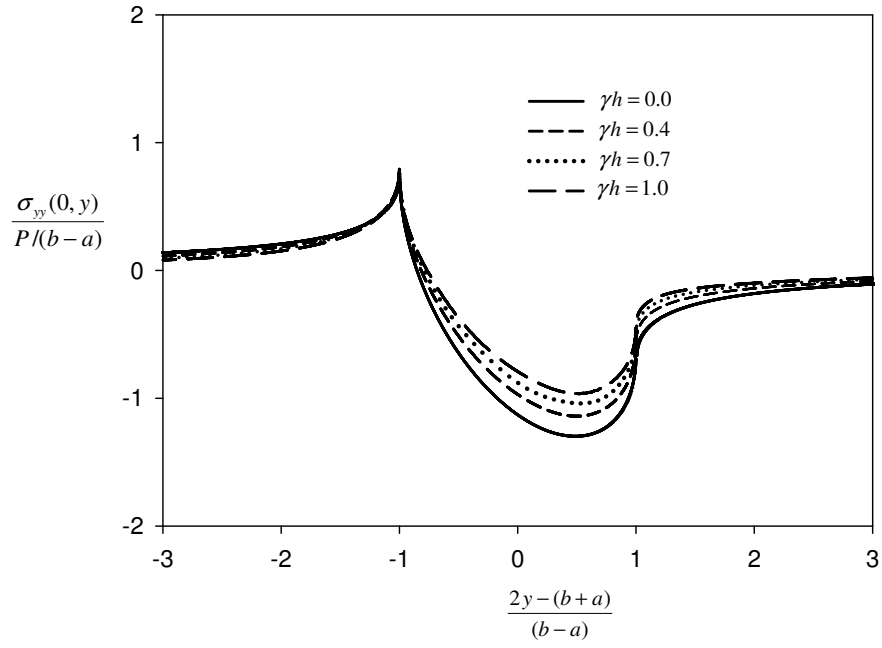


Figure 4.36: Effect of normalized non-homogeneity parameter γh variations on the normalized lateral contact stress for a triangular stamp problem, $(b-a)/h = 1.0$, $\eta = 0.3$.

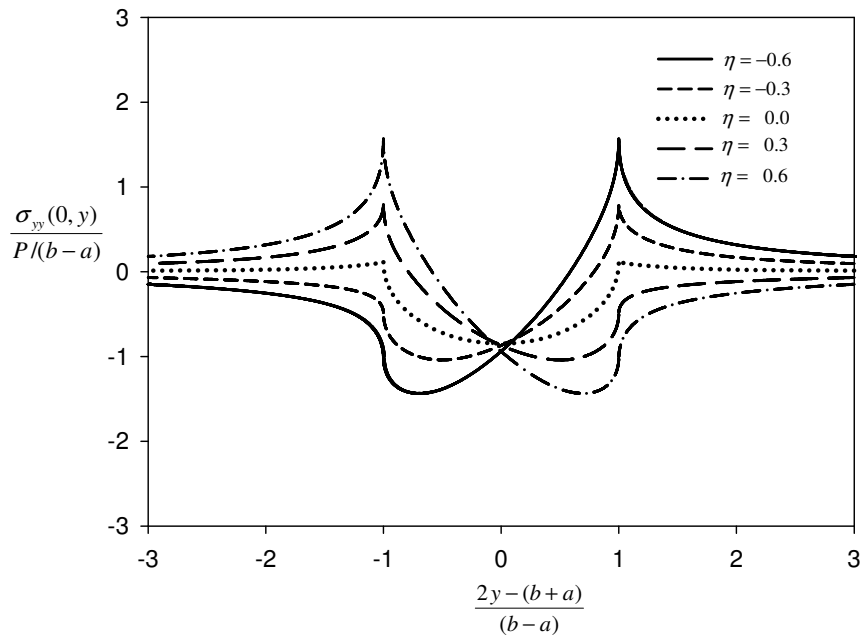


Figure 4.37: Effect of friction coefficient η variations on the normalized lateral contact stress for a circular stamp problem, $(b-a)/h = 1.0$, $\gamma h = 0.712$.

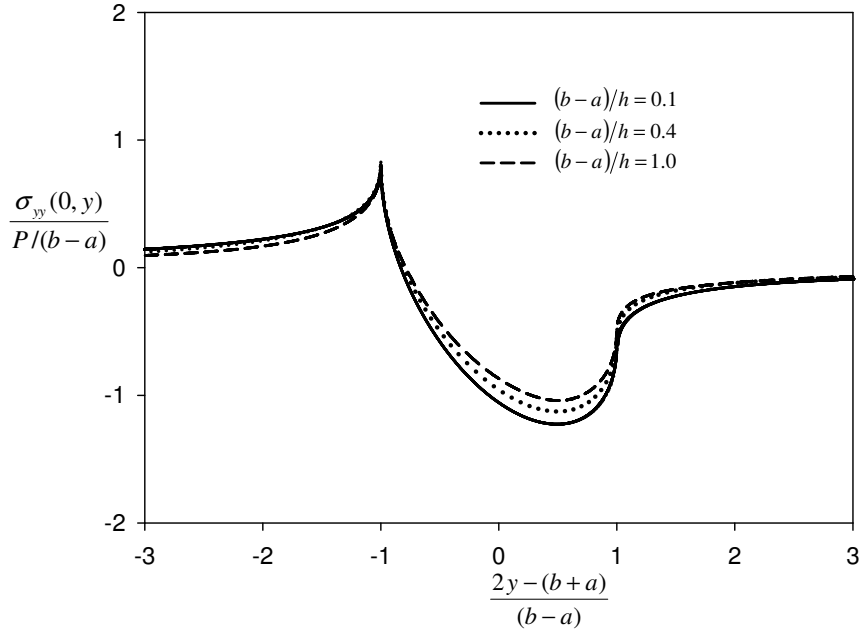


Figure 4.38: Effect of normalized contact length $(b-a)/h$ variations on the normalized lateral contact stress for a circular stamp problem, $\eta = 0.3$, $\gamma h = 0.712$.

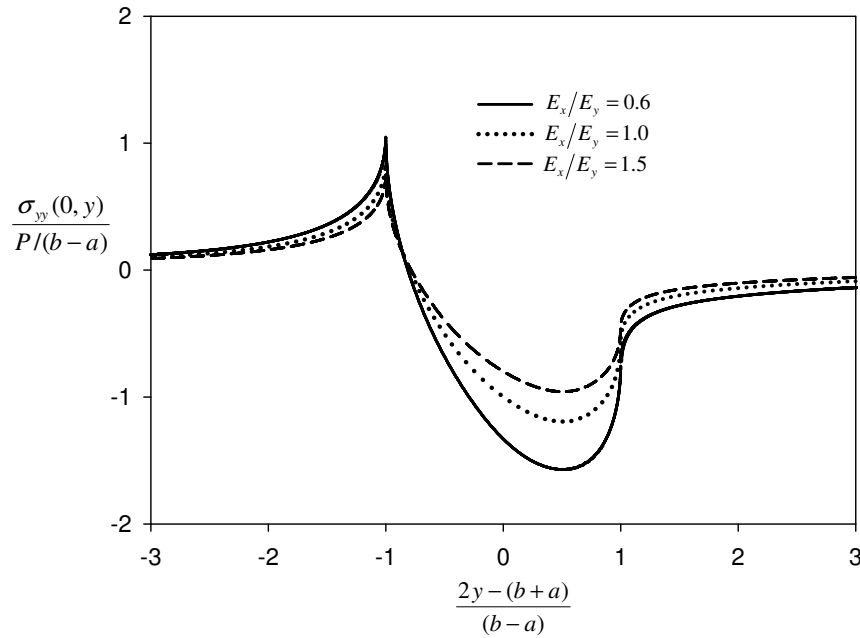


Figure 4.39: Effect of elastic modulus ratio E_x/E_y variations on the normalized lateral contact stress for a circular stamp problem, $(b-a)/h = 1.0$, $\eta = 0.3$, $\gamma h = 0.712$.

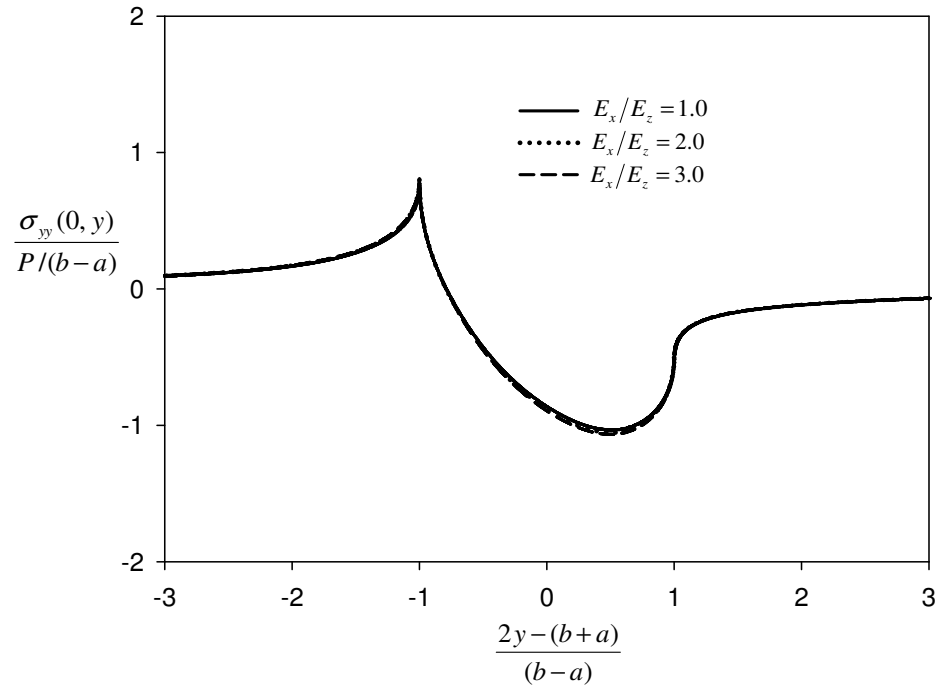


Figure 4.40: Effect of elastic modulus ratio E_x/E_z variations on the normalized lateral contact stress for a circular stamp problem, $(b-a)/h=1.0$, $\eta=0.3$, $\gamma h=0.712$.

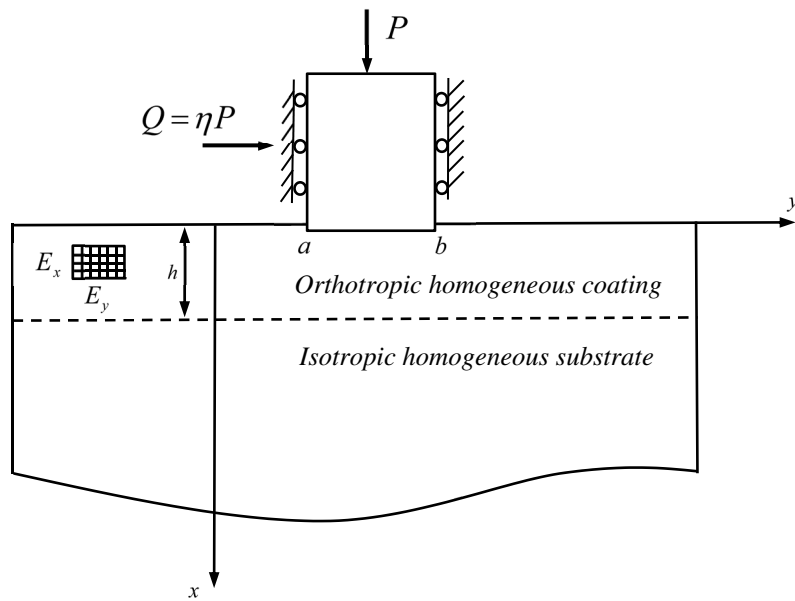


Figure 4.41: The complete contact problem of an orthotropic homogeneous coating.

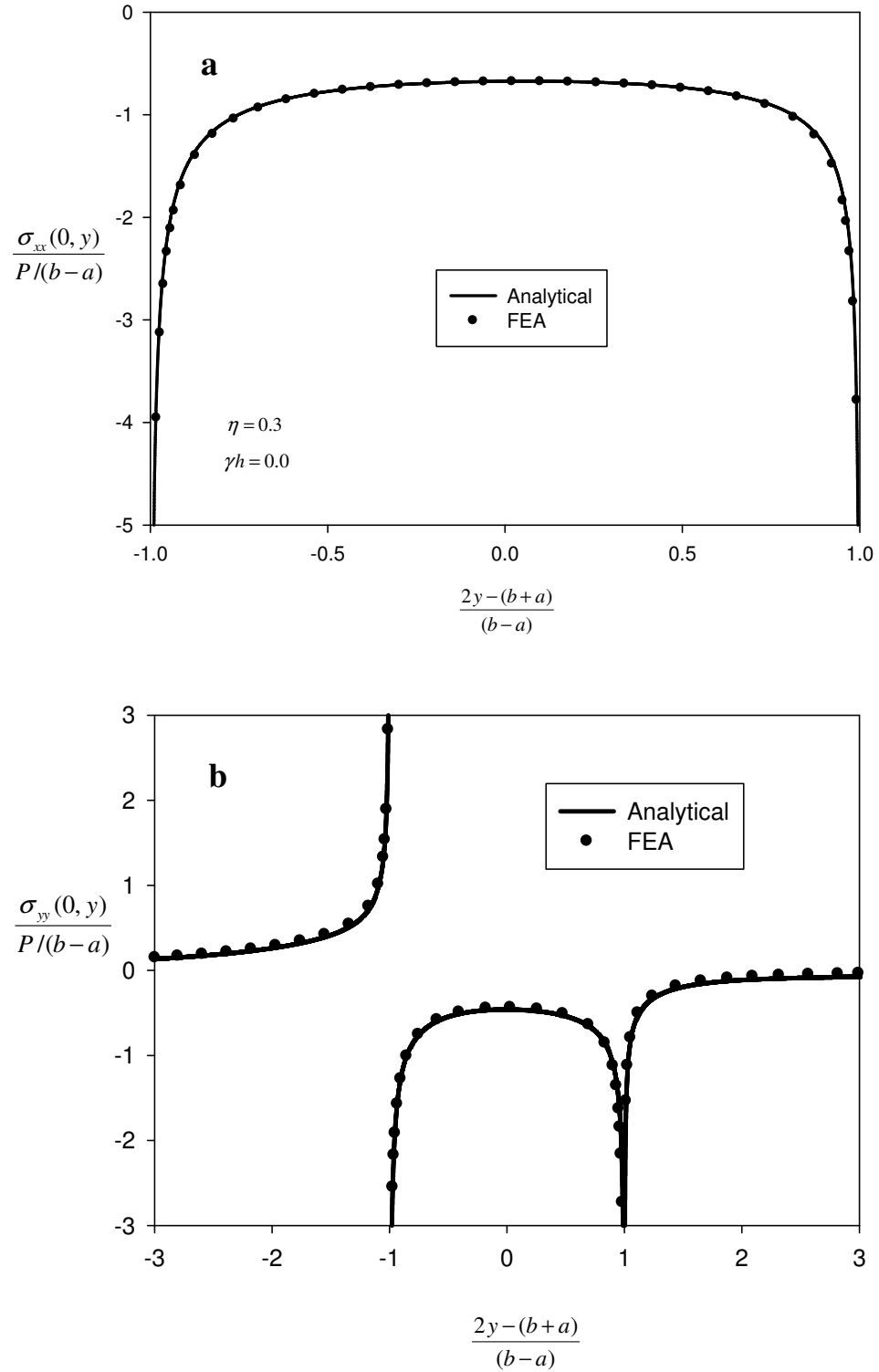


Figure 4.42: Comparison plots of the normalized surface stresses evaluated by the analytical and computational procedures for a flat stamp problem of the homogeneous orthotropic Alumina coating, $(b-a)/h=1.0$, $\eta=0.3$, a) Normalized contact stress, b) Normalized lateral contact stress.

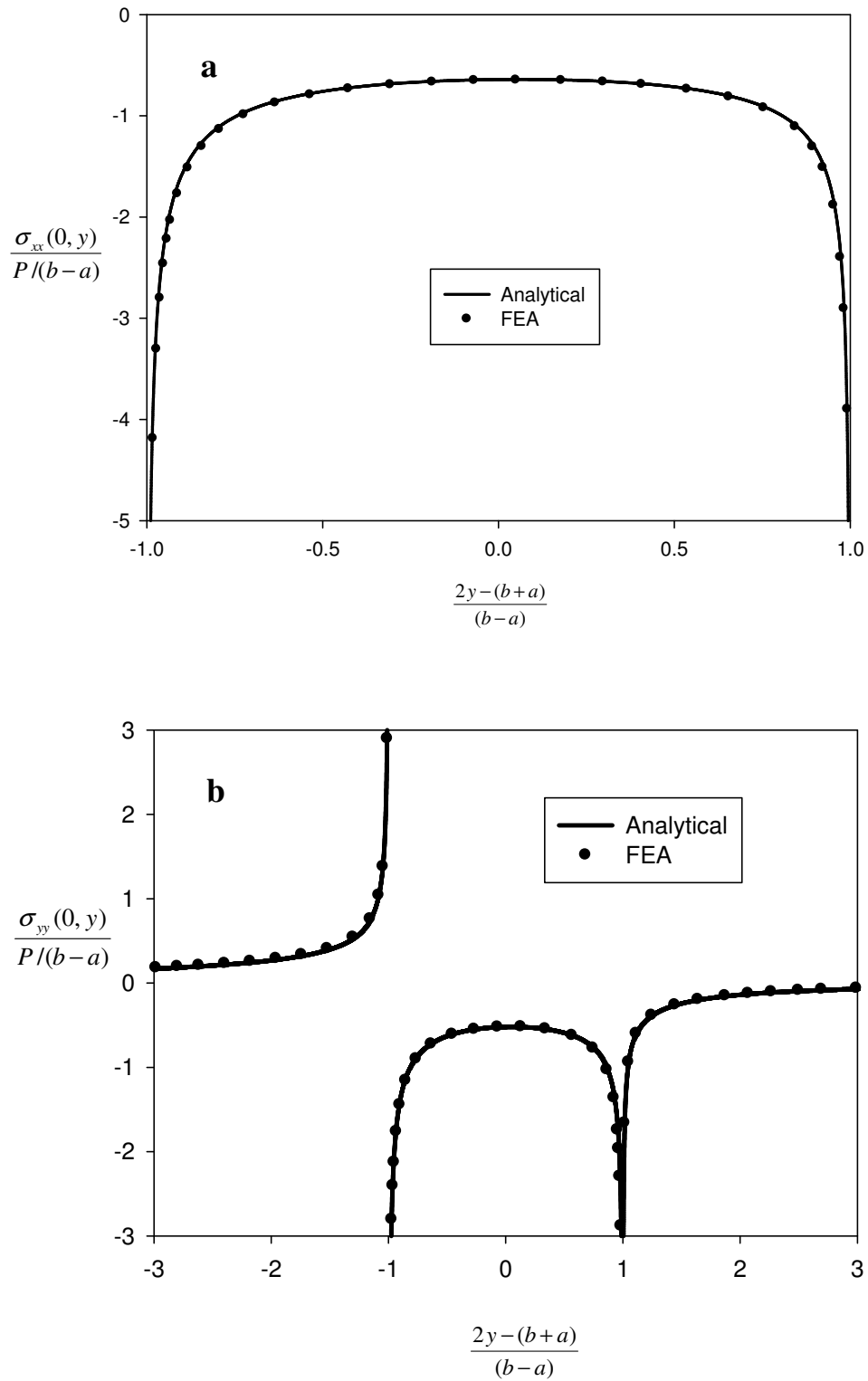


Figure 4.43: Comparison plots of the normalized surface stresses evaluated by the analytical and computational procedures for a flat stamp problem of the homogeneous orthotropic Alumina coating, $(b-a)/h=0.4$, $\eta=0.3$, a) Normalized contact stress, b) Normalized lateral contact stress.

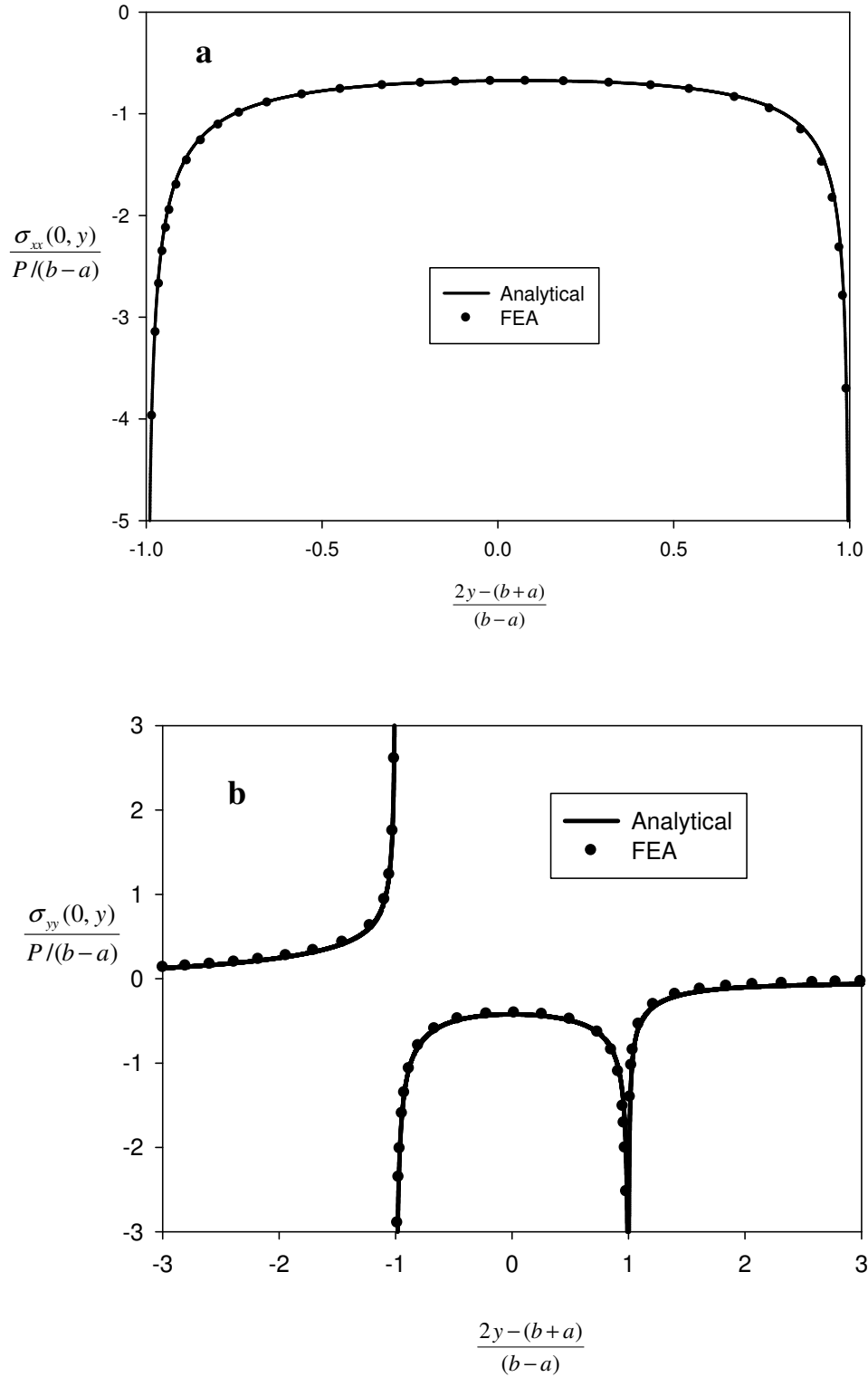


Figure 4.44: Comparison plots of the normalized surface stresses evaluated by the analytical and computational procedures for a flat stamp problem of an homogeneous orthotropic coating, $(b-a)/h = 1.0$, $\eta = 0.3$, $E_1/E_2 = 1.5$, a) Normalized contact stress, b) Normalized lateral contact stress.

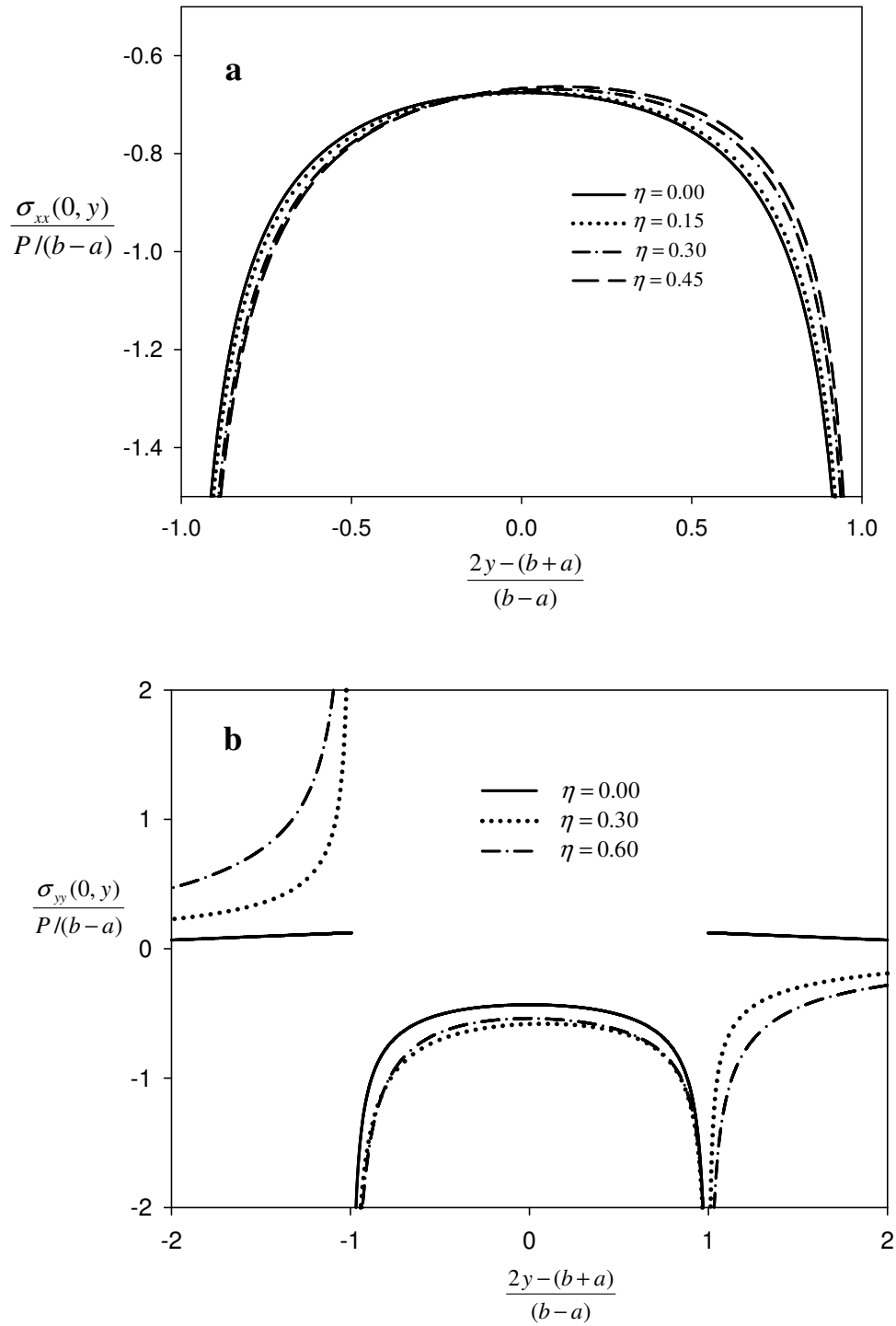


Figure 4.45: Effect of friction coefficient η variations on the normalized surface stresses for a flat stamp problem of the orthotropic homogeneous Alumina coating, $(b-a)/h=1.0$, a) Normalized contact stress, b) Normalized lateral contact stress.

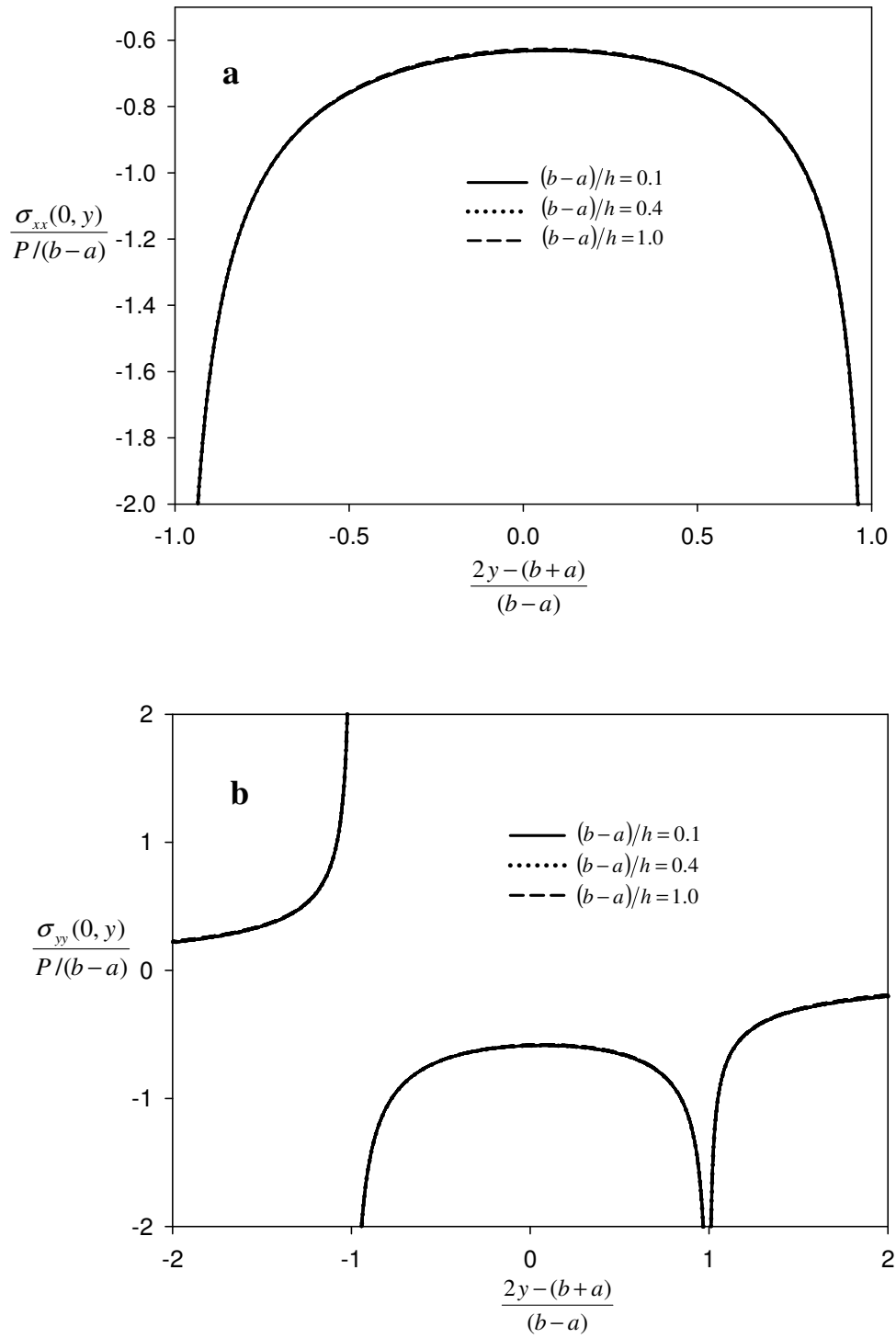


Figure 4.46: Effect of normalized contact length $(b-a)/h$ variations on the normalized surface stresses for a flat stamp problem of the orthotropic homogeneous Alumina coating, $\eta=0.3$, a) Normalized contact stress, b) Normalized lateral contact stress.

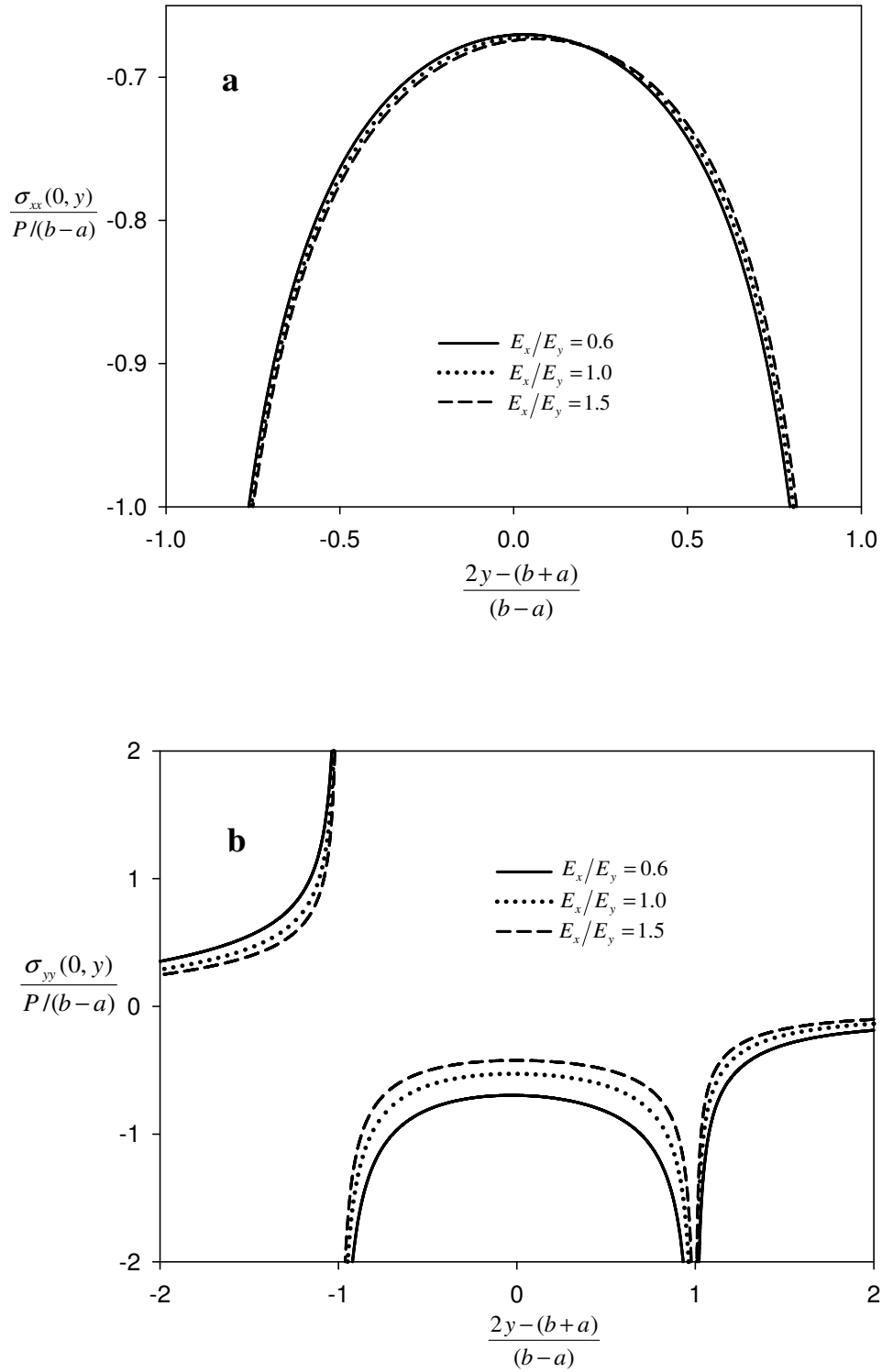


Figure 4.47: Effect of elastic modulus ratio E_x/E_y variations on the normalized surface stresses for a flat stamp problem of orthotropic homogeneous coatings, $(b-a)/h = 1.0$, $\eta = 0.3$, a) Normalized contact stress, b) Normalized lateral contact stress.

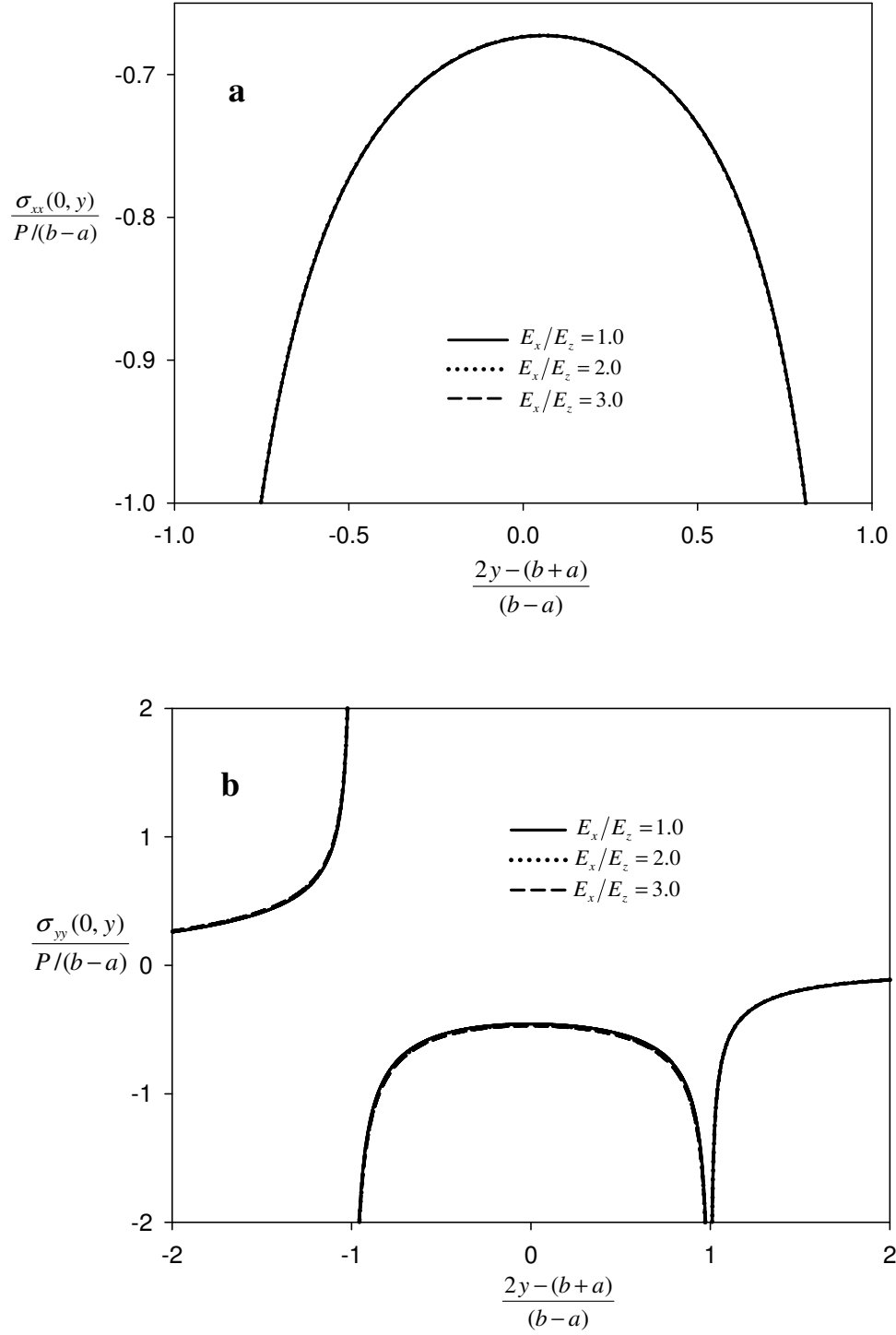


Figure 4.48: Effect of elastic modulus ratio E_x/E_z variations on the normalized surface stresses for a flat stamp problem of orthotropic homogeneous coatings, $(b-a)/h=1.0$, $\eta=0.3$, a) Normalized contact stress, b) Normalized lateral contact stress.

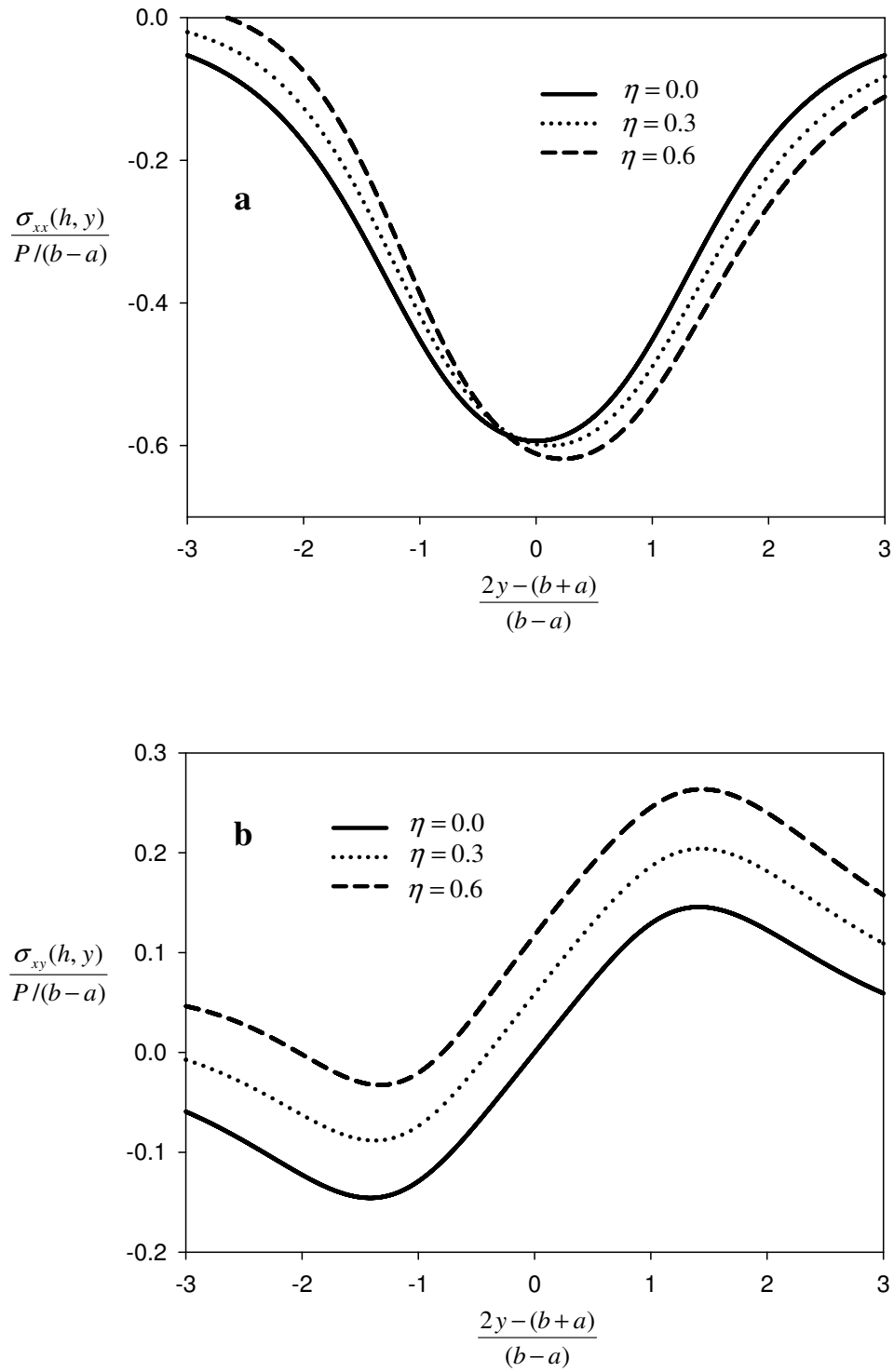


Figure 4.49: Effect of friction coefficient η variations on the normalized interfacial stresses for a flat stamp problem of the orthotropic homogeneous Alumina coating, $(b-a)/h=1.0$, a) Normalized normal stress, b) Normalized shear stress.

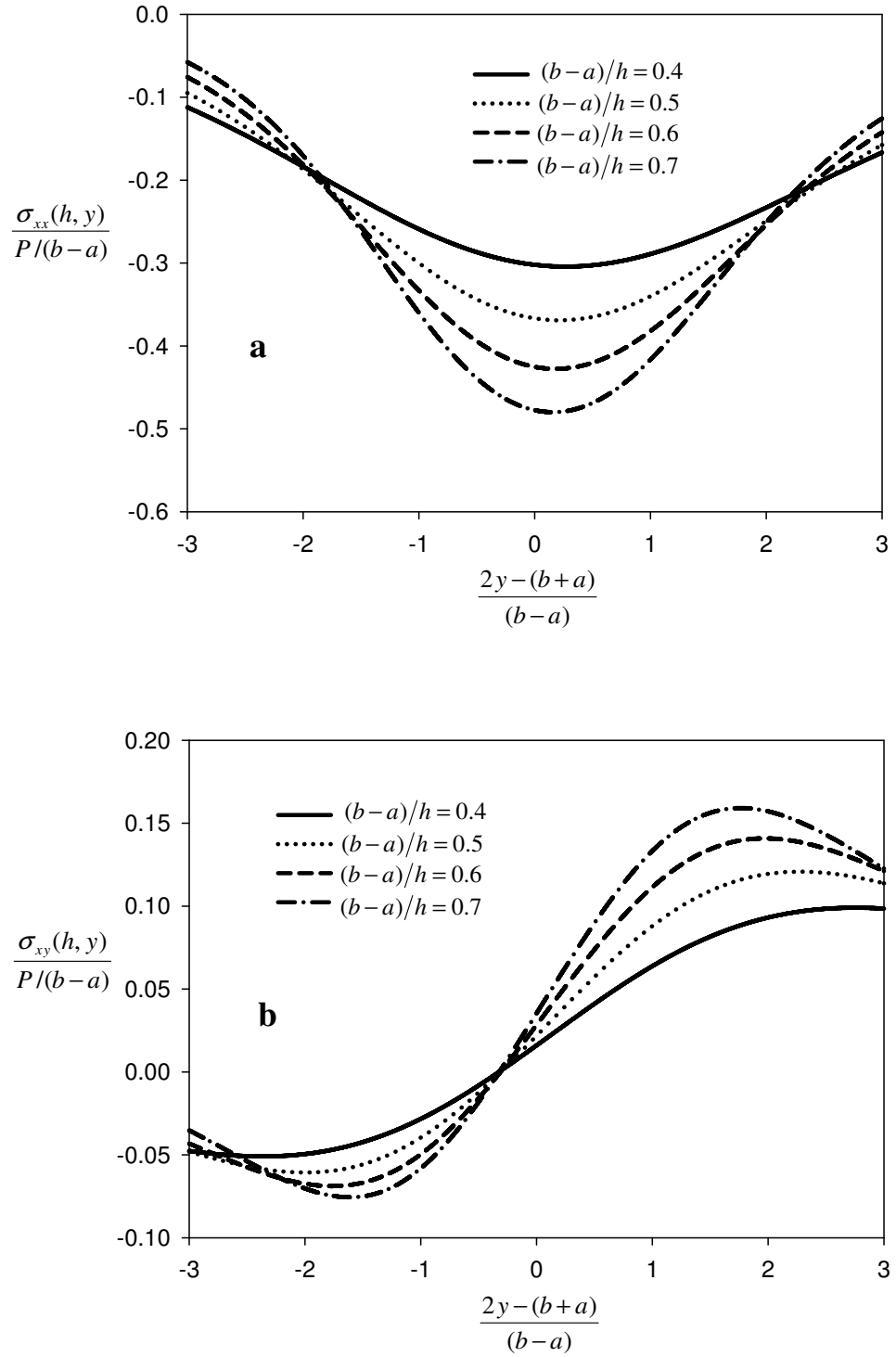


Figure 4.50: Effect of normalized contact length $(b-a)/h$ variations on the normalized interfacial stresses for a flat stamp problem of the orthotropic homogeneous Alumina coating, $\eta=0.3$, a) Normalized normal stress, b) Normalized shear stress.

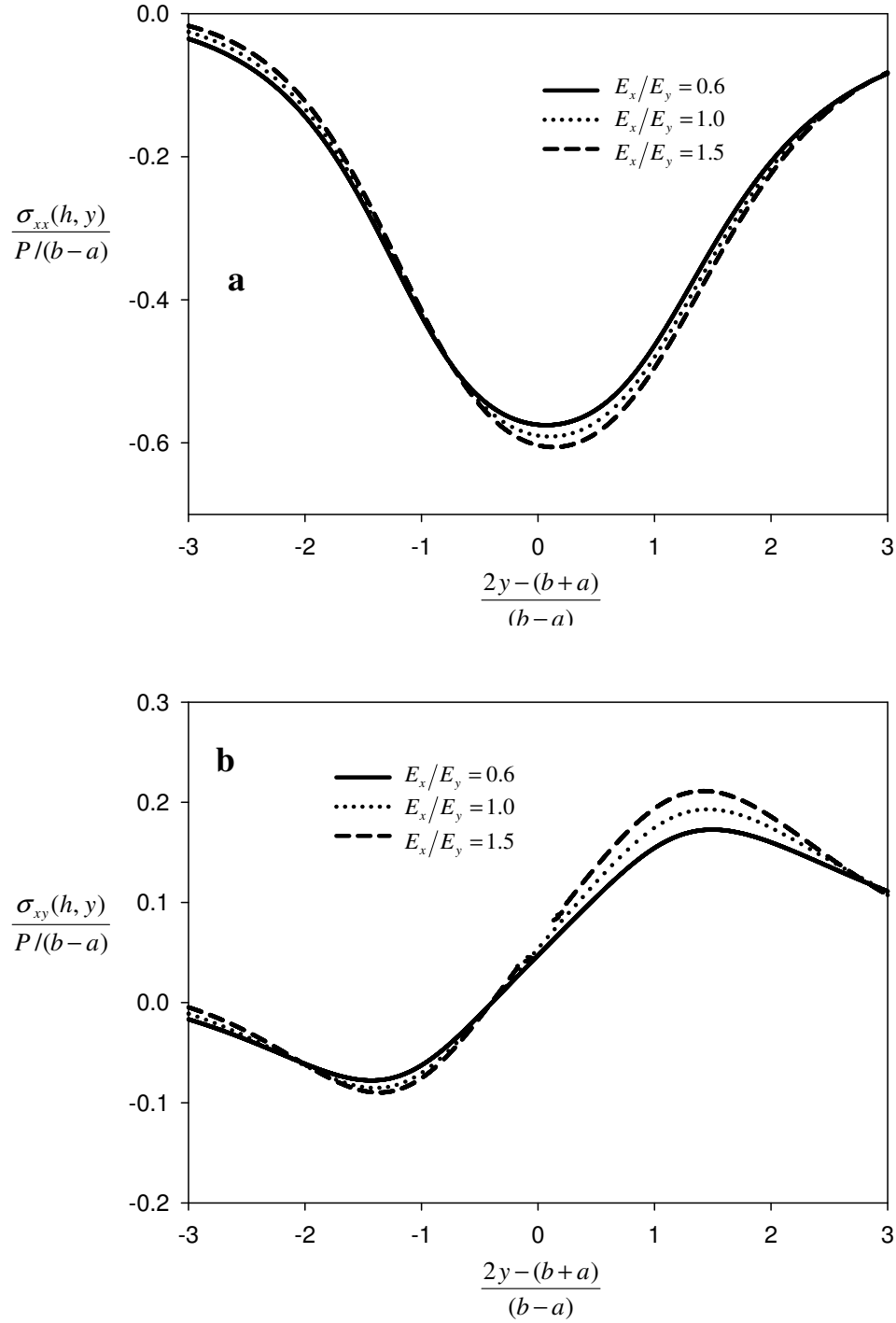


Figure 4.51: Effect of elastic modulus ratio E_x/E_y variations on the normalized interfacial stresses for a flat stamp problem of orthotropic homogeneous coatings, $(b-a)/h = 1.0$, $\eta = 0.3$, a) Normalized normal stress, b) Normalized shear stress.

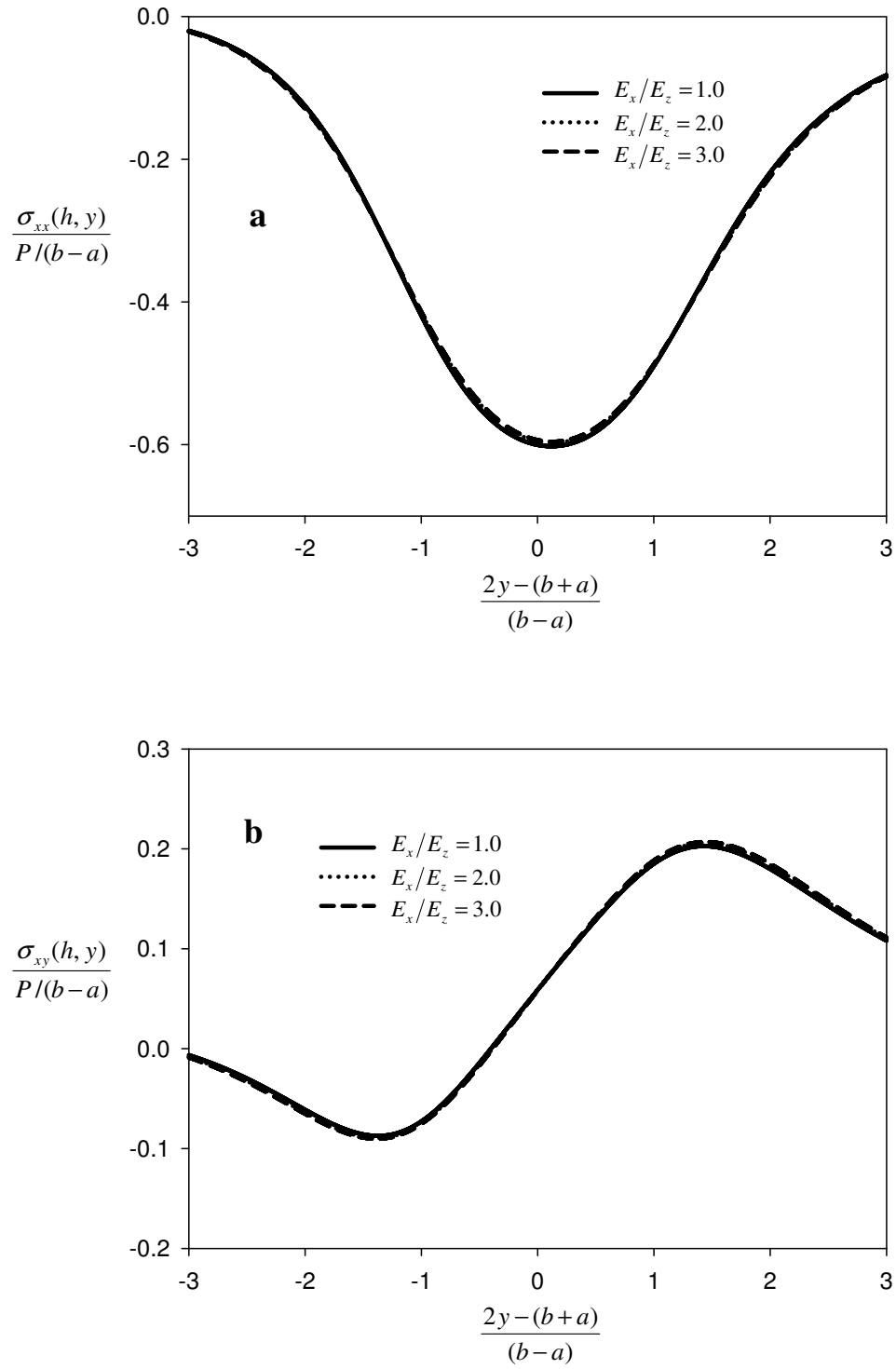


Figure 4.52: Effect of elastic modulus ratio E_x/E_z variations on the normalized interfacial stresses for a flat stamp problem of orthotropic homogeneous coatings, $(b-a)/h = 1.0$, $\eta = 0.3$, a) Normalized normal stress, b) Normalized shear stress.

CHAPTER 5

CONCLUDING REMARKS

5.1 Conclusions

This study presents analytic and finite element based studies for contact problems of orthotropic FGM coatings which are bonded to isotropic homogeneous substrates without any interfacial defects. The analytic procedure is based on the derivation of a SIE. The comparison figures given in Chapter 4 reveals that the results computed two distinct procedure agree with each other with a very good accuracy, which indicates the validity of both methods. The strengths of the singularities described for the orthotropic FGM coating are independent to the coating thickness and the non-homogeneity parameter however, dependent on the engineering parameters and the friction coefficient. Parametric analyses are provided in Section 4 regarding complete and incomplete punch loadings. In the complete loading, the FGM surface is exposed to frictional contact tractions by an inelastic flat stamp. In the related case, the contact stresses tend to infinity at both leading and trailing ends of the rigid stamp for which the normal point load P is not a function of the contact length. However, for the incomplete contact problems, loadings due to rigid triangular and circular stamp profiles are the functions of the contact size. Among the incomplete contact problems, the circular stamp problem solutions take more time compared to the triangular stamp problem. Since the circular stamp problem includes numerically calculated double integrals. In the FEA of all the stamp problems, homogeneous FE technique is used and the orthotropic engineering parameters are defined at the centroids of the finite elements. Compatible results of the analytic and finite element based procedures indicate the utility of the homogeneous FE method. Numerical results are presented to demonstrate the effects of the non-homogeneity constant γh , the friction

coefficient η , the normalized contact length $(b - a)/h$, the elastic modulus ratio E_x/E_y and the elastic modulus ratio E_x/E_z on the contact stresses. The effects of the problem parameters are realized to be remarkable particularly for the lateral contact stress $\sigma_{yy}(0, y)$. It is known that the existence of the lateral tensile stress triggers the initiation of surface crackings on the ceramic materials. We can infer for all the stamp problems that; the normalized lateral contact stress decreases as positive elastic gradation is introduced to an orthotropic coating. Hence, introducing elastic gradation to a coating it might be possible to avoid the contact driven damages. If the risk of damage due to lateral contact stress is concerned, the selection of orthotropic materials having relatively higher elastic modulus ratio E_x/E_y should be also taken into account. It is also observed that the change in the elastic modulus ratio E_x/E_z has no significant effect on the normalized contact and lateral contact stresses. Additionally, for all the stamp problems, the way of decreasing the size of the coating thickness (relative to the contact length) seems such a remarkable alternative to reduce the risk of damage.

In the computational analyses, the triangular stamp inclination angle θ is taken as small as possible whereas the circular stamp radius R is taken as large as possible with respect to the other dimensions of the problems for the convergence purposes of the iterative Augmented Lagrange contact algorithm.

As far as the normalized contact forces are concerned, when the coating gets stiffer in the thickness direction, the normalized contact forces increase significantly for all the stamp problems for any combination of the other problem parameters. When the magnitude of the friction coefficient η is raised, the normalized contact force increases significantly in the triangular stamp case and decreases slightly in the case of circular stamp problem. When the coating thickness is reduced, the normalized contact force increases slightly for the triangular stamp case and increases significantly for the circular stamp case. We can also infer from these tables that when the elastic modulus ratios E_x/E_y and E_x/E_z are increased, then the normalized contact forces decrease for all the incomplete stamp problems regardless of the change in other parameters of the problems. It should be also emphasized that the effect of the variations of the normalized non-homogeneity

parameter γh on the normalized forces become much more significant for the circular and triangular stamp cases, as the coating gets thinner.

Some results investigating the behavior of homogeneous orthotropic coatings under contact loads are presented in this study. It is shown by the comparison figures that the developed analytical and computational approaches work accurately in the homogeneous coating cases. The homogeneous coatings are under the risks of interface debonding and the surface damages when they are exposed to contact loadings. Therefore, in the contact analysis of orthotropic homogeneous coatings, the effects problem parameters on surface and interfacial stresses are illustrated. For that reason, the effect of problem parameters on the interfacial and surface stresses are examined. When orthotropic materials having greater elastic modulus ratio E_x/E_y are selected as a coating material, the risks of surface crackings are reduced however the risks of interfacial debonding is increased in that case. Therefore, depending on the application, an optimization should be carried out during selection of the orthotropic material as far as the effect of the elastic modulus ratio E_x/E_y on the contact stresses are concerned. Increasing the coating thickness, it could be possible to lower the delamination risks without providing any negative effect on the surface resistance of the coating surface to the contact loadings. Finally, if the frictional forces are increased the surface and interfacial stresses raise, which may encourage the surface and interfacial failures due to the contact loads.

5.2 Future work

This study can be extended to a partial slip contact problem of an orthotropic FGM coatings bonded to a homogeneous substrate. Partial slip contact problems have a great physical correspondence because the damage caused by slip within stationary contacts play an important role on the formation of fatigue cracks [80].

It might also important to discuss the relative motion for contact problem of anisotropic materials since dynamic frictional elastic contact may cause dynamic instabilities [81]. Thus a dynamic contact model between the rigid stamp and the

FGM coating can be modelled such that the rigid stamp moves frictionally at a constant speed relative to the FGM surface, as done in the study by Zhou and Lee [82].

In the sliding frictional contact problems, a remarkable amount of heating due to frictional motion between the two contacting bodies, which leads to the thermos-elastic distortion and surface crackings at the contacting surface [83]. In addition, temperature rise resulting from the sliding frictional contact may considerably affect the performance of the FGM coated structures [83]. Thus a numerical study can be handled showing the effect of heat generation on the contact stress on orthotropic FGM coatings loaded by a rigid stamp.

REFERENCES

- [1] Khor, K.A., Gu, Y., 2000. Thermal properties of plasma-sprayed functionally graded thermal barrier coatings. *Thin Solid Films* 372, 104–113.
- [2] Cannillo, V., Lusvarghi, L., Siligardi, C., Sola, A., 2007. Prediction of the elastic properties profile in glass–alumina functionally graded materials. *Journal of the European Ceramic Society* 27, 2393–2400.
- [3] Yang, J., Xiang, H.J., 2007. Thermo–electro-mechanical characteristics of functionally graded piezoelectric actuators. *Smart Materials and Structures*.
- [4] Park, C.W., Lee, B.S., Walker, J.K., Choi, W.Y., 2000. A new processing method for fabrication of cylindrical objects with radially varying properties. *Industrial & Engineering Chemistry Research* 39, 79–83.
- [5] Yue, T.M., Li, T., 2008. Laser cladding of Ni/Cu/Al functionally graded coating on magnesium substrate. *Surface & Coatings Technology* 202, 3043–3049. 16, 784–797.
- [6] Zhang, J., Sun, K., Wang, J., Tian, B., Wang, H., Yin, Y., 2008. Sliding wear behavior of plasma sprayed Fe₃Al—Al₂O₃ graded coatings. *Thin Solid Films* 516, 5681–5685.
- [7] Kim J.W., Liu L., Zhang Y., 2010. Improving the resistance to sliding contact damage of zirconia using elastic gradients. *J. Biomed. Mater. Res. B*. 94B, 347–352.
- [8] Jitcharoen J., Padture NP., Giannakopoulos AE., Suresh S., 1998, Hertzian-crack suppression in ceramics with elastic-modulus-graded surfaces, *J Am Ceram Soc.*, 81, 2301–8.
- [9] Pender, D.C., Padture, N.P., Giannakopoulos, A.E., Suresh, S., 2001. Gradients in elastic modulus for improved contact-damage resistance. Part I: The silicon nitride–oxynitride glass system. *Acta Materialia* 49, 3255–3262.
- [10] Pender, D.C., Thompson, S.C., Padture, N.P., Giannakopoulos, A.E., Suresh, S., 2001. Gradients in elastic modulus for improved contact-damage resistance. Part II: The silicon nitride–silicon carbide system. *Acta Materialia* 49, 3263–3268.
- [11] Suresh, S., Olsson, M., Giannakopoulos, A.E., Padture, N.P., Jitcharoen, J., 1999. Engineering the resistance to sliding-contact damage through controlled gradients in elastic properties at contact surfaces. *Acta Materialia* 47, 3915–3926.

- [12] Nomura, T., Moriguchi, H., Tsuda, K., Isobe, K., Ikegaya, A., Moriyama, K., 1999. Material design method for the functionally graded cemented carbide tool. *International Journal of Refractory Metals & Hard Materials* 17, 397–404.
- [13] Mishina, H., Inumaru, Y., Kaitoku, K., 2008. Fabrication of ZrO₂/AISI316L functionally graded materials for joint prostheses. *Materials Science & Engineering A*. 475, 141–147.
- [14] Hertz H., *Über die Berührung elastischer Körper*, 1882, *J.Reine und Angewandte Mathematik*, 92, 156–71.
- [15] Bakirtas I., 1980, The problem of a rigid stamp on a nonhomogeneous elastic half space., *Int J Eng Sci*, 18, 597–610.
- [16] Selvadurai APS., 1986, Singh BM., Vrbik J., A Reissner–Sagoci problem for a non-homogeneous elastic solid., *J.Elas.*, 16, 383–91.
- [17] Giannakopoulos AE., Suresh S., 1997, Indentation of solids with gradients in elastic properties: Part II Axisymmetric indenters, *Int. J. Solids Struct.*, 34, 2393–428.
- [18] Suresh S., Giannakopoulos AE., Alcala J., 1997, Spherical indentation of compositionally graded materials Theory and experiments., *Acta Mater.*, 45, 1307–21.
- [19] Giannakopoulos AE., Pallot P., 2000, Two dimensional contact analysis of elastic graded materials., *J.Mech Phys Solids*, 48, 1597–631.
- [20] Muskhelishvili N.I., 1963, *Some Basic Problems of the Mathematical Theory of Elasticity*, Noordhoff, Groningen, The Netherlands, 1-100.
- [21] Pao, Y.C., Wu, T.S., Chiu, Y.P., 1971, Bounds on the Maximum Contact Stress of an Indented Elastic Layer., *Transactions of ASME, Journal of Applied Mechanics*, 38, 608-614.
- [22] Ratwani, M., Erdogan, F., 1973, On the Plane Contact Problem for a Frictionless Elastic Layer, *Journal of Solids and Structures* ,9, 921-936.
- [23] Civelek, M.B., Erdogan, F., 1974, The Axisymmetric Double Contact Problem for a Frictionless Elastic Layer, *International Journal of Solids and Structures*, 10, 639-659.
- [24] Gecit, M., 1986, The Axisymmetric Double Contact Problem for a Frictionless Elastic Layer Indented by an Elastic Cylinder, *International Journal of Engineering Science*, 24 (9), 1571-1584.

- [25] Chan, S.K., Tuba, I.S., 1971, A Finite Element Method for Contact Problems of Solid Bodies- Part I. Theory and Validation, *Int. J. Mech. Sci.*, 13, 519-530.
- [26] Tsuta, T., Yamaji, S., 1973, Finite Element Analysis of Contact Problems, Theory and Practice in Finite Element Structural Analysis., University of Tokyo Press, Japan, 10-50.
- [27] Ohte, S., 1973, Finite Element Analysis of Elastic Contact Problems, *Bull. JSME*, 16, 797-804.
- [28] Guler M.A, 2000, Contact mechanics of FGM coatings, PhD dissertation, Lehigh University, Bethlehem, PA, USA.
- [29] Giannakopoulos, A.E., Pallot, P., 2000. Two-dimensional contact analysis of elastic graded materials. *Journal of the Mechanics and Physics of Solids* 48, 1596–163.
- [30] Guler, M.A., Erdogan, F., 2004. Contact mechanics of graded coatings. *Int. J. Solids Struct.* 41, 3865–3889.
- [31] Guler, M.A., Erdogan, F., 2006. Contact mechanics of two deformable solids with graded coatings. *Mechanics of Materials* 38, 633–647.
- [32] Guler, M.A., Erdogan, F., 2007. The frictional sliding contact problems of rigid parabolic and cylindrical stamps on graded coatings. *International Journal of Mechanical Sciences* 49, 161–182.
- [33] Ke, L.L., Wang, Y.S., 2006. Two-dimensional contact mechanics of functionally graded materials with arbitrary variations of material properties. *Int. J. Solids Struct.* 43, 5779–5798.
- [34] Ke, L.L., Wang, Y.S., 2007. Two-dimensional sliding frictional contact of functionally graded materials. *European Journal of Mechanics A – Solids* 26, 171–188.
- [35] Ke, L.L., Wang, Y.S., 2007. Fretting contact with finite friction of a functionally graded coating with arbitrarily varying elastic modulus. Part 1: Normal loading. *Journal of Strain Analysis for Engineering Design* 42, 293–304.
- [36] Ke, L.L., Wang, Y.S., 2007. Fretting contact with finite friction of a functionally graded coating with arbitrarily varying elastic modulus. Part 2: Tangential loading. *Journal of Strain Analysis for Engineering Design* 42, 305–313.
- [37] Yang, J., Ke, L.L., 2008. Two dimensional contact problem for a coating-graded layer–substrate structure under a rigid cylindrical stamp., *International Journal of Mechanical Sciences*, 50, 985–994.

- [38] Choi, H.J., Paulino, G.H., 2008. Thermoelastic contact mechanics for a flat stamp sliding over a graded coating/substrate system with frictional heat generation. *Journal of the Mechanics and Physics of Solids* 56, 1673–1692.
- [39] Guler, M.A., 2008. Mechanical modeling of thin films and cover plates bonded to graded substrates. *Journal of Applied Mechanics – Transactions of the ASME* 75, 051105.
- [40] Dag S., Guler M.A., Yildirim B, A. Ozatag C., 2009. Sliding frictional contact between a rigid stamp and a laterally graded elastic medium. *Int. J. Solids Struct.* 46, 4038–4053.
- [41] Dag S., Guler M. A., Yildirim B., and A. Ozatag C., 2013. Frictional Hertzian contact between a laterally graded elastic medium and a rigid circular stamp, *Acta Mech.* 224, 1773–1789.
- [42] Dag S., 2015. Consideration of spatial variation of the friction coefficient in contact mechanics analysis of laterally graded materials, *Z. Angew. Math. Mech.*, 1–16.
- [43] Hasebe N., Okumura M., Nakamura T., 1989, Frictional stamp and crack in plane elasticity, *ASCE, J.EngMech*, 115, 1137–49.
- [44] Choi HJ., 2001, Effects of graded layering on the tip behavior of a vertical crack in a substrate under frictional Hertzian contact.,*Engng. Fract. Mech*, 1033–59.
- [45] Dag S., Erdogan F., 2002, A surface crack in a graded medium loaded by a sliding rigid stamp, *Eng. Fract. Mech.*, 69, 1729–51.
- [46] Choi HJ., Paulino GH., 2010, Interfacial cracking in a graded coating/substrate system loaded by a frictional sliding flat stamp, *P Roy Soc A – Math Phys*, 466, 853–80.
- [47] Dağ, S., 2001, Crack and Contact Problems in Graded Materials, PhD. Thesis, Lehigh University.
- [48] Dağ S., Apatay T., Guler M.A, Gülgeç M, A., 2012, Surface crack in a graded coating subjected to sliding frictional contact, *Eng. Fract. Mech.*, 80, 72–91.
- [49] Apatay T., 2011, Crack and Contact Problems in Functionally Graded Materials, PhD. Thesis, Gazi University.
- [50] Lajnef, N., 2005, Surface Crack in a Functionally Graded Coating Bounded to a Homogeneous Substrate, PhD. Thesis, Tunusia Polytechnic School, 1-100.

- [51] El-Borgi, S., Abdelmoula, R., Dag, S., Lajnef, N., 2007, A Surface Crack in a Graded Coating Bonded to a Homogeneous Substrate Under General Loading Conditions, *Journal of Mechanics of Materials and Structures*, 2, 1331-1353.
- [52] Borodich F., 2000. Some contact problems of anisotropic elasto-dynamics: integral characteristics and exact solutions. *Int. J. Solids Struct.* 37, 3345–73.
- [53] Ciavarella, M., Demelio G., 2001. Schino M., Vlassak JJ., The general 3D Hertzian contact problem for anisotropic materials. *Key Eng. Mater.* 221, 281–92.
- [54] Lin, Y. and Ovaert, T. C., 2004, Thermoelastic Problems for the Anisotropic Elastic Half-Plane, *ASME Trans., Journal of Tribology*, 126, 3, 459-465.
- [55] Rand, O., Rovenskii, V., 2005. *Analytical methods in anisotropic elasticity: with symbolic computational tools*. Birkhauser.
- [56] Ning, X., Lovell, MR., Slaughter WS., 2006. Asymptotic solutions for axisymmetric contact of a thin transversely isotropic elastic layer. *Wear* 260, 693–8.
- [57] Li X., Wang M., 2006. Hertzian contact of anisotropic piezoelectric bodies. *J. Elast.* 84, 153–66.
- [58] He, L., Ovaert T., 2008. Three-dimensional rough surface contact model for anisotropic materials. *J. Tribol.* 130, 021402–6.
- [59] Larijani N., Brouzoulis J., Schilke M., Ekh M., The effect of anisotropy on crack propagation in pearlitic rail steel. *Wear* 314, 57-68.
- [60] Sampath S., Herman H., 1995, Shimoda N., Saito T., Thermal spray processing of FGMs, *MRS Bull*, 20(1), 27–31.
- [61] Kaysser W.A., Ilschner B., 1995, FGM research activities in Europe, *MRS Bull*, 20(1), 22–6.
- [62] Bakirtas I., 1984. The contact problem of an orthotropic non-homogeneous elastic half-space. *Int. J. Eng. Sci.* 22, 347–59.
- [63] Hwu, C., Fan, CW., 1998. Solving the stamp problems by analogy with the interface crack problems. *Int. J. Solids Struct.* 35, 3945–60.
- [64] Shi, D., Lin, Y., 2003. Ovaert TC., Indentation of an orthotropic half-space by a rigid ellipsoidal indenter. *J. Tribol–Trans ASME*, 223–31.
- [65] Swanson, SR., 2004. Hertzian contact of orthotropic materials., *Int. J. Solids Struct.*, 41, 1945–59.

- [66] Willis, JR., 1966. Hertzian contact of anisotropic bodies. *J. Mech. Phys. Solids* 14, 163–76.
- [67] Pagano, NJ., 1970. Exact solutions for rectangular bidirectional composites and sandwich plates., *J. Compos. Mater.* 4, 20–34.
- [68] Ramirez G., 2006, Frictionless contact in a layered piezoelectric medium characterized by complex eigenvalues, *Smart Mater. Struct.*,15, 1287–1295.
- [69] Guler, M.A., 2014. Closed-form solution of the two-dimensional sliding frictional contact problem for an orthotropic medium. *International Journal of Mechanical Sciences* 87, 72-88.
- [70] Guo L., Wu L., Zeng T., Ma L., 2004, Mode I crack problem for a functionally graded orthotropic strip, *European Journal of Mechanics*, 23, 219-234.
- [71] Erdogan F., 1978, Mixed boundary value problems in mechanics. In: Nemat-Nasser S, editor. *Mechanics today*, Pergamon Press, 4, 1–86.
- [72] Muskhelishvili NI., 1953, *Singular integral equations.*, Groningen: P. Noordhoff.
- [73] Dağ S., Apatay T., Guler M.A, Gülgeç M, A., 2012, Surface crack in a graded coating subjected to sliding frictional contact, *Eng. Fract. Mech.*, 80, 72–91.
- [74] Tricomi, F.G., 1951, “On the Finite Hilbert Transformation”, *The Quarterly Journal of Mathematics Oxford Series*, 2, 199-211.
- [75] ANSYS, 2009. *ANSYS Basic Analysis Guide*. Release 12, ANSYS Inc., Canonsburg, PA, USA.
- [76] Santare, M.H., Lambros, J., 2000. Use of graded finite elements to model the behavior of nonhomogeneous materials. *Journal of Applied Mechanics – Transactions of the ASME* 67, 819–822.
- [77] Yildirim, B., Dag, S., Erdogan, F., 2005. Three dimensional fracture analysis of FGM coatings under thermomechanical loading. *International Journal of Fracture*, 132, 371–397.
- [78] Dag S., Guler M.A., Yildirim B, A. Ozatag C., 2009. Sliding frictional contact between a rigid stamp and a laterally graded elastic medium. *Int. J. Solids Struct.* 46, 4038–4053.
- [79] Mijar A. R., Arora J.S., 2004, An augmented Lagrangian optimization method for contact analysis problems, 1: formulation and algorithm, *Struct Multidisc Optim*, 28, 99–112.

- [80] Kartal M.E., Barber J.R., Hills D. A., Nowell D., Partial slip problem for two semi-infinite strips in contact, *International Journal of Engineering Science*, 49, 203–211.
- [81] Zhou Y.T., Lee K.Y., 2013, Theory of sliding contact for multiferroic materials indented by a rigid stamp, *Int. J. Mech Sci.*, 66, 156–167.
- [82] Zhou Y.T., Lee K.Y., 2014, Dynamic behavior of a moving frictional stamp over the surface of anisotropic materials, *Applied Mathematical Modelling*, 38, 2311–2327.
- [83] Liu J., Ke L., Wang Y., Two-dimensional thermoelastic contact problem of functionally graded materials involving frictional heating, *Int. J. Solids Struct.*, 48, 2536–2548.

APPENDIX A

ASYMPTOTIC EXPANSION COEFFICIENTS

The asymptotic expansion coefficients of kernels that appear in (2.58) and (2.75) are determined using MAPLE and given below. Due to the long structures of these coefficients, the first 16 terms in (2.58) are given explicitly:

$$f_{10} = -\frac{8\eta C_{r2}(c_{120} + c_{660})}{c_{660}\lambda_2} \quad (\text{A.1})$$

$$f_{20} = \frac{4C_{r1}C_{r2}(c_{120} + c_{660})}{c_{660}\lambda_2} \quad (\text{A.2})$$

$$s_{10} = \frac{8\eta C_{r1}(c_{120} + c_{660})}{c_{660}\lambda_1} \quad (\text{A.3})$$

$$s_{20} = -\frac{4C_{r1}C_{r2}(c_{120} + c_{660})}{c_{660}\lambda_1} \quad (\text{A.4})$$

$$f_{11} = \frac{8\eta\gamma}{c_{660}\lambda_2} \left(\frac{2C_{r2}^2 c_{110}(C_{r1} - C_{r2})(c_{120} + c_{660})}{\lambda_2} - c_{660} + c_{120} \right) \quad (\text{A.5})$$

$$f_{21} = \frac{4\gamma}{c_{660}\lambda_2} \left(-\frac{2C_{r2}^2 C_{r1} c_{110}(C_{r1} - C_{r2})(c_{120} + c_{660})}{\lambda_2} + (c_{660} - c_{120})C_{r1} - (c_{660} + c_{120})C_{r2} \right) \quad (\text{A.6})$$

$$f_{12} = \frac{8\eta\gamma^2 C_{r2} c_{110}(C_{r1} - C_{r2})}{c_{660}\lambda_2} \left(\frac{2(c_{660} - c_{120})}{\lambda_2} - \frac{(3C_{r2}^2 c_{110} - 4c_{120})(c_{120} + c_{660})}{\lambda_2(C_{r2}^2 c_{110} + 4c_{120})} \right) \quad (\text{A.7})$$

$$f_{22} = \frac{4\gamma^2}{c_{660}\lambda_2} \left[\frac{C_{r2}c_{110}(C_{r1}-C_{r2})}{\lambda_2} \begin{pmatrix} C_{r1}(c_{120}+c_{660}) \frac{3C_{r2}^2c_{110}-4c_{120}}{C_{r2}^2c_{110}+4c_{120}} \\ -2C_{r1}(c_{660}-c_{120}) \\ +2C_{r2}(c_{660}+c_{120}) \end{pmatrix} - c_{660} + c_{120} \right] \quad (\text{A.8})$$

$$s_{11} = -\frac{8\eta\gamma}{c_{660}\lambda_1} \left(\frac{2C_{r1}^2c_{110}(C_{r1}-C_{r2})(c_{120}+c_{660})}{\lambda_1} - c_{660} + c_{120} \right) \quad (\text{A.9})$$

$$s_{21} = \frac{4\gamma}{c_{660}\lambda_1} \left(\frac{2C_{r1}^2C_{r2}c_{110}(C_{r1}-C_{r2})(c_{120}+c_{660})}{\lambda_1} + (c_{120}+c_{660})C_{r1} - (c_{660}-c_{120})C_{r2} \right) \quad (\text{A.10})$$

$$s_{12} = \frac{16\eta\gamma^2C_{r1}c_{110}(2.5C_{r1}^2c_{110}c_{120}+0.5c_{660}c_{110}C_{r1}^2+c_{120}^2-3c_{660}c_{120})}{c_{660}\lambda_1(C_{r1}^2c_{110}+4c_{120})^2} \quad (\text{A.11})$$

$$s_{22} = -4\gamma^2 \frac{\left(C_{r1}^4c_{110}^2(3c_{120}+c_{660}) + C_{r1}^3C_{r2}c_{110}^2(5c_{120}+c_{660}) + 16C_{r1}^2c_{110}c_{120}^2 \right.}{c_{660}\lambda_1(C_{r1}^2c_{110}+4c_{120})^2} \quad (\text{A.12})$$

$$d_{10} = -\frac{2C_{r1}(c_{110}C_{r2}^2-4c_{660})}{c_{660}\lambda_2} \quad (\text{A.13})$$

$$d_{20} = -\frac{4\eta(c_{110}C_{r2}^2-4c_{660})}{c_{660}\lambda_2} \quad (\text{A.14})$$

$$h_{10} = \frac{2C_{r2}(c_{110}C_{r1}^2-4c_{660})}{c_{660}\lambda_1} \quad (\text{A.15})$$

$$h_{20} = \frac{4\eta(c_{110}C_{r1}^2-4c_{660})}{c_{660}\lambda_1} \quad (\text{A.16})$$

where

$$\lambda_1 = (C_{r1}-C_{r2})(c_{110}C_{r1}^2+4c_{120}) \quad (\text{A.17})$$

$$\lambda_2 = (C_{r1}-C_{r2})(c_{110}C_{r2}^2+4c_{120}) \quad (\text{A.18})$$

APPENDIX B

CLOSED FORM AND RECURRENCE TYPE SOLUTIONS OF CAUCHY PRINCIPAL VALUE INTEGRALS

The closed form solution of Cauchy principal value integrals for are calculated by Tricomi [74] and given by

$$\begin{aligned} \frac{1}{\pi} \int_{-1}^1 \frac{(1-t)^\alpha (1+t)^\beta}{t-r} P_n^{\alpha,\beta}(r) dt &= \cot(\pi\alpha)(1-r)^\alpha (1+r)^\beta P_n^{\alpha,\beta}(r) \\ &- \frac{2^{\alpha+\beta} \Gamma(\alpha) \Gamma(n+\beta+1)}{\pi \Gamma(n+\alpha+\beta+1)} F\left(n+1, -n-\alpha-\beta, 1-\alpha, \frac{1-r}{2}\right) \end{aligned} \quad -1 < r < 1 \quad (\text{B.1})$$

where $\alpha > -1$, $\beta > -1$, $\alpha \neq 0, 1, 2, \dots$, Γ is the Gamma function, $F()$ is the Hypergeometric function. (B.1) can be reduced to the following form for $\chi = -(\alpha + \beta) = (-1, 0, 1)$ as:

$$\begin{aligned} \frac{1}{\pi} \int_{-1}^1 \frac{(1-t)^\alpha (1+t)^\beta}{t-r} P_n^{\alpha,\beta}(r) dt &= \cot(\pi\alpha)(1-r)^\alpha (1+r)^\beta P_n^{\alpha,\beta}(r) \\ &- \frac{2^{-\chi}}{\sin(\pi\alpha)} P_{n-\chi}^{-\alpha, -\beta}(r) \end{aligned} \quad -1 < r < 1 \quad (\text{B.2})$$

The recurrence type closed form solutions of Cauchy principal value integrals are calculated by Guler [28]. The integral can be defined as

$$L_n(r) = \int_{-1}^1 \frac{(1-t)^\alpha (1+t)^\beta}{t-r} P_n^{\alpha,\beta}(r) dt \quad -\infty < r < \infty \quad (\text{B.3})$$

where

$$L_n(r) = \frac{1}{P_{n-1}^{\alpha,\beta}(r)} \left(P_n^{\alpha,\beta}(r) L_{n-1}(r) + \frac{h_{n-1}}{G_{n-1}} \right) \quad -\infty < r < \infty \quad n = 1, 2, \dots \quad (\text{B.4})$$

$$h_0 = \frac{2^{\alpha+\beta+1} \Gamma(\alpha+1) \Gamma(\beta+1)}{\Gamma(\alpha+\beta+2)} \quad (\text{B.5})$$

$$h_n = \frac{2^{\alpha+\beta+1} \Gamma(n+\alpha+1) \Gamma(n+\beta+1)}{(2n+\alpha+\beta+1) n! \Gamma(n+\alpha+\beta+1)} \quad n=1,2,\dots \quad (\text{B.6})$$

$$G_n = \frac{2(n+1)(\alpha+\beta+n+1)}{(\alpha+\beta+2n+1)(\alpha+\beta+2n+2)} \quad n=0,1,2,3,\dots, \quad (\text{B.7})$$

for $\alpha < 0$, $\beta < 0$ and $\alpha + \beta = -1$,

$$L_0(r) = \frac{\pi}{\sin(\pi\alpha)} \begin{cases} -(-r+1)^\alpha (-r-1)^\beta & -\infty < r < -1 \\ (-r+1)^\alpha (r+1)^\beta \cos(\pi\alpha) & -1 < r < 1 \\ (r-1)^\alpha (r+1)^\beta & 1 < r < \infty \end{cases} \quad (\text{B.8})$$

for $\alpha > 0$, $\beta < 0$ and $\alpha + \beta = 0$,

$$L_0(r) = \frac{\pi}{\sin(\pi\alpha)} \begin{cases} (-r+1)^\alpha (-r-1)^\beta - 1 & -\infty < r < -1 \\ (-r+1)^\alpha (r+1)^\beta \cos(\pi\alpha) - 1 & -1 < r < 1 \\ (r-1)^\alpha (r+1)^\beta - 1 & 1 < r < \infty \end{cases} \quad (\text{B.9})$$

for $\alpha > 0$, $\beta > 0$ and $\alpha + \beta = 1$,

$$L_0(r) = \frac{\pi}{\sin(\pi\alpha)} \begin{cases} -(-r+1)^\alpha (-r-1)^\beta - r + \alpha - \beta & -\infty < r < -1 \\ (-r+1)^\alpha (r+1)^\beta \cos(\pi\alpha) - r + \alpha - \beta & -1 < r < 1 \\ (r-1)^\alpha (r+1)^\beta - r + \alpha - \beta & 1 < r < \infty \end{cases} \quad (\text{B.10})$$

APPENDIX C

FUNCTION THEORETIC ANALYSES

The dominant part of the singular integral equation (2.68) have analogous structure to that derived for isotropic FGM coatings. Therefore, a similar procedure can be used in order to define the strength of singularities of the contact end for orthotropic FGM coatings. The aforementioned procedure is given as follows [28]:

Let the dominant part of the SIE is given as

$$A\phi(r) - \frac{1}{\pi} \int_{-1}^1 \frac{\phi(s)}{s-r} ds = F(r) \quad -1 < r < 1 \quad (\text{C.1})$$

where the bounded function $F(r)$ contains part of the integral with the Fredholm kernels. Defining

$$\phi(z) = \frac{1}{2\pi i} \int_{-1}^1 \frac{\phi(s)}{s-z} ds \quad (\text{C.2})$$

And utilizing the consecutive Plemelj formulations

$$\Phi^+(r) - \Phi^-(r) = \begin{cases} \phi(r) & -1 < r < 1 \\ 0 & r < -1, r > 1 \end{cases} \quad (\text{C.3})$$

$$\Phi^+(r) + \Phi^-(r) = \begin{cases} \frac{1}{\pi i} \int_{-1}^1 \frac{\phi(s)}{s-r} ds & -1 < r < 1 \\ 2\Phi(r) & r < -1, r > 1 \end{cases} \quad (\text{C.4})$$

(C.1) can be reduced to the consecutive Riemann-Hilbert problem for partially holomorphic function $\Phi(z)$ as

$$\Phi^+(r) = G\Phi^-(r) + g(r) \quad (\text{C.5})$$

where

$$G = \frac{A+i}{A-i} \quad (\text{C.6})$$

$$g(r) = \frac{F(r)}{A-i} \quad (\text{C.7})$$

Considering the corresponding homogeneous equation

$$X^+(r) - GX^-(r) = 0 \quad (\text{C.8})$$

The fundamental solution $X(z)$ and the fundamental function $\omega(x)$ of (C.1) are obtained as

$$X(z) = (z-1)^\alpha (z+1)^\beta \quad (\text{C.9})$$

$$\omega(r) = (1-r)^\alpha (r+1)^\beta \quad (\text{C.10})$$

where

$$\alpha = a_1 + ib_1 + N \quad (\text{C.11})$$

$$\beta = a_2 + ib_2 + M \quad (\text{C.12})$$

$$a_1 + ib_1 = \frac{\ln G}{2\pi i} \quad (\text{C.13})$$

$$a_2 + ib_2 = -\frac{\ln G}{2\pi i} \quad (\text{C.14})$$

If $A > 0$, the angle φ can be defined for:

$$A + i = re^{i\varphi} \quad (\text{C.15a})$$

$$A - i = re^{-i\varphi} \quad (\text{C.15b})$$

$$\varphi = \arctan\left(\frac{1}{A}\right) > 0 \quad (\text{C.15c})$$

Therefore (C.13) and (C.14) becomes

$$a_1 + ib_1 = \frac{1}{2\pi i} \ln e^{2i\varphi} = \frac{\varphi}{\pi} \quad (\text{C.16})$$

$$a_2 + ib_2 = -\frac{1}{2\pi i} \ln e^{2i\varphi} = -\frac{\varphi}{\pi} \quad (\text{C.17})$$

yielding

$$\alpha = N + \frac{\theta}{\pi} \quad (\text{C.18})$$

$$\beta = M - \frac{\theta}{\pi} \quad (\text{C.19})$$

However, If $A = -A_0 < 0$, the angle φ can be defined as

$$\varphi = \arctan\left|\frac{1}{A}\right| > 0 \quad (\text{C.20a})$$

From equation (C.6), G becomes

$$G = \frac{A_0 - i}{A_0 + i} \quad (\text{C.20b})$$

The angle φ can be defined for

$$A_0 + i = re^{i\varphi} \quad (\text{C.21})$$

$$A_0 - i = re^{-i\varphi} \quad (\text{C.22})$$

$$\varphi = \arctan\left(\frac{1}{A_0}\right) > 0 \quad (\text{C.23})$$

Therefore (C.13) and (C.14) becomes

$$a_1 + ib_1 = \frac{1}{2\pi i} \ln e^{-2i\varphi} = -\frac{\varphi}{\pi} \quad (\text{C.24})$$

$$a_2 + ib_2 = -\frac{1}{2\pi i} \ln e^{2i\varphi} = -\frac{\varphi}{\pi} \quad (\text{C.25})$$

Then, α and β yield

$$\alpha = N - \frac{\theta}{\pi} \quad (\text{C.26})$$

$$\beta = M + \frac{\theta}{\pi} \quad (\text{C.27})$$

where N and M arbitrarily selected integers which are related to the nature of the problem.

VITA

PERSONAL INFORMATION

Surname, Name: Arslan, Onur
Nationality: Turkish (TC)
Date and Place of Birth: 7 April 1984, Elbistan
Marital Status: Single
Phone: +90 312 297 62 08 – 124

EDUCATION

| Degree | Institution | Year of graduation |
|--------|----------------------|--------------------|
| MS | Hacettepe University | 2011 |
| BS | Gaziantep University | 2007 |

WORK EXPERIENCE

| Year | Place | Enrollment |
|--------------|----------------------|--------------------|
| 2008-Present | Hacettepe University | Research Assistant |
| 2007-2008 | TUBITAK Project | Project Assistant |
| 2007-2007 | Sanko Makina | R & D Engineer |

HONORS

| Title | Institution | Year |
|---|----------------------|------|
| Top grad-student in engineering faculty | Gaziantep University | 2007 |

PUBLICATIONS

Dag, S., Yildirim, B., Arslan, O., Arman, E.E., 2012. Hygrothermal fracture analysis of orthotropic materials using J_k - integral. Journal of Thermal Stresses, 35, 596-613.

PATENTS

Yıldırım, N., Kapucu S., Göğüş, F., Arslan, O., 2011, An olive oil extraction unit, Turkish Patent Institute, Patent No: 2008 02778.